UNIVERSITÀ DI PARMA

UNIVERSITA' DEGLI STUDI DI PARMA

DOTTORATO DI RICERCA IN
SCIENZA E TECNOLOGIA DEI MATERIALI

CICLO XXXV

Responsive materials *via* vinylogous urethane chemistry and host-guest interactions.

Coordinatore:

Prof. Enrico Dalcanale

Tutore:

Prof. Enrico Dalcanale

Dottorando: Giuseppe Soavi

Anni Accademici 2019/2020-2022/2023

Abstract

Responsive materials exhibit remarkable macroscopic responses upon specific external stimuli, providing solutions to today's progress challenges. The growing demand for more sustainable technological development is becoming a necessity in many fields, prompting the scientific community to push the boundaries of the progress even further. The goal is to provide ever more performing materials with a well-defined end-of-life management strategy. For this purpose, polymers incorporating dynamic bonds or weak interactions represent the best tradeoff between a well-consolidated platform of synthetic polymers and a new generation of materials, more durable or, alternatively, able to easily be reintroduced in a circular economy.

The envisaged dynamicity in these new polymeric materials can be imparted by the incorporation of weak interactions, such as hydrogen bonding, host-guest interactions, metal-ligand coordination, or more robust reversible covalent bonds, giving arise to covalent adaptable networks.

This PhD thesis reports design, synthesis, and properties of responsive materials for application in a wide variety of fields: from promoter for interlayer adhesion in composites until the tailoring of new recyclable insulators, as well as the generation of new self-reporting polymers.

The main investigated covalent adaptable networks (CANs) were those based on the vinylogous urethane chemistry. In Chapter 2, a systematic study of the thermal, rheological, and mechanical properties of phenoxy-based vitrimers was presented. They relied on the transamination of vinylogous urethane. The aforementioned vitrimers were obtained by a two-steps synthesis from a commercial phenoxy resin via partial conversion of hydroxyl groups to acetoacetates (AcAc), followed by network formation by reaction with a 20% molar excess of m-xylylendiamine (XYDIA) as crosslinker. Three different vitrimers with variable crosslinking density were obtained by tuning the density of AcAc moieties along the phenoxy resin scaffold (5%, 10% and 15% conversion of hydroxyl groups). The conversion of linear polymers to dynamic crosslinked networks was confirmed by DMTA and rheology measurements, followed by stress relaxation tests to investigate the kinetics of bond exchanges. The calculation of activation energies for the relaxation process showed the negligible existence of additional relaxation modes, compared to the relaxation due to

vinylogous bond exchanges, especially for higher vinylogous urethane crosslinking %. Tensile tests as a function of reprocessing cycles revealed an increase of the maximum elongation and stress at break and proved the good recyclability of the vitrimers. Enhanced adhesive properties compared to pristine phenoxy resins were demonstrated, including the possibility to thermally re-join the assembly after its mechanical failure. Finally, the solvent-free preparation of vitrimer was exploited for 5% crosslinked vitrimer via melt reactive blending, providing a valuable alternative to the less environmentally sustainable synthesis in solution.

As adhesion promoters for carbon fiber-reinforced epoxy matrices, phenoxy resins and their functionalized counterparts with acetoacetate units were studied in Chapter 3. Multilayer objects are known to be susceptible to failure in a variety of modes in the thickness direction since their main weakness is the fiber/matrix interface. This phenomenon is called interlaminar delamination. Delamination is detrimental for composites because it is capable to worsen drastically their mechanical properties, therefore the enhancement of the interlaminar adhesion becomes a crucial factor. Our purpose was to address this issue playing on different factors, including the type of bonds introduced to the polymeric component of the composite, the topology of connection between the epoxy resin of the composite, the polymeric chains of the adhesion promoter and the ability to dissipate mechanical stresses.

We proposed the application of two commercial phenoxy resins with different average molecular weights (PKHB and PKHP). They are amorphous thermoplastic mixable with epoxy resin, ensuring mutual diffusion of the relevant polymeric chains, hence able to give arise to a physical entanglement, which is one of the enhancing factors of interlaminar adhesion. A further step was the introduction of a properly functionalized phenoxy resin (PKHP-AcAc 20% and PKHB-AcAc 20%) It was thought that the presence of acetoacetate units could be crucial for the formation in situ of a vitrimeric network, once crosslinked with the amines of the crosslinker present in the epoxy matrix of the composite. The interlaminar adhesion would also be enhanced due to the development of a stitch-stitch topology entanglement, which entails the diffusion of acetoacetylated phenoxy chains into the epoxy networks of the two adherends, crosslinking into a third covalent adaptable-based polymer, in topological entanglement with both pre-existing polymer networks. The third polymer network acts like a molecular suture. To separate, at least one of the three polymer networks

must break. These polymeric adhesion promoters were applied to a commercial prepreg (DT120), as thin films or dissolved in a suitable solvent. Mechanical characterization of bonded joint was evaluated in single lap shear configuration and fracture toughness configuration.

The application of vitrimeric networks as recyclable alternative to the wide-spread thermosets-based insulators was analyzed in Chapter 4. The replacement of crosslinked polyethylene is becoming a prominent issue to relieve the environmental imprint due to the end-life high voltage cables disposal. Thereby, the design of a new vitrimer which intrinsically presenting high free volume was identified as the best solution to address this problem. As building blocks, triptycene-based molecules were chosen thanks to the ability to create interstitial space around them.

We were interested to develop a vinylogous transamination-based CAN, attainable by the reaction between aminic crosslinkers and acetoacetylated amorphous thermoplastics. Several routes were explored to generate triptycene-based phenoxy resins, in which the triptycene unit ideally replaces the bisphenol A. The synthetic attempts concerned the reactions between the diglycidylated triptycene (9,10-benzenoanthracene-1,4-diol diglycidyl ether) with the hydroquinone homologous (9,10-benzenoanthracene-1,4-diol) or primary amines. The polymerization experiments showed only the formation of oligomers even varying the conditions in terms of temperature, base/catalyst, and time.

To overcome the limited growth of the polymeric chain, a more straightforward approach was also studied, thus avoiding the challenging synthesis of the linear polymer and its functionalization. The 9,10-benzenoanthracene-1,4-diol was properly acetoacetylated, becoming a suitable raw material for the reaction with tris(2-aminoethyl) amine (TREN), to generate a vinylogous urethane-based vitrimer.

In Chapter 5 cavitand-based host-guest chemistry has been tested to produce self-diagnostic polyurethanes. The purpose was to introduce a supramolecular unit in a polyurethane matrix, designed for the non-destructive and non-invasive detection of micro–damages. A nonemissive supramolecular complex was prepared and embedded into a rigid PU for the assessment of the mechanical-induced stress in the polymeric matrix. Indeed, internal stress detection in polymers used for high performance applications is critical in preventing structural failures when the integrity is crucial. The investigated system is based on the complex between a fluorescent N-methyl pyridinium salt (PyPyr-OH) and a

tetraphosphonate cavitand, CavPOPh (mono -OH). Both the host and the guest have a peripheral OH group to be embedded in the polyurethane matrix. In the complex the radiation emitted by the fluorophore is immediately quenched upon the complexation and theoretically restored by the mechanical stress-induced dissociation of the supramolecular complex. The photophysical behavior of the host-guest probe was investigated. Absorption and fluorescence emission titrations were performed, proving the emission quenching of PyPyr-OH in the complex. The spectroscopic characterization in solution was preparatory to perform investigation when the system was chemically linked to a polyurethane matrix. A polyol, in which a solution of the probe was dispersed, was polymerized with an isocyanate. The non-fluorescent behavior of the complex was retained in the polymer matrix. Tensile tests were carried out on dog-bone specimens to evaluate how the fluorescent response of the probe changed as stress level increased.

The fluorescence of PyPyr-OH remained quenched in the specimens after a mechanical stress application.

Finally, the effect of the host-guest interaction between cucurbit[8]uril (CB[8]) and a model trimethine indocyanine (Cy3) on dye spectral properties and aggregation in water was investigated in Chapter 6. Inclusion of polymethine cyanine dyes in the cavity of macrocyclic receptors is an effective strategy to alter their absorption and emission behavior in aqueous solution. Solution studies, performed by a combination of spectroscopic and calorimetric techniques, indicate that the addition of CB[8] disrupted Cy3 aggregates, leading to the formation of a 1:1 host-guest complex with an association constant of 1.5×10^{6} M^{-1}. At concentrations suitable for NMR experiments, the slow formation of a supramolecular polymer was observed, followed by precipitation. Single crystals X-ray structure elucidation confirmed the formation of a polymeric assembly with 1:1 stoichiometry in the solid state.

Nomenclature

^{1}H NMR	proton nuclear magnetic resonance
^{31}P NMR	phosphorous nuclear magnetic resonance
A	absorbance
AcAc	acetoacetate
CAN	covalent adaptable network
CB[n]	cucurbit[n]uril
d	doublet
dd	doublet of doublets
ddd	doublet of doublets of doublets
DCM	dichloromethane
DICY	dicyandiamide
DLS	dynamic light scattering
DMF	dimethylformamide
DMSO	dimethyl sulfoxide
DMTA	dynamic mechanical thermal analysis
DSC	differential scanning calorimetry
E′	elastic modulus (DMTA)
E″	loss modulus (DMTA)
FT-IR	Fourier transformed infrared spectroscopy
FTIR-ATR	attenuated total reflectance Fourier transformed infrared
G_{1c}	mode I

G_{2c}	mode II
G′	storage modulus (rheology)
G″	loss modulus (rheology)
GPC	gel permeation chromatography
HPLC	high pressure liquid chromatography
I	emission intensity
ILSS	interlaminar shear stress
ITC	isothermal titration calorimetry
J	spin-spin coupling
K_a	association constant
k_r	radiative process rate
n	refractive index
m	multiplet
M_n	number average molecular weight
M_w	weight average molecular weight
MALDI-TOF	matrix-assisted laser desorption/ionization-time of flight
MEK	methyl ethyl ketone
MS	mass spectrometry
mol%	molar percentage
o.n.	overnight
OD	optical density
-OH	hydroxy group

PDI	polydispersity index
PMMA	poly(methyl methacrylate)
PS	polystyrene
PU	polyurethane
Q	quantum yield
r_0	fundamental anisotropy
r	anisotropy
r.t.	room temperature
ROMP	ring-opening metathesis polymerization
s	singlet
t	triplet
T_g	glass transition temperature
T_m	melting temperature
T_v	topology freezing temperature
THF	tetrahydrofuran
TLC	thin layer chromatography
XLPE	crosslinked polyethylene
XRD	X-ray diffraction
XYDIA	m-xylylendiamine
UV-Vis	ultraviolet-visible spectroscopy
VU	vinylogous urethane
WLF	Williams-Landel-Ferry
δ	chemical shift

ε	dielectric constant
λ	wavelength
η	viscosity
η*	complex viscosity
θ	rotational correlation time
τ	relaxation time
τ	fluorescence lifetime
τR	tensile strength
υ	Poisson's ratio

Contents

Chapter 1

Adaptable Polymer Networks

The IUPAC Gold Book defines a macromolecule as: "*A molecule of high relative molecular mass, the structure of which essentially comprises the multiple repetition of units derived, actually or conceptually, from molecules of low relative molecular mass*".[1]

In polymer science topology plays a crucial role. Different topologies, along with the chemical composition of the material, can result in different macroscopic physical properties.[2,3] Polymeric molecules can have several spatial features, such as linear, branched, or cyclic architectures.[4] Topology can also refer to polymer networks that exhibit distinct topologies due to special crosslinkers.[5]

Thermoplastic and thermosets are the two main categories into which polymers are classified. [6,7]

Thermoplastics are characterized by long linear chains, not chemically connected each other, but physically entangled due to their high molecular weight. They entail a macroscopically flow like viscoelastic liquids when they are heated well above the glass transitions temperature, T_g (or the melting temperature, T_m, for semi-crystalline polymers), allowing them to be repeatedly melted and molded.[8] On the other hand, they are not suitable for applications requiring high thermal and chemical stability, high mechanical resistance, and dimensional stability. For these purposes, thermosets are the best candidates to address the aforementioned limitations: they have an extensive three-dimensional network, which endows to the material creep resistance, solvent resistance and high mechanical strength, preventing reprocessing and recycling.

Nowadays, the demand of recyclable high-performance materials[9] is becoming more prominent because of their attractiveness for lightweight structural applications, combined with the ability to be recycled.[10-12] The incompatibility between the classical thermoplastic and thermosets kicked off the development of dynamic polymer networks. Several weak interactions have been used for dynamic network formation ranging from host-guest interaction to metal-ligand coordination to the use of hydrogen bonding patterns (Figure 1).[13-17] They can be exploited to direct the self-assembly, which can provide the preorganization of macromolecules. The resulting architectures, otherwise difficult to make, are useful to realize unprecedented properties and functions.[18-23]

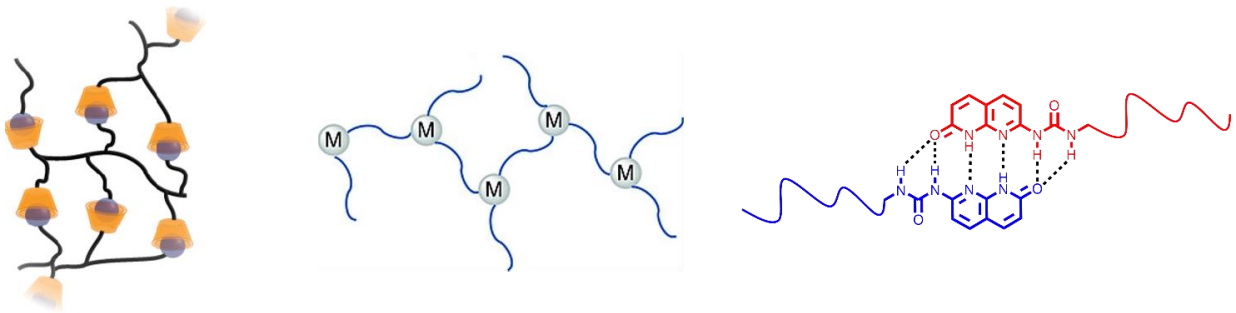

Figure 1 *Examples of weak interactions on which dynamic polymeric networks can rely on: host-guest interactions (Left), metal-ligand coordination (Middle) and hydrogen bonds (Right).*

High mechanical properties are critical for a variety of applications. As a result, the implementation of a new class of polymeric materials that are both robust and reprocessable is becoming appealing. This tradeoff has made possible by the incorporation of covalent dynamic crosslinks in CANs, which are conceptually similar to noncovalent crosslinked networks but differ in terms of interaction strength and lifetime. These materials are known as covalent adaptable networks (CANs), and they exhibit intrinsically dynamic behavior by two possible mechanisms: dissociative CANs show the cleavage of bonds into their constituents before the regeneration of the new functionality (Figure 2).

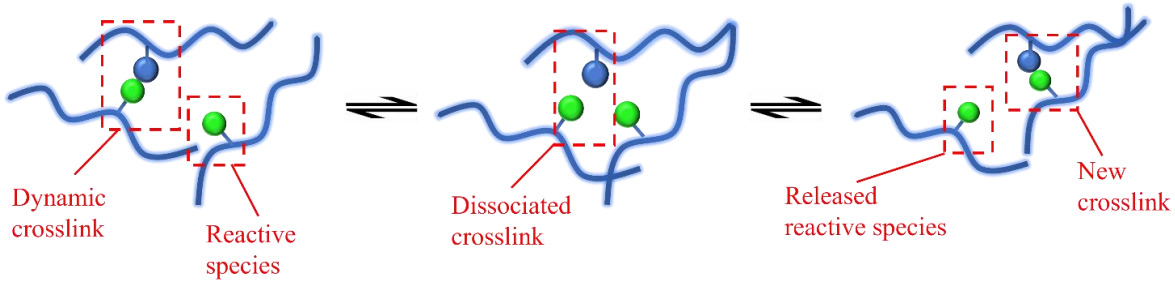

Figure 2 *General mechanism of dissociative bond exchange (adapted from reference 24).*

By contrast, the associative mechanism (Figure 3) occurs throughout an associative intermediate since a reactive moiety undergoes a concerted substitution reaction with another reactive species. Vitrimers belong to this latter category.

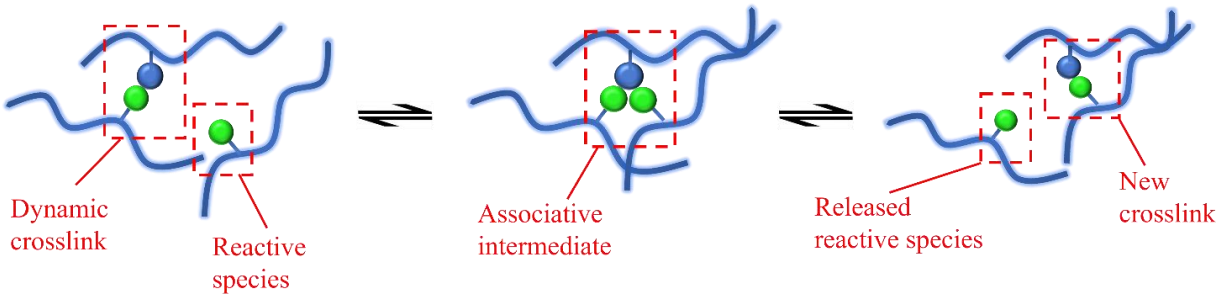

Figure 3 *General mechanism of associative bond exchange (adapted from reference 24).*

As the research topics described in this thesis are mainly concerned with the synthesis and the implementation of vitrimeric systems, this introduction deals with the discussion of associative CANs and their properties.

The name vitrimer was coined by Leibler because of the similarity in terms of viscosity variations with the temperature between the associative CANs and vitreous silica.[25] The dynamicity that characterizes these materials is reached by topological rearrangement due to thermally activated degenerated reactions between dynamic covalent units allowing these systems to fully relax external stresses.

Because both sides of the equilibrium (Figure 3) are identical in associative networks, temperature is not a factor that can favor one of the two sides. This means that the thermodynamic constant is always equal to 1, ensuring that the number of chemical bonds remains constant regardless the temperature. However, increasing the temperature has an important effect: it can increase the rate for both the direct and inverse reaction to the same extent, causing an enhancement of the dynamic character of the network.[26] Considering the temperature-dependent behavior of the flow properties of vitrimers, the rate of dynamic crosslink exchange determines the viscous flow of the polymer. To describe the viscous flow in a vitrimer, two critical temperatures must be evaluated: the glass transition temperature (T_g) and the topology freezing temperature (T_v). The former is a temperature that is common to all amorphous polymers, whereas the latter is only found in vitrimers. Indeed, crosslink exchange reactions in a vitrimeric network theoretically occur at all temperature, but only at T_v they become fast enough to allow network reorganization. This temperature is defined as when the system reaches a viscosity of 10^{12} Pa · s.[27]

Vitrimers necessitate sufficient network strand mobility, attainable above T_g, and a fast enough rate of crosslink rearrangement to accommodate deformations. Therefore, the start of the viscous flow is determined by the highest transition temperature that can be the T_v or the T_g. In almost all cases, vitrimers have the T_v higher than T_g, enabling a decrease of the viscosity according to an Arrhenius dependence with temperature (Figure 4, Left). Less frequently, vitrimeric systems have a lower T_v than T_g. This is the case of very rigid polymeric backbones, where having polymeric strands mobility requires more energy than triggering exchange reactions. At all temperatures below T_g, the material is a glass because bond exchange is suppressed due to the lack of chain mobility. The initial viscosity trend with temperature can be described by the Williams-Landel-Ferry (WLF) model before

following the Arrhenius dependence for gradually increasing temperatures (Figure 4, Right).[28]

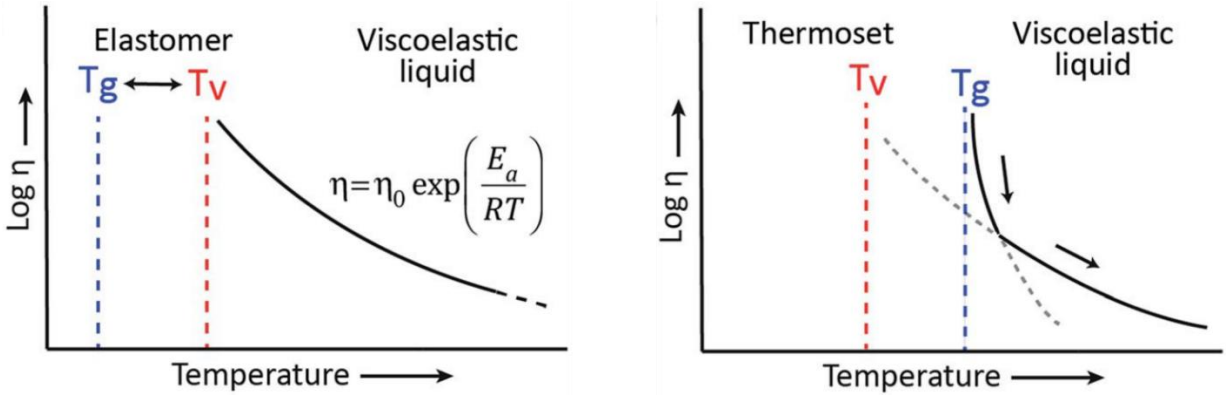

Figure 4 *Representation of the viscoelastic behavior of vitrimers with (Left) a glass transition, T_g, lower than the topology freezing transition temperature, T_v. Upon heating, the vitrimer evolves from a glassy solid ($T < T_g$) to an elastomer ($T_g < T < T_v$) to a viscoelastic liquid ($T > T_v$) that follows the Arrhenius law. (b) A hypothetical T_v is situated well below T_g. Upon heating, the vitrimer evolves from a glassy solid to a viscoelastic liquid with a viscosity that is first controlled through diffusion (WLF) and then by the exchange kinetics (Arrhenius).*[29]

Among the explored chemistries amenable to obtain associative CANs, transesterification and transamination are the most exploited reactions (Figure 5).

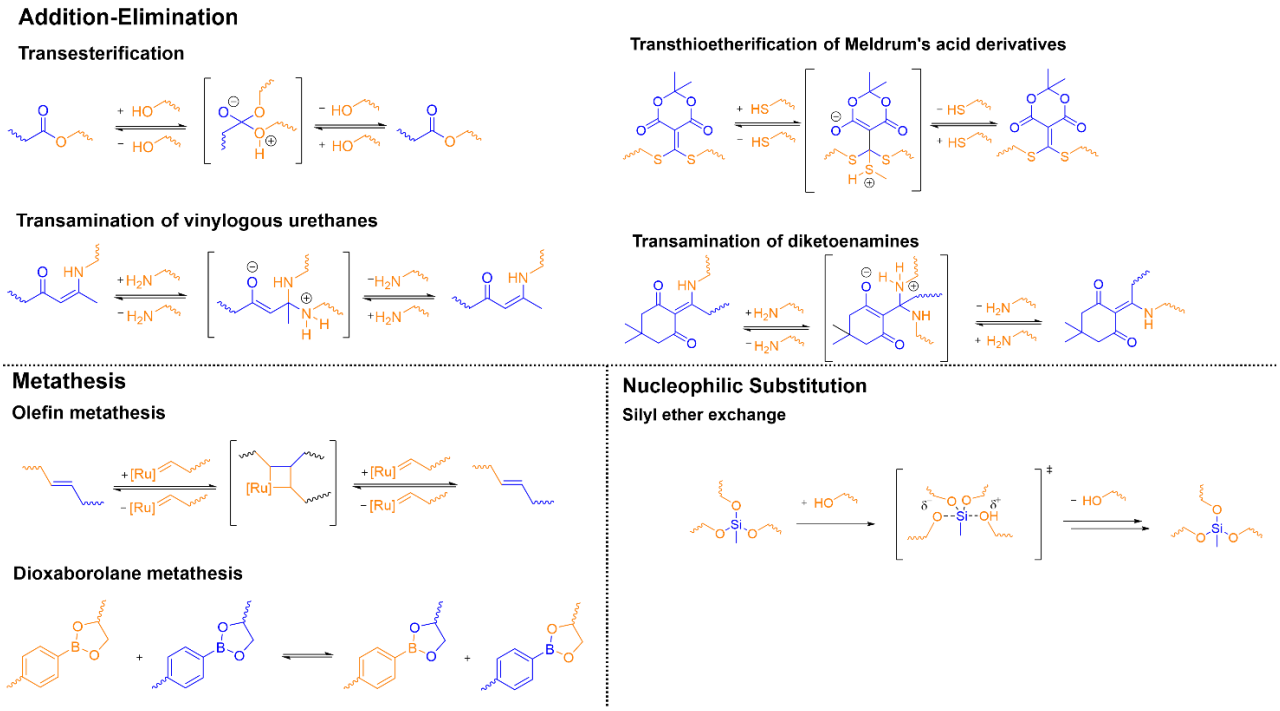

Figure 5 *Overview of crosslinking chemistries utilized for associative covalent adaptable networks.*[24]

Du Prez and co-workers[30] reported the first example of catalyst-free vitrimer, based on transamination reactions on vinylogous urethane moieties. Vinylogous urethane units are stable towards hydrolysis[31] because the exchangeable carbon-nitrogen bond is like the same

bond in a urethane or amide bond. This is possible thanks to the conjugation with the carbonyl group mediated by the carbon-carbon bond.

Vinylogous urethane group has the same reactivity of a Michael acceptor towards the nucleophilic addition of an amine. Vinylogous urethane-based polymers are prepared by the condensation reaction between acetoacetylated monomers and a slight excess of amines, to ensure free amines for the exchange reactions.

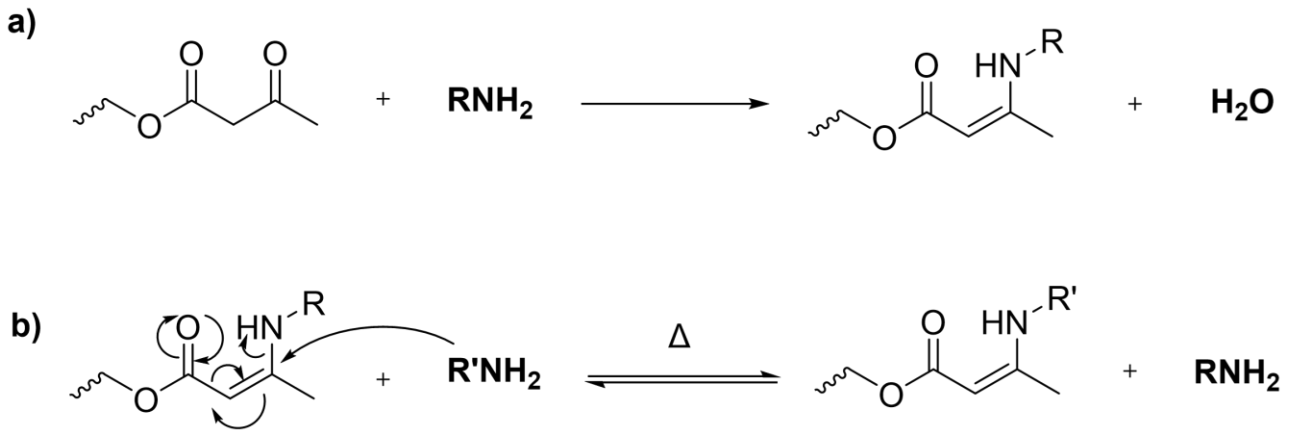

Scheme 1 *(a) Synthesis of vinylogous urethane; this reaction can even be performed in water. (b) Exchange of vinylogous urethanes and amines occurs at temperatures above 100 °C without catalyst via a Michael addition.*[30]

1.1. References

(1) M. McNaught, A. Wilkinson, *IUPAC. Compendium of Chemical Terminology,* **1997**, 2nd edition.

(2) P. J. Flory, *British Polymer Journal* **1985**, *17*, 96–102.

(3) R. Wang J. A. Johnson, B. D. Olsen, *Macromolecules* **2017**, *50*, 2556–2564.

(4) Y. Tezuka, H. Oike, *Progress in Polymer Science* **2002**, *27*, 1069–1122.

(5) Y. Gu, J. Zhao, J. A. Johnson, *Trends in Chemistry* **2019**, *1*, 318–334.

(6) E. N. Peters, *Applied Plastics Engineering Handbook*, 2nd edition.

(7) J. P. Pascault, R. J. J. Williams, *Thermosets*, 2nd edition.

(8) J. M. Garcia, M. L. Robertson, *Science* **2017**, *358*, 870-872.

(9) B. S. Sumerlin, *Science* **2018**, *362*, 150-151.

(10) D. J. Fortman, J. P. Brutman; G. X. De Hoe, R. L. Snyder, W. R. Dichtel, M. A. Hillmyer, *ACS Sustainable Chem. Eng.* **2018**, *6*, 11145−11159.

(11) R. J. Wojtecki, M. A. Meador, S. J. Rowan, *Nat. Mater.* **2011**, *10*, 14−27.

(12) C. N. Bowman, C. J. Kloxin, *Angew. Chem. Int. Ed.* **2012**, *51*, 4272−4274.

(13) C. Heinzmann, C. Weder, L. M. de Espinosa, *Chem. Soc. Rev.* **2016**, *45*, 342−358.

(14) N. Roy, B. Bruchmann, J. M. Lehn, *Chem. Soc. Rev.* **2015**, *44*, 3786−3807.

(15) G. R. Whittell, M. D. Hager, U. S. Schubert, I. Manners, *Nat. Mater.* **2011**, *10*, 176−188.

(16) L. Voorhaar, R. Hoogenboom, *Chem. Soc. Rev.* **2016**, *45*, 4013−4031.

(17) J. Tellers, S. Canossa, R. Pinalli, M. Soliman, J. Vachon, E. Dalcanale, *Macromolecules* **2018**, *51*, 7680-7691.

(18) D. Philp, J. F. Stoddart, *Angew. Chem. Int. Ed.* **1996**, *35*, 1154-96.

(19) V. Balzani, A. Credi, F. M. Raymo, J. F. Stoddart, *Angew. Chem. Int. Ed.* **2000**, *39*, 3348-91.

(20) N. C. Seeman, *Angew. Chem. Int. Ed.* **1998**, *37*, 3220-38.

(21) E. Regis, *Boston: Little Brown*, **1995**.

(22) J. F. Stoddart, *Acc. Chem. Res*. **2001**, 34:6.

(23) J. P. Sauvage, *Structure and bond* **2001**, 99.

(24) G. M. Scheutz, J. J. Lessard, M. B. Sims, B. S. Sumerlin, *J. Am. Chem. Soc.* **2019**, *141*, 16181-16196.

(25) D. Montarnal, M. Capelot, F. Tournilhac, L. Leibler, *Science* **2011**, *334*, 965−968.

(26) C. J. Kloxin, C. N. Bowman, *Chem. Soc. Rev.* **2013**, *42*, 7161−7173.

(27) D. J. Fortman, J. P. Brutman, C. J. Cramer, M. A. Hillmyer, W. R. Dichtel, *J. Am. Chem. Soc.* **2015**, *137*, 14019-14022.

(28) Y. Nishimura, J. Chung, H. Muradyan, Z. Guan, *J. Am. Chem. Soc.* **2017**, *139*, 14881−14884.

(29) W. Denissen, J. M. Winne, F. E. Du Prez, *Chem. Sci.* **2016**, *7*, 30–38.

(30) W. Denissen, G. Rivero, R. Nicolaÿ, L. Leibler, J. M. Winne, F. E. Du Prez, *Adv. Funct. Mater.* **2015**, 25, 2451–2457.

(31) H. A. Stefani, I. M. Costa, D. de O. Silva, *Synthesis* **2000**, 1526–1528.

Chapter 2

Phenoxy Resin-based Covalent Adaptable Networks*

*The content of this chapter has been submitted for publication. Mechanical characterization was carried out by the group of Professor Fina (PoliTO).

2.1. Introduction

Epoxy resins are widely used in several large-scale applications, including electronics, structural composites and adhesives. Standard epoxy resins are thermosets, therefore unsuitable to be repaired and recycled. However, their non-recyclability poses environmental problems, whose solution asks for sustainable alternative materials, as required by the EC Circular Economy Action Plan.[1] In the last few years, this drawback has been addressed in an innovative way, by introducing epoxy vitrimers.[2] Vitrimers bridge the gap between thermoplastics and thermosets, having the mechanical properties of the latter at service temperature and malleability like glass at temperature above the topology transition temperature (T_v).[3] This bimodal behavior is obtained by introducing covalent adaptable networks (CANs) in the polymer in the form of thermally activated reversible covalent bonds. The cross-link density in vitrimers is constant, due to bond cleavage occurring only after formation of new bonds.[2] As a consequence, the viscosity in the melt is controlled by the exchange reactions, following an Arrhenius-like decrease with temperature akin to vitreous silica,[2] providing glass-like weldability.[4] Pioneered by Leibler and co-workers, the earliest examples of epoxy vitrimers were based on dynamic transesterification reactions, catalyzed by zinc acetate.[2,3] Subsequently, other different exchange chemistries have been explored for the preparation of epoxy vitrimers such as disulfide metathesis,[5] imine amine exchange,[6,7] vinylogous urethane[8] and silyl ether exchange.[9] All these epoxy vitrimers are prepared by reacting the epoxy resins with a suitable hardener, either forming or containing the exchangeable bond. Absent in this scenario is the post-polymerization approach, where an epoxy-based linear thermoplastic is converted into a vitrimer. Phenoxy resins are commercially available amorphous thermoplastic polymers with molecular weight in the range 10,000-100,000 g/mol. They are miscible with epoxy resins, with whom they are often blended. Due to their excellent mechanical properties including flexibility, toughness, adhesive and cohesive strength, as well as chemical and heat resistance, phenoxy resins are widely employed in composites and adhesives. Phenoxy resin vitrimers are unknown in the literature. The pendant hydroxyl groups in phenoxy resins are amenable to a variety of functionalization. Among the several CAN chemistries available, we selected vinylogous transamination[10] to turn phenoxy resins into vitrimers (Scheme 1). For this aim, commercial phenoxy resins were

partially derivatized with acetoacetate (AcAc) groups and the resulting polymers were crosslinked with m-xylylendiamine (XYDIA). Mechanical and viscoelastic properties were thoroughly investigated, to exploit the vitrimeric properties in reprocessability and toward the development of reversible adhesives. Finally, the solvent-free preparation of phenoxy vitrimers *via* melt reactive blending was explored.

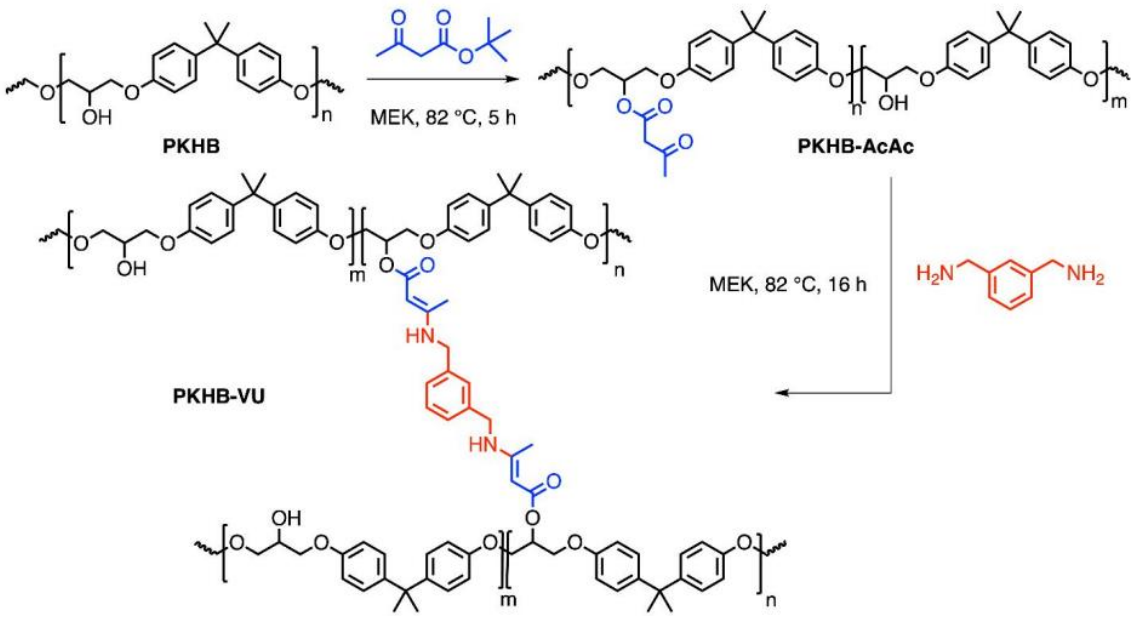

Scheme 1 *Synthetic scheme for the preparation of PKHB n% AcAc and PKHB n% VU compounds (n% = 5, 10, 15).*

2.2. Results and discussion

PKHB-based vitrimers were prepared in solution in two steps. Partial functionalization of PKHB with acetoacetate (AcAc) groups was carried out using t-butoxy acetoacetate in refluxing MEK (Scheme 1). The degree of functionalization was determined *via* ^{1}H NMR (Figure 1), by integrating the diagnostic triplet of the methyne α to AcAc at 5.54 ppm against the triplet of the methyne bearing the unreacted PHKB hydroxyl groups at 4.37 ppm. Functionalized PKHB n% AcAc were then reacted with XYDIA (20% excess) in refluxing MEK, to produce vinylogous urethane exchangeable crosslinking between linear chains.

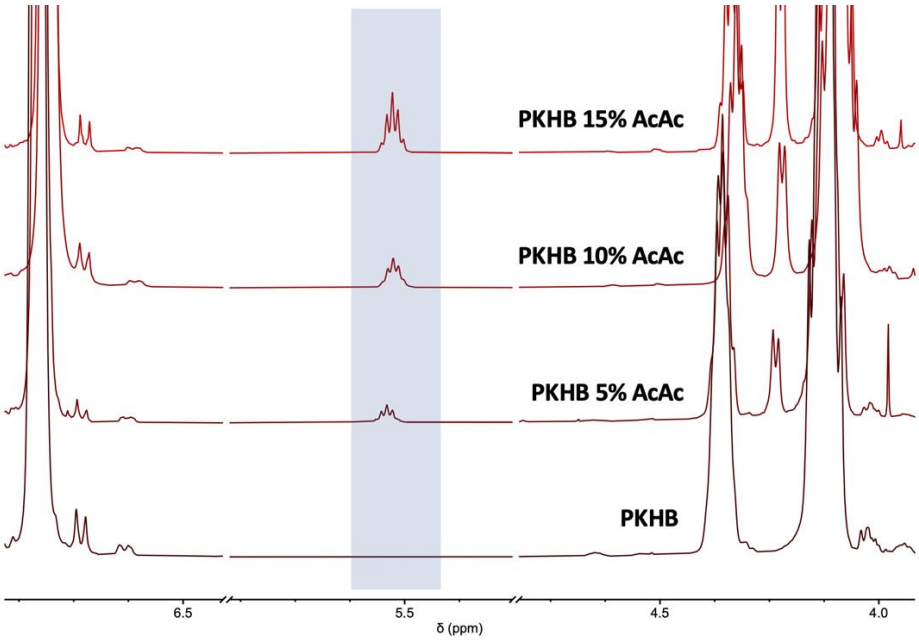

Figure 1 *Stacked ^{1}H NMR spectra of PKHB n% AcAc (n = 5, 10, 15) in $CDCl_3$.*

Conversion to vinylogous urethane was monitored by FTIR. Infrared spectra (Figure 2) for PKHB n% AcAc evidences the appearance of two signals at ca. 1744 and 1714 cm^{-1}, corresponding to the C=O stretching modes in the ester and ketone, respectively, with intensities proportional to the % of grafted AcAc groups. After reaction with XYDIA (Scheme 1), conversion to vinylogous urethane is supported by the appearance of a new broad band at ca. 1660 cm^{-1}, typically assigned to the conjugated C=O ester stretching in vinylogous urethane,[10] and the disappearance of the 1744 and 1714 cm^{-1} AcAc bands. The second characteristic band of VU, namely the C=C stretching, is overlapping to the PKHB and XYDIA aromatic C=C stretching at 1606 cm^{-1} (Figure 2).

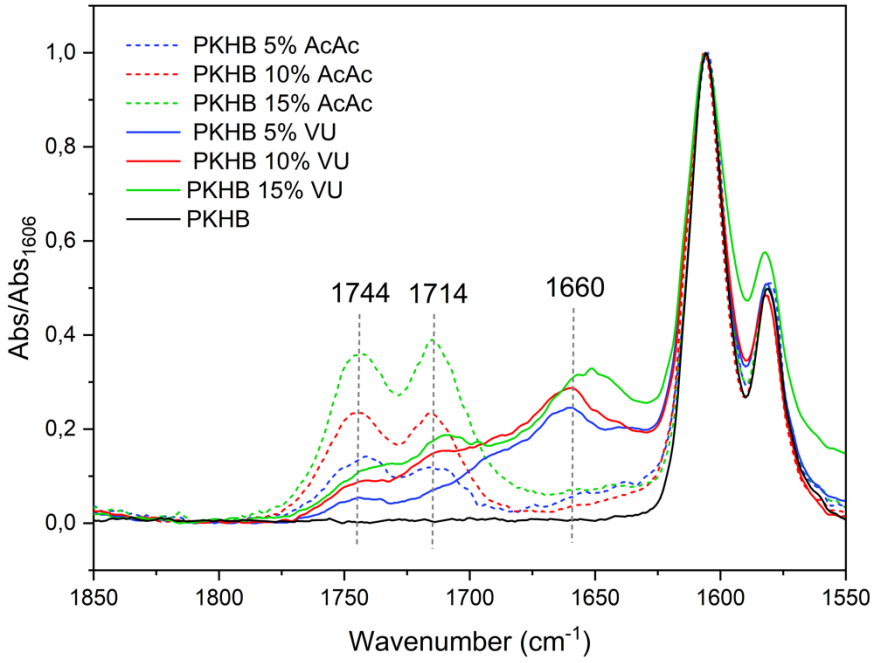

Figure 2 *Spectral window of FTIR of PKHB n% AcAc (dashed lines) and PKHB n% VU (solid lines), evidencing the diagnostic absorption bands relative to the carbonyl stretching.*

To verify the crosslinked character and improved solvent resistance of PKHB n% VU, the samples were kept in MEK at 60°C for 24 h. The remaining insoluble fractions after solvent removal and vacuum oven drying were 78, 97 and 100% for 5, 10 and 15% VU, respectively. By comparison, pristine PKHB resulted completely soluble in MEK at room temperature. Such high residues in the 10 and 15% samples reflect high crosslinking degrees in PKHB-based vitrimers, in line with previously reported polyvinylogous urethanes.[10] Reprocessability of PKHB n% VU was tested by compression molding, allowing simple preparation of films and slabs under mild conditions, thus evidencing the dynamic nature of the crosslinking bonds. Gel fractions were re-evaluated after compression molding into sheets, to evaluate the evolution of crosslinking upon reprocessing. The residue after extraction of the soluble fraction increased to 90% for PKHB 5% VU, suggesting that the temperature treatment allows completing the reaction, whereas residual fractions for 10 and PKHB 15% VU remained constant, as the crosslinking obtained from the synthesis was quantitative, within experimental errors of the gel fraction method. Viscoelasticity of PKHB vitrimers was investigated by DMTA on heating (Figure 3). Pristine PKHB exhibits a room temperature storage modulus E' at about 1.75 GPa, quickly decaying above 70°C due to the α relaxation of linear chains, with a maximum temperature (T_α) of ca. 93°C (Figure 3 top). Vitrimers resulted in slightly higher storage modulus (ranging between 2.1 and 2.9 GPa)

and variable T_α, (Figure 3 bottom) with a broad transition suggesting coexistence of relatively long linear fractions together with regions with high crosslinking densities. However, the most relevant result from the DMTA analysis is the higher thermomechanical resistance of vitrimers compared to the pristine PKHB, at temperatures above α relaxation. Indeed, at 5% VU, the storage modulus is slowly decreasing with increasing temperature, reflecting a partial crosslinking, whereas at higher % VU clear rubbery plateaus are observed at 1.9 and 3.0 MPa for 10% and 15% VU, respectively.

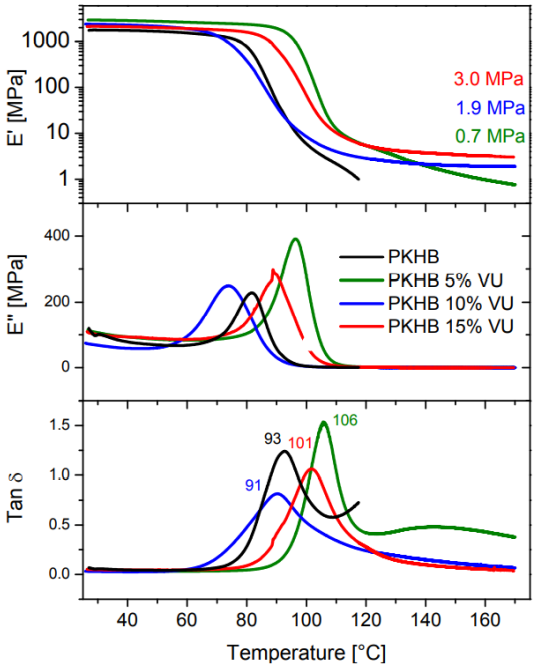

Figure 3 *DMTA plots for pristine PKHB and PKHB n% VU (n = 5, 10, 15).*

To further investigate the viscoelastic properties at high temperature, rheological analysis was carried out at variable frequency and different temperatures in the linear viscoelastic regime. In Figure 4, storage modulus (G'), loss modulus (G'') and complex viscosity (η*) plots obtained at 200 °C are plotted vs. the oscillation frequency. Remarkable G' values, in the range 10^4 to 10^5 Pa, were obtained for the vitrimers: in 5% VU a weak dependence on frequency is observed, whereas for 10 and 15% VU frequency-independent plateau values are obtained, increasing with the concentration of crosslinking. This behavior is completely different to that of linear PKHB and PKHB n% AcAc (Figure 4), confirming conversion of linear polymers to highly crosslinked networks, characterized by a solid-like rheological behavior.

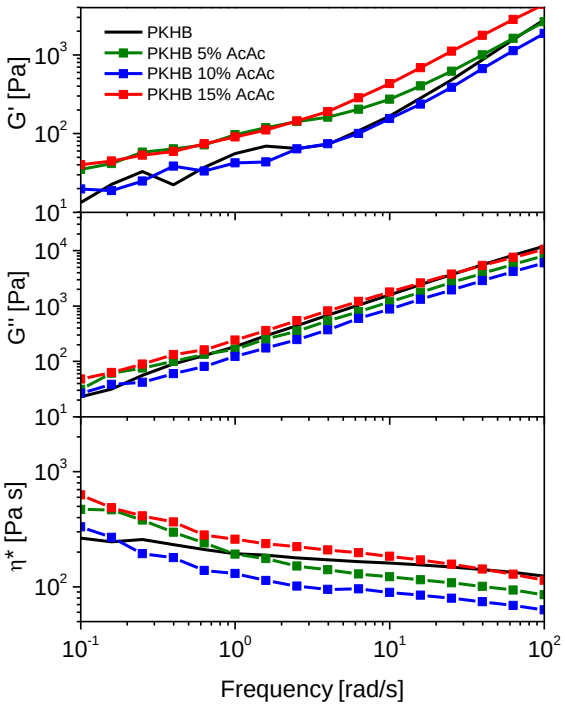

Figure 4 *Rheological plots pristine PKHB and PKHB-AcAc n% (n=5, 10, 15).*

This is further supported by the analysis of G'' values, being significantly lower than G' for all vitrimers, and the η* plots evidencing for extremely high viscosity up to ca. 10^6 Pa·s at low frequency, with a strong shear thinning effect as the frequency increases (Figure 5).

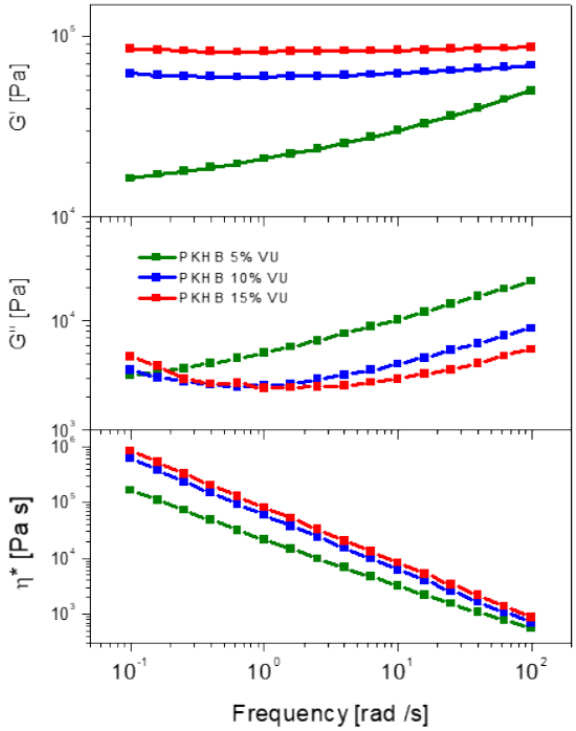

Figure 5 *Rheological plots for PKHB n% VU (n = 5, 10, 15).*

Such a viscoelastic behavior is clearly due to the covalent crosslinking of vitrimers while the exchange of bonds is not significant under these testing conditions, characterized by low deformation and limited relaxation time for the given temperature. To investigate the dynamics of bond exchanges in the covalent associative network, stress relaxation tests were also carried out. In these conditions, the rearrangement of the network is possible and a characteristic relaxation time as well as the activation energy can be estimated. The simplest model applicable to the stress relaxation of vitrimers assumes a simple exponential decay according to Maxwell model, with a characteristic decay time τ corresponding to the time at which the normalized stress reaches 1/e threshold. This model was applied to different vitrimers with high crosslinking density, including vinylogous urethanes.[12] However, at low crosslinking density, deviations from the Maxwell model were reported[11] and explained by the contribution of additional relaxation modes other than the exchange reaction in CAN. These modes may include networks strands, dangling chains and trapped loops[13] as well as direct associative interaction between linear chains, including hydrogen bonding, π-π interaction and Van der Waals forces. While these additional relaxation modes may be better described in terms of a continuous relaxation spectrum,[14] a simpler approach was also proposed by the use of modified decay functions,[11] aiming at the estimation of an average relaxation time. Alternatively, relaxation times in vitrimers were calculated from the initial slope of the stress relaxation curve[15] or from the G'-G'' crossover frequency.[14] Regardless the method to calculate the relaxation time, the temperature dependence of relaxation times may provide information on the exchange of dynamic bonds, as vitrimers follow an Arrhenius dependency.

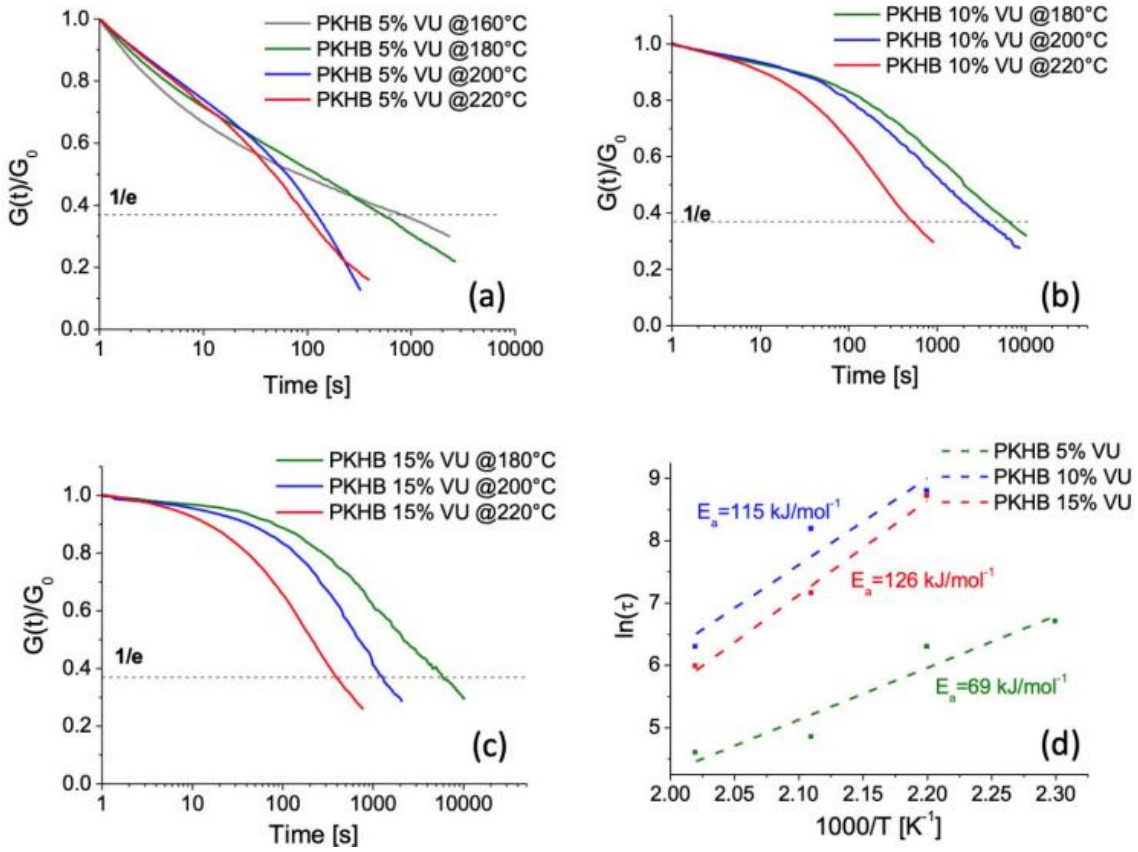

Figure 6 *Normalized stress relaxation plots at different isotherms for PKHB 5% VU (a), PKHB 10% VU (b), and PKHB 15% VU (c). Panel (d) reports Arrhenius plots for the relaxation times (τ) and fitting to calculate activation energies for the relaxation process.*

Stress relaxation plots for PKHB vitrimers (Figure 6a-c) exhibit very different feature depending on the % of crosslinkers. For samples PKHB 10 and 15% VU, stress relaxation qualitatively follows the usual trend for vitrimers, with slow stress decay vs time, whereas for sample PKHB 5% VU the decay is much faster in the early stage of the test, confirming the limited crosslinking. Fitting of these relaxation plots with the Maxwell model (Figure 7 left) did not provide good match for any of the PKHB vitrimers. However, a much better fit (Figure 7 right) for the same was obtained with a "stretched" exponential decay function $\frac{G(t)}{G_0} = Ae^{\left(\frac{t}{\tau}\right)^{\alpha}}$ with typical values between 0.4 and 0.6 for PKHB 10 and 15% VU, in agreement with previously reported stress relaxation of vinylogous urethane crosslinked polyethylene.[11] The observed deviation from the Maxwell relaxation is explained by the additional relaxation modes (e.g. networks strands, dangling chains, trapped loops as well as associative interaction between linear chains) beside vinylogous urethane bond exchange. The contribution of the additional relaxation modes is more evident at low

crosslinking density (5% VU), resulting in low α values (Figure 7 right), whereas the deviation from the ideal relaxation model becomes less important at higher % VU.

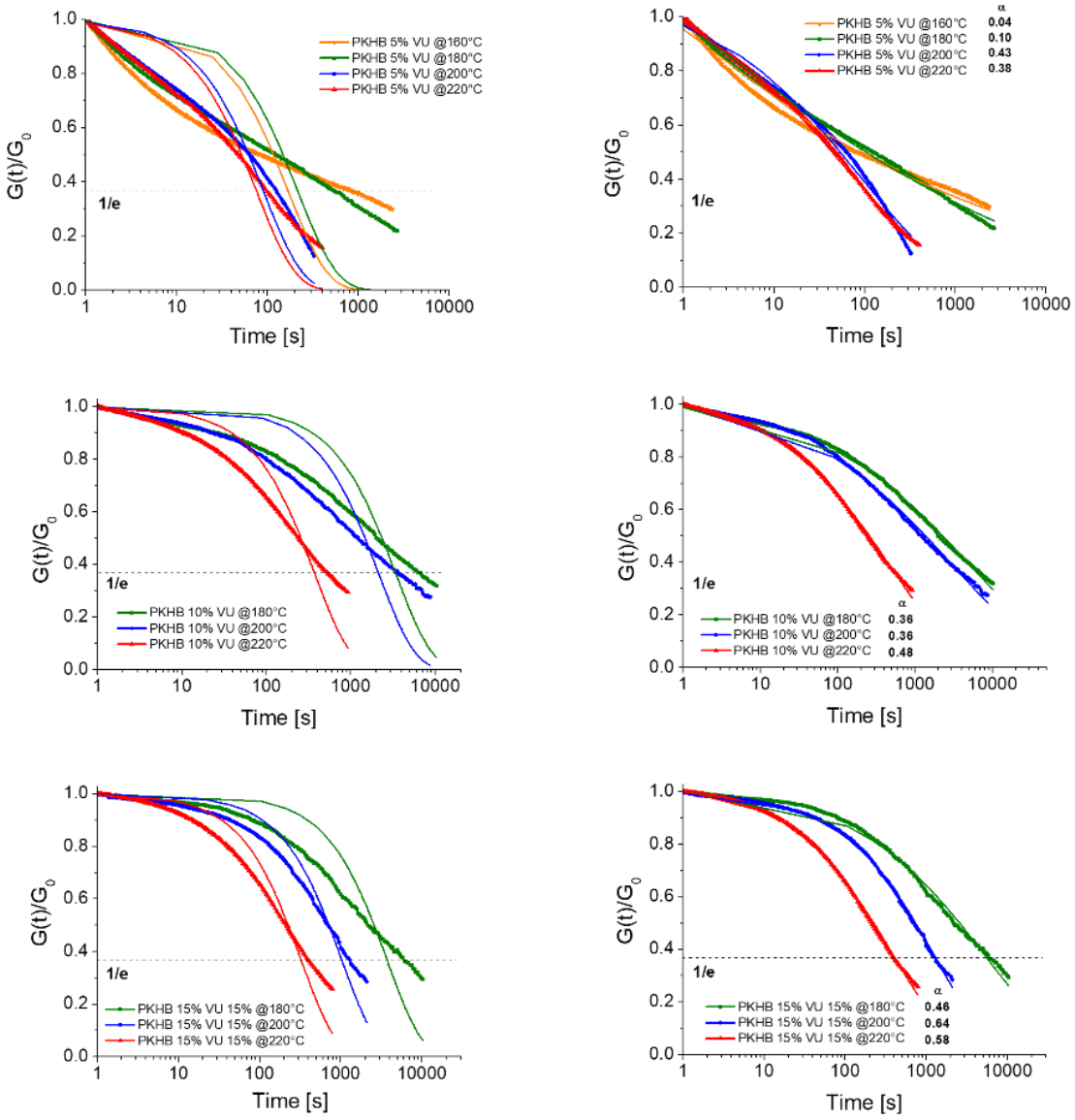

Figure 7 *Fitting of stress relaxation plots, accordingly with: left) simple decay (Maxwell model) and right) stretched exponential function. Dots represent experimental data, lines represent fittings.*

Representing the multi-mode relaxation with a single averaged relaxation time appears a reasonable approximation to discuss the evolution of relaxation time with temperature and to calculate the energy of activation for the relaxation process. Results reported in Figure 6d confirm the Arrhenius type temperature dependence of the relaxation time, with best ln(τ) vs. 1/T linear fit obtained for PKHB 15% VU, whereas limited scatter observed at lower crosslinking density may reflect the complexity of relaxation discussed above. Expectedly, activation energies for the relaxation process are also dependent on the VU %. At 5% VU

the calculated energy of activation is as low as 69 kJ/mol, reflecting a significant contribution of non-crosslinked chains to the materials relaxation. The activation energy increases with cross-linking density, namely 115 and 126 kJ/mol at 10% and 15% VU, respectively. These values are higher than the ones reported for polyvinylogous urethane[10] and VU crosslinked polyethylene[11] owing to the higher conformational stiffness of the aromatic structure of the phenoxy resin. Nevertheless, similar values are reported in the literature for other vitrimeric systems[16,17,18] and these values do not hamper the flow of the vitrimers during reprocessing at moderate temperatures.[19] The topology-freezing transition temperature (T_v) was defined by Leibler et al.[12] as the temperature at which "the mechanical relaxation time controlled by the exchange reaction rate becomes longer than the experimental timescale and, on this timescale, the network topology is frozen". Assuming a liquid-solid transition at $\eta=1\cdot10^{12}$ Pa·s and relaxation according to Maxwell's equation $\eta=(E^{'}/2(1+\nu))\cdot\tau$, where E' is the elastic modulus at the rubbery plateau and ν is the Poisson's ratio, Tv values are easily estimated. This simple model was largely applied in vitrimers literature[20,21] and results correlated with the possibility to reprocess the vitrimers at temperatures above T_v. As the bond exchange within a vitrimer network requires sufficient chain mobility, topology freezing transition is expected to occur above the glass transition temperature (T_g), as originally proposed by Leibler et al. However, T_v values below T_g were also reported in literature,[10,20] yielding materials in which stress relaxation is controlled by the segmental motion of linear chains. It is worth mentioning that the above discussed assumptions for the calculation of T_v might not be accurate for vitrimers exhibiting a rheological complex behavior. In particular, when the vitrimer relaxation is based on both bond exchanges and additional relaxation modes (e.g., networks strands, dangling chains, trapped loops etc.) Maxwell's equation may not be a good approximation and its application may lead to misleading T_v values. In this work, since at low crosslinking degree the co-existence of different relaxation modes is apparent based on the above stress-relaxation plots (Figure 6a), calculation of T_v for PKHB 5% VU is not possible by the Maxwell model. Instead, in highly crosslinked PKHB n% VU vitrimers, the contribution to any additional relaxation mode appears negligible compared to the relaxation by vinylogous bond exchanges and the Maxwell equation can be applied, resulting a T_v of 120 °C for PKHB 15% VU, which is slightly higher than the glass transition temperature for linear PKHB.

The tensile properties and recyclability of the synthesized vitrimers were evaluated. Both pristine PKHB and derived vitrimers exhibited brittle fracture, regardless of the processing cycles, as expected by the relatively high glass transition temperature. Stress-strain plots (Figure 7a for cycle 1 and Figure 8 for cycles 2 and 3) show significant differences between vitrimers and PKHB.

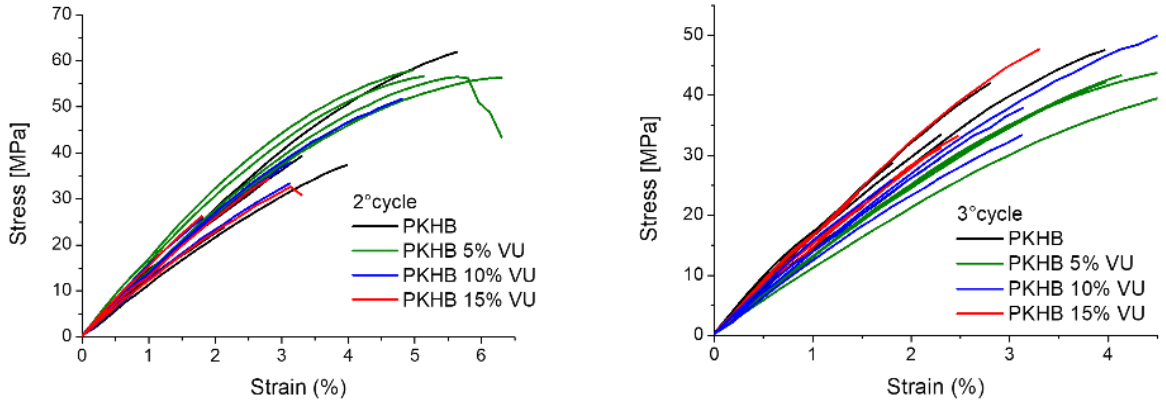

Figure 8 *Stress-strain plots on second and third tensile test cycles.*

Elastic modulus, elongation at break and resistance at break values for the different formulations and processing cycles are resumed in Figure 9b, c and d, respectively.

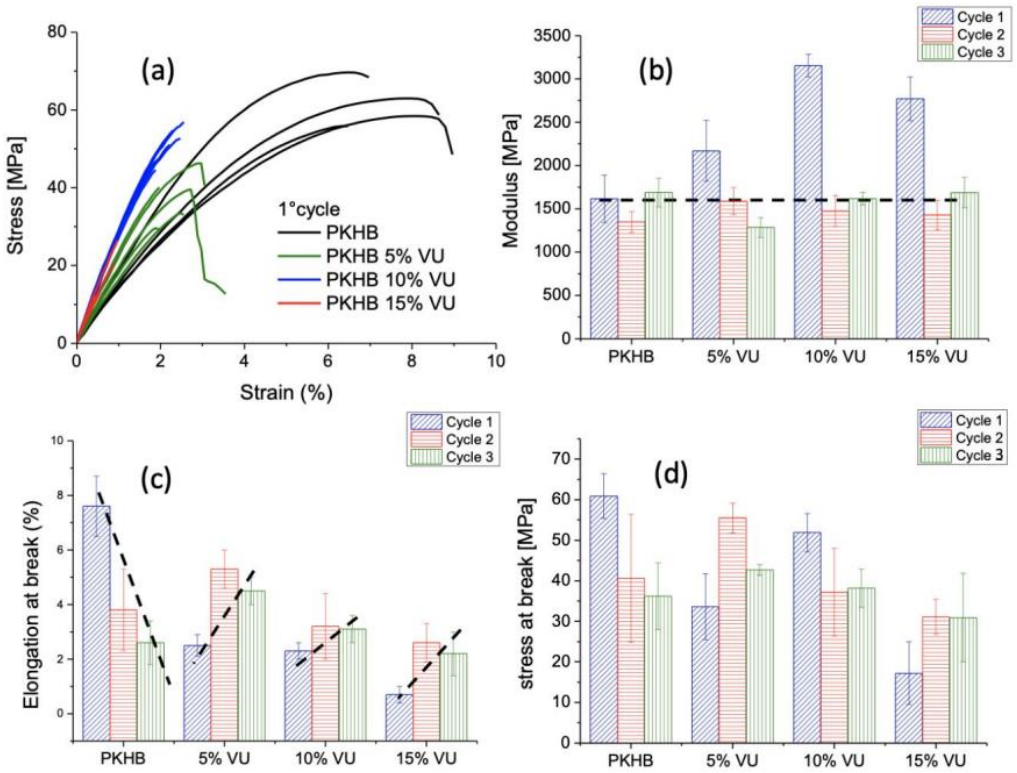

Figure 9 *Stress-strain plots on first tensile test cycle (a) and comparative histograms for different formulation and processing cycles, regarding elastic modulus (b), elongation at break (c) and stress at break (d).*

Elastic modulus of PKHB was measured in the range of 1.6 GPa, with variations upon reprocessing cycles within the experimental error. On cycle 1, significantly higher stiffness was observed for the vitrimers, up to 3.2 GPa for PKHB 10% VU. However, this stiffening effect is not retained on subsequent processing cycles, in which the different vitrimers appear to level off in stiffness at the value for PKHB, within the experimental uncertainty. For PKHB both elongation at break and stiffness decrease upon reprocessing cycles, according to the progressive thermo-mechanical degradation of the polymer. On the other hand, vitrimers exhibit a different trend, with typically higher elongation and resistance after reprocessing. Indeed, in CANs the polymer degradation by chain scission is still possible but the effect is not relevant as the crosslinking between linear PKHB chains does not lead to a decrease in the average molecular weight, which is typically associated with embrittlement. Adhesive properties of vitrimers were also explored and compared to pristine PKHB in lap shear test using aluminum plates. PKHB exhibits moderate adhesive properties, quantified as 3.7 ± 0.6 % strain and 2.5 ± 0.4 MPa stress at failure, which occurs by cohesive-adhesive mixed mode fracture, with traces of adhesive on both surfaces of the substrate. PKHB n% VU vitrimers displayed enhanced properties compared to PKHB (Figure 10a); in particular, in PKHB 5% VU ultimate strain and stress increase to 6.5 ± 0.8 % and 4.8 ± 0.5 MPa respectively. Further increase in crosslink density did not provide further enhancement but rather a decrease in joints performance, with failure by a clear adhesive mechanism (Figure 10b). This may be related to the differences in conformational mobility of the vitrimers during the joining process and suggest slow relaxation of the highly crosslinked vitrimers, requiring higher time/temperature to optimize adhesion onto the substrate.

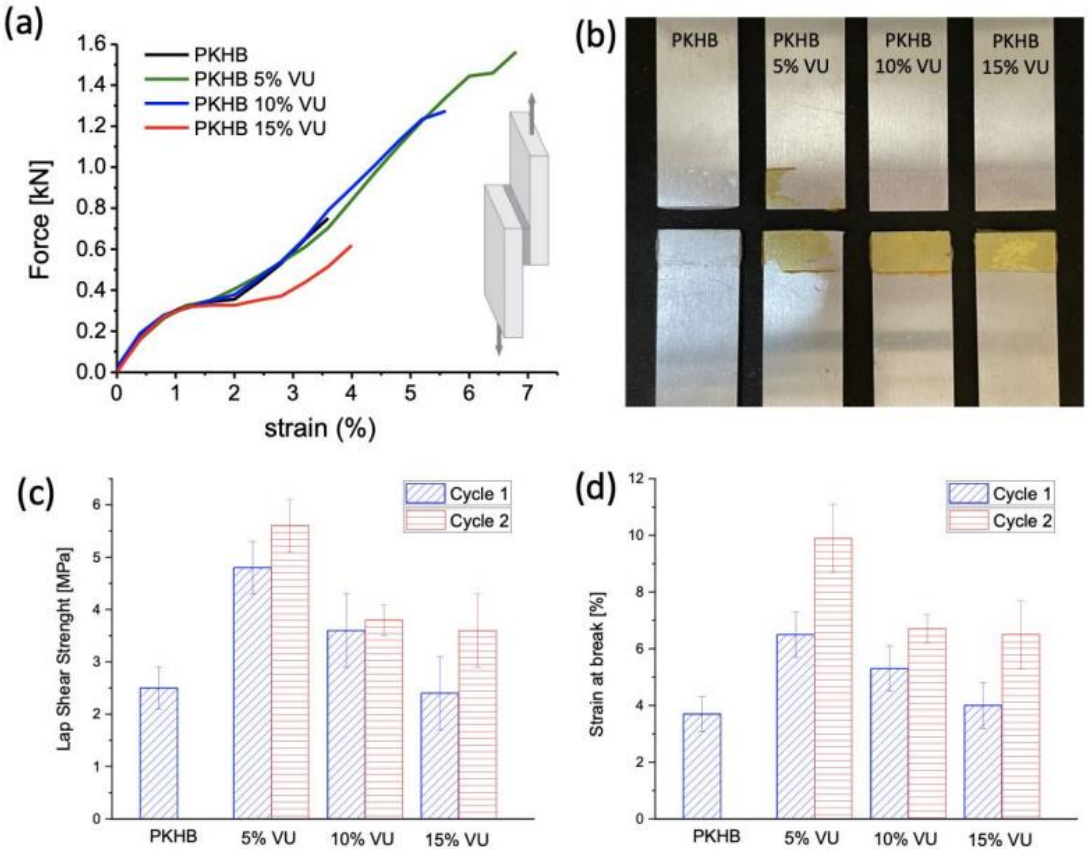

Figure 6 *Force vs strain plots for lap shear test using PKHB or vitrimers as adhesive (a) and pictures of the two plates after joint failure, for each of the adhesives (b). Panels (c) and (d) resume lap shear strength and strain at break for the different adhesives, on first and second joining cycle.*

Instead, the co-existence of different relaxation modes observed at weakly crosslinked PKHB 5%VU appears to couple good substrate adhesion with mechanical resistance, which demonstrates potential for the development of vitrimeric adhesives. Indeed, this class of adhesive allows multiple debonding and re-bonding, based on the retained mechanical properties upon reprocessing demonstrated above. The possibility to re-join the two parts after the lap shear test was explored by simple restacking and pressing in the same conditions as for the initial bonding. While re-joining was not successful with pristine PKHB, all vitrimers joints were qualitatively satisfactory and were tested again in lap shear. Results demonstrated enhancement both in lap shear strength and in strain at break, that are, for all vitrimers, higher compared to the first cycle. For instance, PKHB 5%VU on test #2 showed 9.9 ± 1.2% strain (+52% compared to PKHB) and 5.6 ± 0.5 MPa (+16% compared to PKHB), thus demonstrating the adhesive reversibility (Figure 10c, d). Because industrial application of vitrimers is currently limited by the large use of organic solvents in vitrimers preparation processes, the solvent-free preparation of phenoxy vitrimers was explored.

Compared to vitrimers based on conventional thermoplastic polymers in which melt reactive blending preparation was previously reported, such as polyethylene,[11] PMMA and PS,[22] melt processing of phenoxy resin is significantly more challenging, owing to its relatively high glass transition temperature coupled with adhesive properties onto the metal surfaces in melt mixers. Based on the mechanical and adhesive properties discussed above, PKHB 5% VU was selected for preparation *via* melt reactive blending, exhibiting a strong increase in melt viscosity during mixing (Figure 11), almost up to the limit of the micro compounding system used.

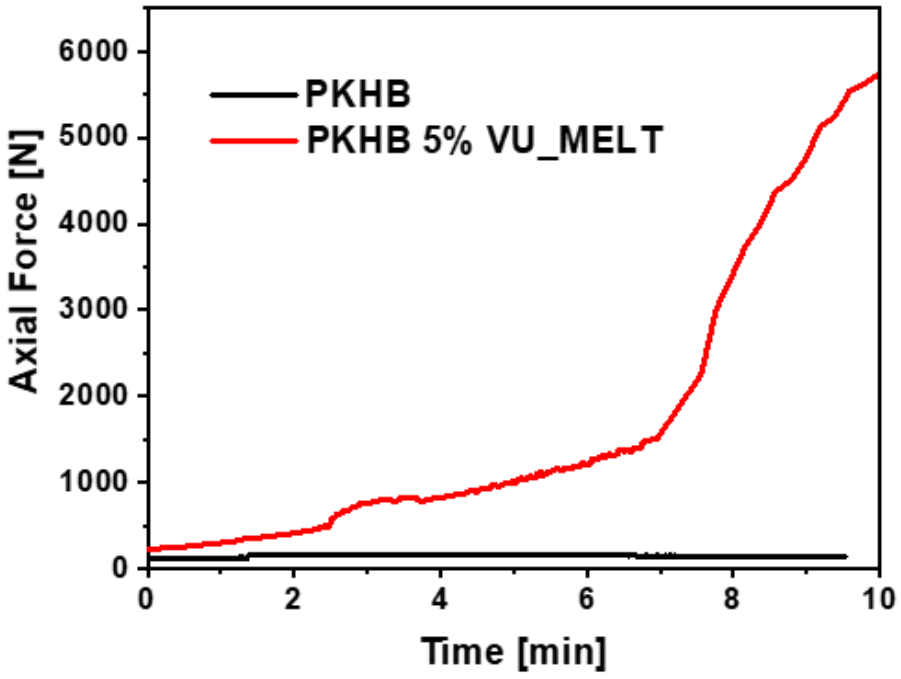

Figure 7 *Axial force plots measured during compounding in mini extruder for PKHB and PKHB 5% VU_MELT.*

The gel fraction of the extruded materials was 89%, which is higher than the corresponding formulation prepared in solvent, confirming the efficiency of melt reactive blending to promote chemical reaction, thank to both high temperature and shear deformation in the melt. PKHB 5% VU_MELT was also compression molded to obtain suitable specimens for DMTA (Figure 12a) and rheological analysis (Figure 12b), which were found fully consistent with the reference formulation *via* the solvent process. Thus, the melt reactive blending is a viable route to obtain phenoxy vitrimers.

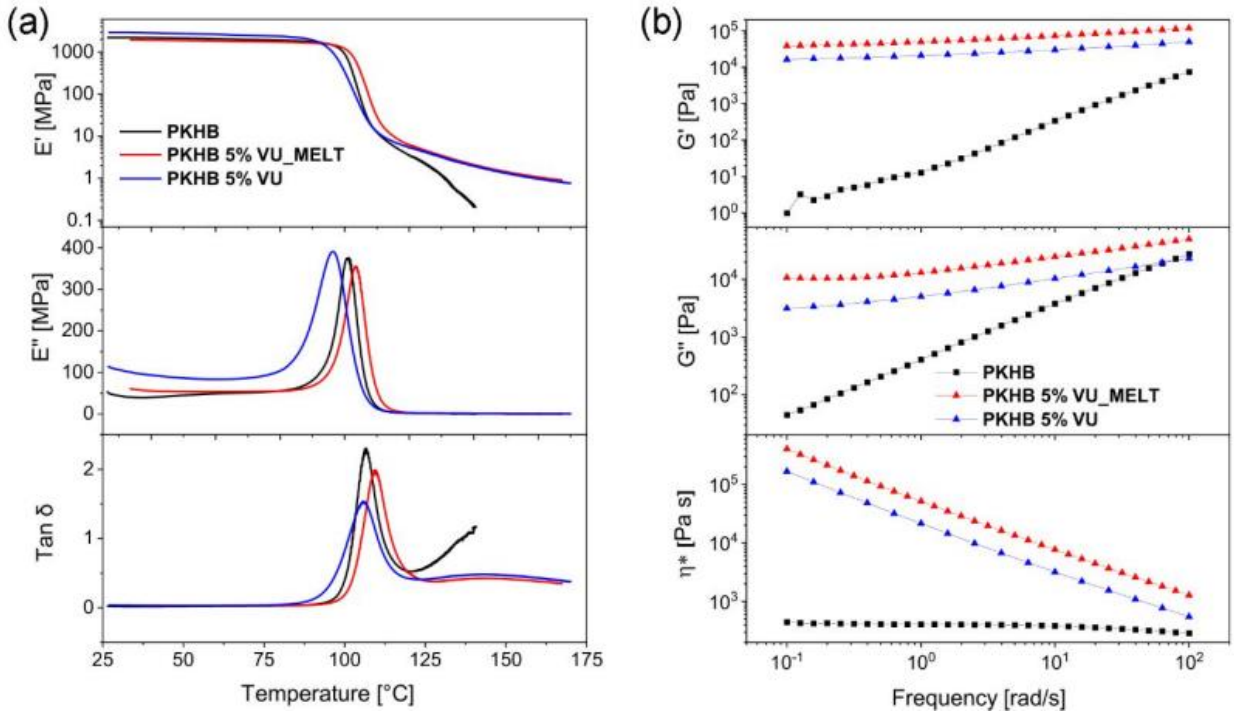

Figure 8 *Comparison between dinamomechanical (a) and rheological (b) properties for PKHB 5% VU prepared via the conventional solvent processing or by melt reactive processing.*

2.3. Conclusions

Linear phenoxy resins were functionalized with acetoacetate groups to introduce reactive moieties for subsequent reaction with a diamine to produce vinylogous urethane exchangeable bonds. This allowed preparing covalent adaptable networks based on a linear equivalent of conventional epoxy, providing epoxy vitrimers, which have been validated for melt processability and recycling. The novel approach demonstrated in this work allows tailoring the crosslinking density, by varying the density of AcAc moieties along the phenoxy resin, yielding tailorable rheological properties. Indeed, full crosslinking of the polymer was obtained at relatively high density of functional groups (e.g. 15% conversion of hydroxyl groups along the phenoxy chains), whereas incomplete crosslinking was observed at low density (e.g. 5% conversion of hydroxyl groups), yielding a rheological behavior intermediate between typical vitrimers and thermoplastic polymers. This is evidenced by the elastic and viscous moduli as a function of deformation frequency at high temperature, as well as the stress relaxation results, suggesting the combination of secondary relaxation modes related to networks strands and dangling chains as well as associative interaction between linear segments, in addition to vinylogous urethane bonds exchange. The adhesive properties were studied in lap shear mode, showing best

performance for PKHB 5% VU, including the possibility to thermally re-join the assembly after its mechanical failure. This is obtained thanks to the rapid relaxation times of this vitrimer, allowing strong adhesion to aluminum (typical of phenoxy resin), together with stiffness reinforcement typical of the crosslinked networks. The preparation of PKHB 5% VU *via* melt reactive blending in a lab-scale micro extruder was also proved to yield consistent thermomechanical and rheological properties, thus demonstrating the production of phenoxy-based vinylogous urethane vitrimers in a solventless process, which opens for an industrially viable upscale of this class of materials, as a potential alternative to conventional epoxy thermosets.

2.4. Experimental section

2.4.1. General procedure for the synthesis of PKHB 5,10,15% VU

8 g of PKHB 5,10,15% AcAc corresponding to ≈27 mmol of each polymer, were dissolved in 40 mL of MEK, then m-xylylendiamine (XYDIA) diluted in 1 mL of MEK was added to the solution in a 0.6 molar ratio with respect to the molar amount of AcAc groups present on PKHB (0.11 mL for 5%, 0.22 mL for 10% and 0.32 mL for 15%). After stirring for 16 h in refluxing MEK, a yellow precipitate was formed. The resulting suspension was treated with 300 mL of methanol, and the resulting precipitate was filtered and dried in vacuum oven at 10^{-2} torr and 60 °C for 24 h.

2.4.2. Preparation of PKHB 5% VU in melt reactive blending

Solventless synthesis was implemented into a co-rotating twin-screw mini-extruder DSM Xplore 15 cm^3 under nitrogen flow, at 240°C, 100 rpm, 10 min. 10.0 g of PKHB-AcAc 5% (1.73 mmol eq. AcAc) were pre-wet with 0.137 mL of xylene diamine (1.04 mmol corresponding to a molar ration AcAc/XYDIA = 0.6), loaded in the chamber at 50 rpm, then increased to 100 rpm for the mixing stage (10 min) and the final extrusion. Vitrimer prepared by melt reactive blending is referred to as PKHB-VU 5%_MELT.

2.4.3. Gel fraction determination

Gel fractions were calculated based on dry residual weight after dissolution in methyl ethyl ketone (MEK) for 24 h. Specimen's pieces were placed in a 10 mL closed vial and heated in MEK at 60°C for 24 h. After Büchner filtration, the samples were dried in vacuum oven at 10^{-2} torr and 100 °C for 24 hours. The gel fraction was determined according to the equation below:

$$Gel\ fraction\ (\%) = \frac{m_{final}}{m_{initial}} \cdot 100$$

2.4.4. Dynamic mechanical analysis (DMTA)

DMTA analyses were carried out on bars with a cross-section of around 6 x 1 mm^2, 30 mm length, cut from compression-molded plates, tested in tensile mode on a Q800 equipment (TA Instruments). Temperature scan was from room temperature to 170°C, at 2°C/min heating rate and 1 Hz frequency in strain-controlled mode, deformation amplitude at 0.05% and 0.01 N preload. All samples were conditioned at 23°C and 50% of relative humidity for at least 48 h before analyses.

2.4.5. Rheology

Rheological properties were investigated using an ARES rheometer (TA Instruments) operated with a 25 mm parallel plate geometry and 1 mm thickness samples. Dynamic frequency sweep tests were carried out to determine G', G'' and complex viscosity (η*) between 0.1 and 100 rad/s at 1% strain (linear viscoelasticity) at a constant temperature of 200°C. Isothermal relaxation tests were also carried out at 5% strain, till below 30% of the initial stress was reached. Stress G(t) is reported normalized on G_0, i.e. the stress recorded at t = 1 s to get rid of instrumental transient at the start for relaxation test.[11]

2.4.6. Mechanical properties

Tensile tests were done on 60 x 10 mm^2 compression molded films, thickness in the range of 150 to 200 µm, on an Instron 5966 machine equipped with a 50 N loading cell and flat faces pneumatic clamps, gauge length of 30 mm. Strain rate was 1 mm/min up to 0.3% strain and then 2 mm/min to break. The samples were conditioned at 23°C and 50% of relative humidity for at least 48 h before analyses. Tests carried out on films prepared from as-obtainment vitrimers are referred to as cycle 1. After testing, broken specimens were

recovered and reprocessed by compression molding into new films in the same conditions and tested again, with results referred to as cycle 2. Further reprocessing with the same procedure provided tensile results referred to as cycle 3.

2.4.7. Adhesion tests

Single lap shear adhesion tests were carried out on the same machine, on samples prepared according to ISO 4587, using 1.5 mm thick aluminum plates pre-cleaned with ethanol. Films of 200 µm were placed between Al plates, preheated for 3 min and hot pressed under 1 ton for 5 min at 240°C for vitrimers and 170°C for pristine PKHB, using a lab made support to hold metal plates in proper position during compression.

2.5. References

(1) https://eur-lex.europa.eu/resource.html?uri=cellar:8a8ef5e8-99a0-11e5-b3b7-01aa75ed71a1.0012.02/DOC_1&format=PDF and https://ec.europa.eu/environment/circular-economy

(2) D. Montarnal, M. Capelot, F. Tournilhac, L. Leibler, S*cience* **2011**, *334*, 965-968.

(3) W. Denissen, J. M. Winne, F. E. Du Prez, *Chem. Sci.* **2016**, *7*, 30-38.

(4) M. Capelot, D. Montarnal, F. Tournilhac; L. Leibler, *J. Am. Chem. Soc.* **2012**, *134*, 7664-7667.

(5) A. Ruiz de Luzuriaga, R. Martin, N. Markaide, A. Rekondo, G. Cabañero, J. Rodríguez, I. Odriozola, *Mater. Horiz.* **2016**, *3*, 241–247.

(6) S. Zhao, M. M. Abu-Omar, *Macromolecules* **2018**, *51*, 9816−9824.

(7) H. Memon, H. Liu, M. A. Rashid, L. Chen, Q. Jiang, L. Zhang, Y. Wei, W. Liu, Y. Qiu, *Macromolecules* **2020**, *53*, 621-630.

(8) Y. Spiesschaert, M. Guerre, I. De Baere, W. Van Paepegem, J. M. Winne, F. E. Du Prez, *Macromolecules* **2020**, *53*, 2485−2495.

(9) T. Debsharma, V. Amfilochiou, A. A. Wróblewska, I. De Baere, W. Van Paepegem, F. E. Du Prez, *J. Am. Chem. Soc.* **2022**, *144*, 12280-12289.

(10) W. Denissen, G. Rivero, R. Nicolaÿ, L. Leibler, J. M. Winne F. E. Du Prez, *Adv. Funct. Mater.* **2015**, *25*, 2451-2457.

(11) J. Tellers, R. Pinalli, M. Soliman, J. Vachon, E. Dalcanale, *Polym. Chem.* **2019**, *10*, 5534-5542.

(12) M. Capelot, M. M. Unterlass, F. Tournilhac, L. Leibler, *ACS Macro Lett.* **2012**, *1*, 789-792.

(13) S. Wu, Q. Chen, *Macromolecules* **2022**, *55*, 697-714.

(14) L. Porath, J. Huang, N. Ramlawi, M. Derkaloustian, R. H. Ewoldt, C. M. Evans, *Macromolecules* **2022**, *55*, 4450-4458.

(15) A. M. Hubbard, Y. Ren, D. Konkolewicz, A. Sarvestani, A.; C. R. Picu, G. S. Kedziora, A. Roy, V. Varshney, D. Nepal, *ACS Appl. Polym. Mater.* **2021**, *3*, 1756-1766.

(16) D. J. Fortman, J. P. Brutman, C. J. Cramer, M. A. Hillmyer, W. R. Dichtel, *J. Am. Chem. Soc.* **2015**, *137*, 14019-14022.

(17) Y. Spiesschaert, C. Taplan, L. Stricker, M. Guerre, J. M. Winne, F. E. Du Prez, *Polym. Chem.* **2020**, *11*, 5377-5385.

(18) F. Snijkers, R. Pasquino, A. Maffezzoli, *Soft Matter*. **2017**, *13*, 258-268.

(19) J. P. Brutman, R. A. Delgado, M. A. Hillmyer, *ACS Macro Lett.* **2014**, *3*, 607-610.

(20) Y. Nishimura, J. Chung, H. Muradyan, Z. Guan, *J. Am. Chem. Soc.* **2017**, *139*, 14881-14884.

(21) B. M. El-Zaatari, J. S. A. Ishibashi, J. A. Kalow, *Polym. Chem.* **2020**, *11*, 5339-5345.

(22) M. Röttger, T. Domenech, R. van der Weegen, A. Breuillac, R. Nicolaÿ, L. Leibler, *Science* **2017**, *356*, 62-65.

Chapter 3

Phenoxy Resins as Adhesion Promoters for Carbon Fiber Reinforced Epoxy Resin Matrix Composites*

Mechanical tests were carried out by Dallara Automobili (Varano de' Melegari).

3.1. Introduction

3.1.1. Composite materials

Composite materials are heterogeneous materials consisting of two or more phases, whose combination give arise to enhanced mechanical properties due to their synergistic action. The typical constitution of composite materials is given by reinforcing fibers dispersed in a matrix resin (Figure 1).[1]

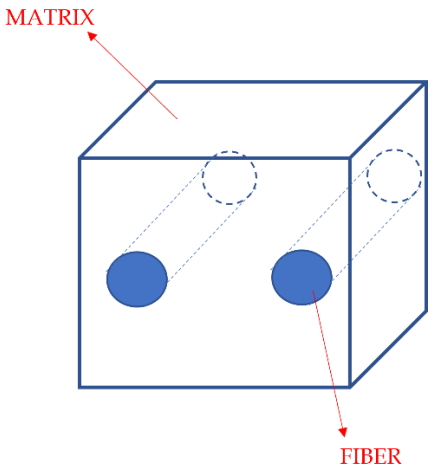

Figure 1 *Schematic representation of a composite material. The fibers are embedded into the polymeric matrix.*

The fibers can be continuous, long, or short and they provide strength and stiffness, especially along the axis of the fibers. Conversely, the matrix is based either on thermoplastic or thermosets resins, whose task is to endow rigidity and environmental resistance.

Nowadays, composites are the materials of choice for all those applications where the combination of high mechanical strength, lightweight and flexible manufacturing are fundamental requirements. In fact, their applications range from automotive, aircraft to military defense, ship, and aerospace industries.[2] One of the most important examples are carbon fiber reinforced epoxy laminates, in which several stacked carbon fiber plies are embedded and held together by an epoxy resin-based matrix.[3] The outstanding lightweight of carbon fibers, combined with the excellent mechanical, chemical and thermal resistance of the epoxy matrix give arise to a structural material that is resistant to high stresses.[1]

3.1.2. Prepregs

Prepregs are one of the most important composite materials used in the manufacture of racing cars. They are, in fact, the materials from which the car bodies are constructed. Prepregs are resin-impregnated fibers that are sold commercially as fabrics or flat mats. The resin can be either thermoplastic or a thermoset polymer (the most used and traded). These materials are created by impregnating the fibers with the resin either through a hot melt process or through solution treatment. The former method involves applying the matrix in its viscous form, avoiding the use of a solvent, but with limited fiber wetting due to the matrix's high viscosity. Conversely, the solvent impregnation entails dissolving the resin in a suitable solvent, resulting in a low-viscosity liquid into which fibers are dipped. The main drawback of this approach is the disposal of the solvent.

The fibers are generally oriented parallel to the main axes of woven, providing the ability to tailor the composite properties in the desired direction, which is especially useful to make highly contoured parts. The drape and tack of prepregs must be evaluated based on the application requirements. The drape is the ability to shape on contoured surfaces, which thermoset prepregs easily achieve. Instead, the tackiness of uncured prepregs should be significant to favor laying and processing. Thermoset prepregs have a limited shelf life and must be stored under refrigeration, preventing the complete curing, and slowing down the kinetic of reaction.[2] In fact, the matrix is partially cured to allow easy handling. Several additives (e.g., flame retardants, catalysts, and inhibitors) are used to endow specific end-use properties, processing and handling needs. Prepregs are commonly used in processes such as hand or automatic lay-up, roll wrapping, and compression molding. After being laid on an object tool, prepregs are cured in the presence of pressure and temperature to produce the final product. [1]

3.1.3. Interlaminar adhesion in prepregs

The most typical failure for multilayer objects is known as interlaminar delamination. Delamination provokes a sudden and drastic downgrading of the mechanical properties, therefore the enhancement of the interlaminar adhesion becomes a crucial factor. The entity of the interlaminar adhesion can be evaluated by a specific parameter, the Interlaminar

Shear Stress (ILSS),[4] whose decreasing affects the load-bearing capacity and the service life of the object. Broadly speaking, strong adhesion could be reached through the synergy of three different factors: (i) the nature of involved chemical bonds, (ii) the topology of connection between polymeric chains and (iii) the ability to dissipate mechanical stresses.[5] The employment of the connection topology between polymeric networks is more promising than using nanofibers or nanoparticles, which are other options that have been suggested in the literature to improve the delamination toughness.[1]

Each polymer has a typical molecular weight above which it starts to entangle. Entanglement can occur as physical restrictions between segments of the polymer chains, hence chains are stuck because they are no longer free to move past each other (Figure 2).[6]

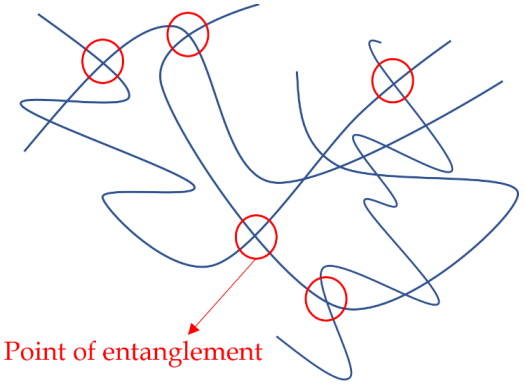

Figure 2 *Model of entanglement network in a high MW polymer.*

A similar behavior can be observed between two different high MW thermoplastics, generating a heterogeneous entanglement, reached annealing the polymers above T_g and cooling right after. Indeed, the two thermoplastics become glassy polymers again, and the penetrating polymers are locked inside. (Figure 3).

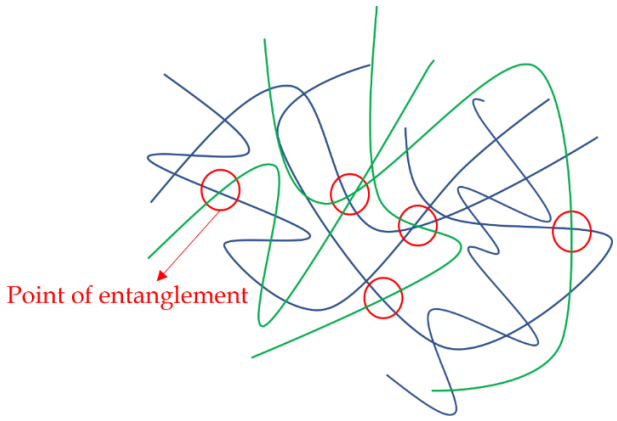

Figure 3 *Physical entanglement between two different polymers.*

A different topology is also widely exploited to enhance the adhesion between two adherends: the stitch-stitch topology. A polymer diffuses into the polymeric networks of the two adherends, crosslinking in topological entanglement with both pre-existing polymer networks. Therefore, the third polymer network acts like a molecular suture, stitching the two polymer networks together. To separate them, at least one of the three polymer networks must be broken (Figure 4).[5]

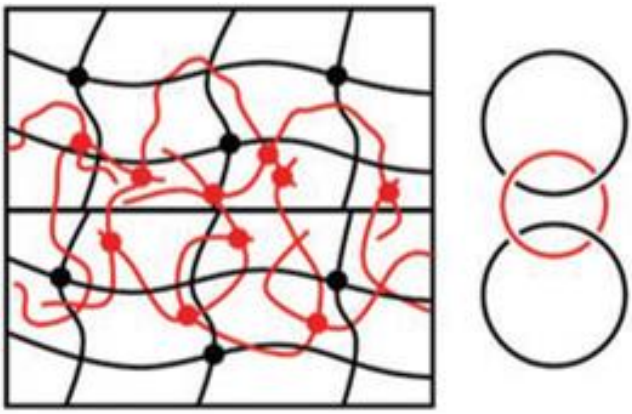

Figure 4 *Schematic representation of a stitch-stitch topology entanglement.*[5]

Here we report the use of phenoxy vitrimers as adhesive between plies to reduce delamination through topological entanglement. Phenoxy resins are the thermoplastic version of epoxy resins (Scheme 1).

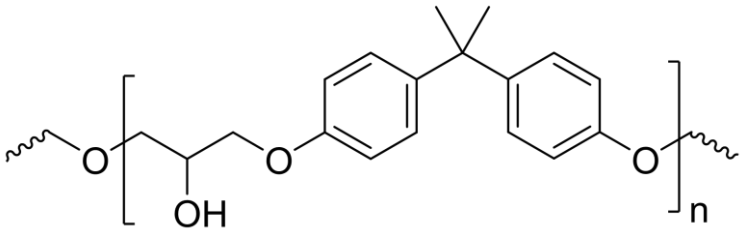

Scheme 1 *Chemical structure of a phenoxy resin.*

Their chemical structure makes them compatible with epoxy resins, ensuring mutual diffusion of the relevant polymeric chains, resulting in an extended physical entanglement with the epoxy matrix. Furthermore, the possible occurrence of a stitch-stitch entanglement was investigated, introducing properly functionalized phenoxy resins with acetoacetate groups capable of reacting with the crosslinker of the formulation. This latter approach is aimed to investigate the possible occurrence of stitch-stitch entanglement between the vitrimeric network and the epoxy matrix.

We proposed the application of two commercial phenoxy resins with different average molecular weights (PKHB and PKHP) and their functionalized derivatives with acetoacetate groups (PKHP-AcAc 20% and PKHB-AcAc 20%) to a prepreg used to create the body of racing cars. These polymeric adhesion promoters were applied as thin films or dissolved in a suitable solvent.

The mechanical characterization of bonded joints in single lap shear configuration and in the fracture toughness configuration were evaluated.

3.2. Results and discussion

3.2.1. Adhesion promoters synthesis

We firstly functionalized the phenoxy resins, PKHB and PKHP, with acetoacetate (AcAc) units (Scheme 2). The synthesis was performed in refluxing methyl ethyl ketone (MEK) using *tert*-butoxy acetoacetate (*t*-BuAcAc) and the degree of functionalization was assessed *via* NMR, by integrating the peak relative to the methyne α to AcAc moiety at 5.54 ppm (see Chapter 2, Figure 1). The chosen percentage of functionalized hydroxyl groups was 20%. The purpose of introducing the PKHP-AcAc 20% into prepregs is to trigger the formation of a vitrimeric network *in situ*, which is generated by the reaction of the acetoacetates moieties and the primary amines of the crosslinker present in the prepreg.

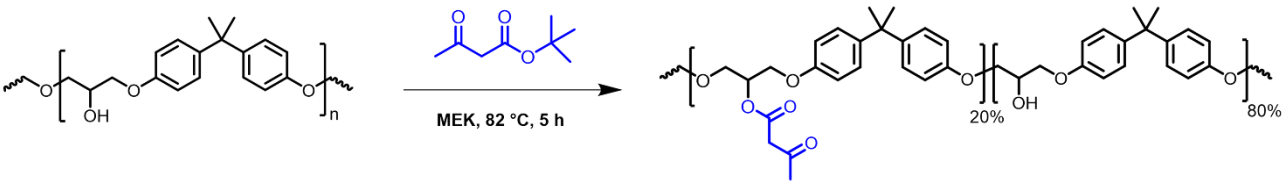

Scheme 2 *Synthetic scheme for the preparation of PKHB/PKHP-AcAc 20%.*

3.2.2. DT120 and ER450 as tested prepregs

DT120 and ER450 were identified as the commercial prepreg on which evaluate the joint performances in Single Lap Shear (SLS) test and fracture toughness.

DT120 resin is a highly toughened thermosetting epoxy resin with a versatile curing range from 80°C to 135°C. DT120 prepregs are mainly suitable for processing by autoclave vacuum bag curing. DT120 is appropriate for structural applications requiring high impact

performance and energy absorption. This matrix has a significantly lower T_g (120 °C) than ER450 and the viscosity minimum is equal to 10 Pa·s, reached at 120 °C.

The latent curing agent in this matrix is dicyandiamide (DICY), extensively employed for the curing of epoxy resins in prepregs.[7-9] DICY is a guanidine nitrile derivative, with a cyano group attached. It exists in two distinct tautomeric forms that differ in terms of the protonation and the bonding of the nitrogen to which the cyano group is attached (Scheme 3).[10]

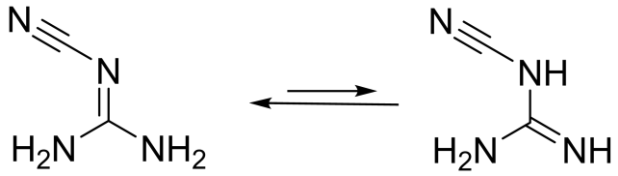

Scheme 3 *Chemical structure of the two possible tautomers of DICY.*

The tautomeric character of DICY regulates the reactivity of the two primary amines, lowering it and prohibiting an undesirable and premature curing prior to lay-up and the subsequent autoclave treatment. Furthermore, the presence of an electron withdrawing unit, such as cyano moiety, contributes to DICY's decreased reactivity.

It is a white powder with a poor solubility in epoxy resin at room temperature. Theoretically, DICY-based latent curing systems cures epoxy resins at temperatures higher than 180 °C, near to the DICY's melting point.[11,12] That curing high temperature is not economically sustainable and, thus the introduction of N-aryl-N',N'-dialkyl ureas (e.g. N,N-dimethyl-N'-phenylurea (fenuron), N-(4-chloro-phenyl)-N',N'-dimethylurea (monouron)), acting as accelerators,[13-18] become essential to enhance the reactivity of the system and reduce the curing temperature (Scheme 4).

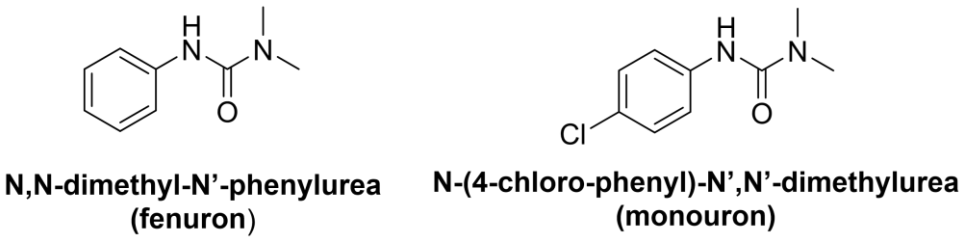

Scheme 4 *Chemical structures of the two most used accelerators in prepregs.*

In order to investigate the reactivity of DICY towards acetoacetate units, a model reaction was carried out between PKHP-AcAc 20% and DICY (Scheme 5).

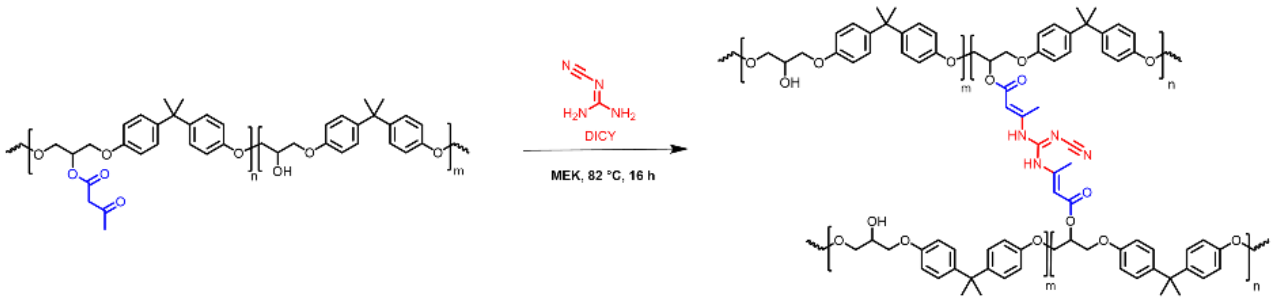

Scheme 5 *Synthesis of the vinylogous urethane crosslinked with DICY.*

To evaluate the crosslinked character of the obtained product, the sample was kept in MEK at 60 °C for 24 hours. The remaining insoluble fractions after solvent removal and vacuum oven drying was 73%. By comparison, pristine PKHP resulted completely soluble in MEK at room temperature.

ER450 is a toughened epoxy prepreg that has been developed for a variety of structural applications. It has a relatively high T_g (210 °C) and a flexible processing cycle with cure temperatures ranging from 80°C to 180°C in autoclave. It is a very viscous resin with a minimum viscosity equal to 1000 Pa·s (at 125 °C), which hinders the easy diffusion of adhesion promoters during curing.

Conversely, ER450 contains a different crosslinker,[19] that is 4,4′-diaminodiphenyl sulfone (Scheme 6).

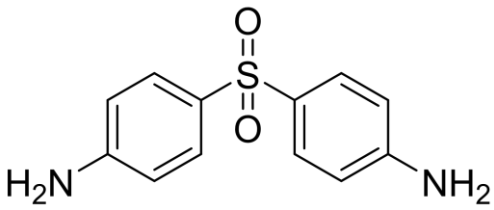

Scheme 6 *Chemical structure of 4,4'-diaminodiphenyl sulfone.*

In order to investigate the reactivity of 4,4′-diaminodiphenyl sulfone towards acetoacetate units, a model reaction was carried out with PKHP-AcAc 20% (Scheme 7).

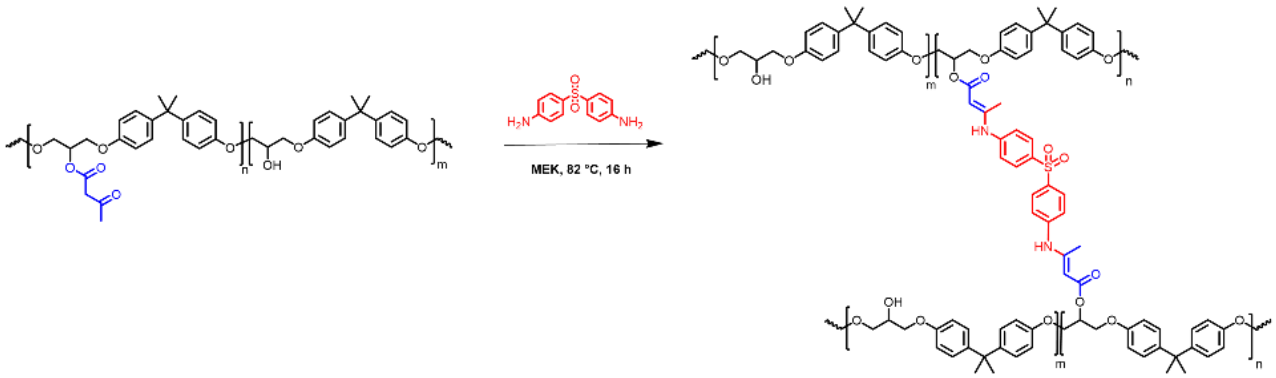

Scheme 7 *Synthesis of the crosslinked vinylogous urethane that it should be formed in the reaction between PKHP-AcAc 20% and with 4,4'-diaminodiphenyl sulfone.*

A gel fraction was conducted after precipitation in methanol to evaluate the crosslinked fraction. The product was kept in MEK at 60 °C. After few hours, the solid was completely dissolved, thus demonstrating that the crosslink reaction did not occur.

The reduced nucleophilic character of the aromatic hardener is the origin of the limited reactivity toward AcAc units, which excludes the use of the vinylogous urethane reaction in this case.

Therefore, we decided to set aside ER450 from the following explained tests and kept our focus on DT120.

3.2.3. Single Lap Shear tests

Mechanical characterization of bonded joints in single lap shear configuration (ASTM D 1002) was carried out. Each of the two joints was formed by stacking 8 plies of prepreg (Figure 5, Right) and, the promoters were manually applied in the 30 mm x 200 mm joint area (Figure 5, Left).

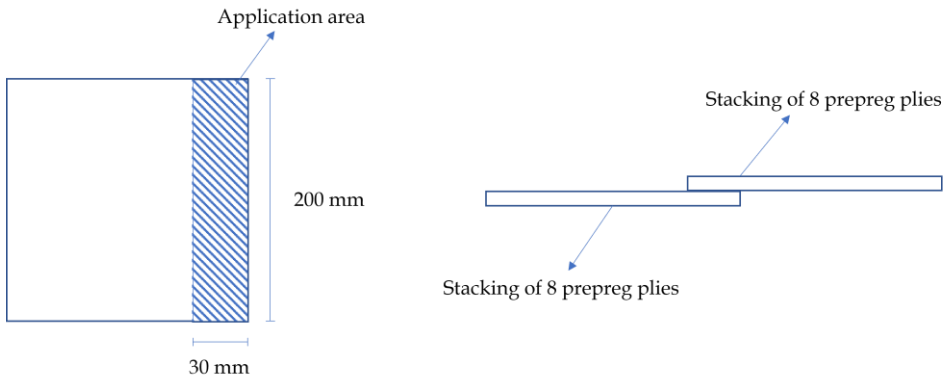

Figure 5 *Frontal view of one of the two adherents composed by 8 stacked prepreg plies (Left); side view of the two jointed adherents, formed by eight stacked plies (Right).*

The specimens were vacuum bagged[20] to remove the air before being placed in an autoclave for 6 hours at 135 °C under a pressure of 6 bar. Following curing, each panel was cut into six specimens. The single lap shear test consists in applying an increasing stress until the specimen, secured by two clamps, breaks.

The campaign started with testing PKHP-AcAc 20% as solid adhesion promoter for DT120 (Figure 6).

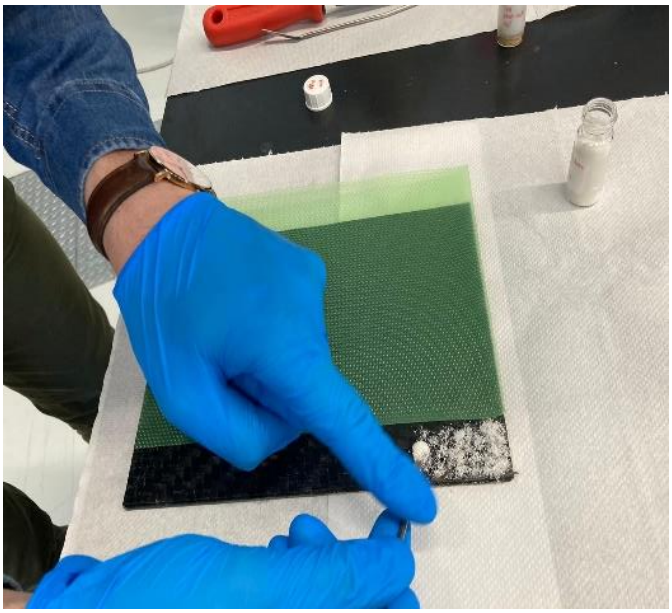

Figure 6 *Application of the adhesion promoter in the joint area of prepreg during the preparation of specimens.*

This polymer dramatically reduced the shear properties of the joint specimens with respect to the reference (specimens with only the cured commercial prepreg). The poor observed joint performances can be explained by a not uniform dispersion of the promoter in the joint area, but also by the not optimized quantity of added promoter. In fact, approximately 1 g of promoter were added. Considering that there are 253.33 g of epoxy resin per m^2, the amount of added promoter corresponded to the 66% of the epoxy resin total weight in the joint area, which is an excessive amount that can reduce the mechanical properties of the object.

Therefore, a different approach was undertaken. To overcome the issue of the not uniform application of the promoters, they were previously dissolved in MEK and applied as solution. Furthermore, the quantity of added promoter was the 15% of the epoxy resin weight contained in the prepreg joint area. This value was thought to be sufficient to have

a proper amount of promoter, but not so high as to negatively impact the object's mechanical properties.

Specimens containing the commercial non-functionalized phenoxy resin PKHP (average molecular weight 52000 Da) were also tested to assess if the addition of a phenoxy thermoplastic, capable of causing physical entanglement with the epoxy matrix network, was enough to improve joint properties. Two other adhesion promoters were tested: they were identical to the previously described, but they differ for the epoxy resin on which they are based. In fact, PKHB, a lower average molecular weight (32000 Da instead of 52000 Da for PKHP) and its corresponding AcAc-20% functionalized polymer were tested in SLS configuration. It was assumed that for a lighter phenoxy resin would be easier for it to interpenetrate in the epoxy matrix networks during curing, resulting in a greater entanglement.

Therefore, four different types of specimens were prepared for DT120:

- PKHP-containing specimens;
- PKHP-AcAc 20% containing specimens;
- PKHB-containing specimens;
- PKHP-AcAc 20% specimens

The promoters were applied as a MEK solution to the joint area (30 mm x 200 mm) by the means of a brush (Figure 7, Left).

Figure 7 *Application of dissolved adhesion promoters in MEK (Left) and the resulting specimens after curing (Right).*

Following application on both sides of the joint area, the two adherends were left exposed to allow the solvent to evaporate. Following the overlapping of the two adherends, a vacuum bag phase was performed followed by the same curing described above (6 hours at 135 °C under a pressure of 6 bar). The obtained specimens, after cutting by waterjet, are reported in Figure 7, Right.

The mechanical tests results (ASTM D 1002) are reported in the following histogram (Figure 8):

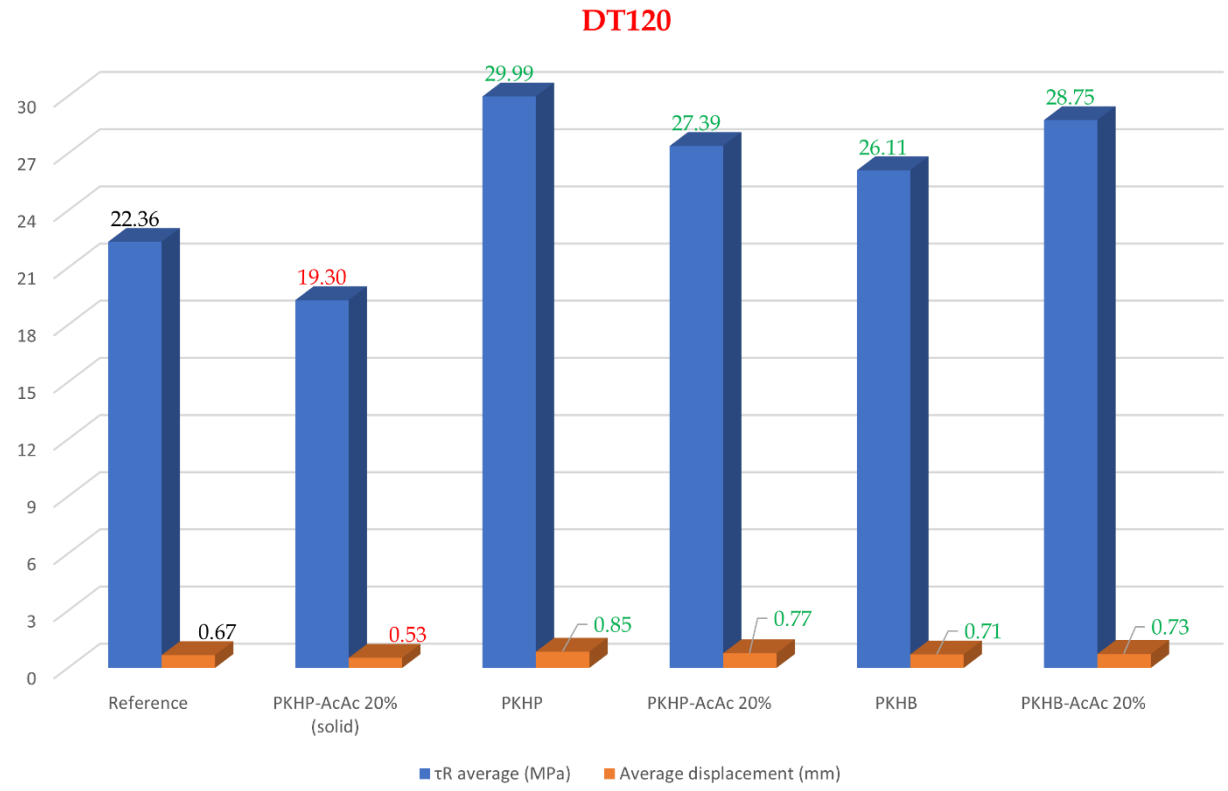

Figure 8 *Results of SLS campaign on DT120. Red data labels stand for worse values respect with the reference. Green data labels stand for better values respect with the reference.*

In conclusion, a significant improvement of the shear properties was observed for all promoters applied as solution. The best result was obtained upon addition of PKHP (+34.0%), demonstrating that the main contribution to the joint performances enhancement is due to the physical entanglement between the phenoxy resin and the epoxy matrix, rather than the formation *in situ* of a vitrimeric network able to give topological entanglement with the matrix.

3.2.4. Fracture toughness test

Fracture toughness tests are typically performed to assess a material's resistance to failure by cracking. The key point of this test is to purposely generate a crack and then calculating the energy needed to propagate it by 1 mm.

As mentioned before, one of the most common failure for composite materials is delamination. It can occur in three different modes, reported in Figure 9.

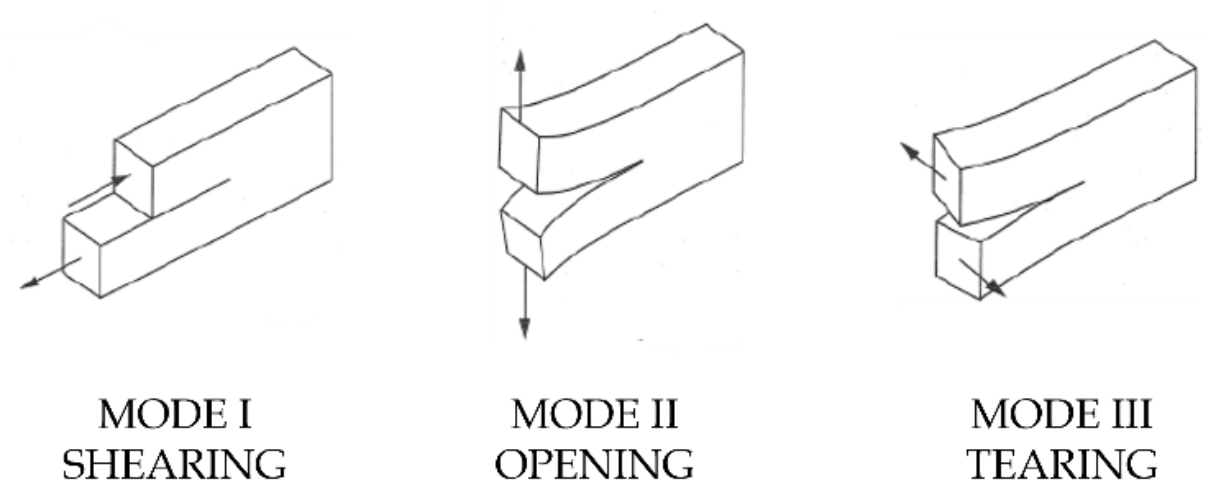

Figure 9 *Possible delamination modes in composite materials.*

We investigated how our adhesion promoters affected the joint performances to prevent mode I and mode II delamination, that are shearing and opening delamination.

G_{1c} and G_{2c}, which represent the force required to propagate the crack for the shearing and the opening, respectively, are the two crucial parameters to be taken into account.

PKHP and PKHB-AcAc 20%, the two adhesion promoters that performed best in the single lap shear configuration, were tested in fracture toughness configuration.

The samples were prepared in the same way followed for SLS tests: adhesion promoters were dissolved in MEK and then applied on the uncured plies on a joint area of 174 mm x 250 mm. The samples underwent a vacuum bag phase before being autoclave-cured for 90 minutes at 135 °C and 6 bar of pressure.

The test for fracture toughness in mode I consists in the setup reported in Figure 10.

Figure 10 *Example of specimen used in fracture toughness test (Left) and the setup for the test (Right).*

To better visualize the configuration of the specimens and the forces playing in this test, a schematic representation is reported in Figure 11.

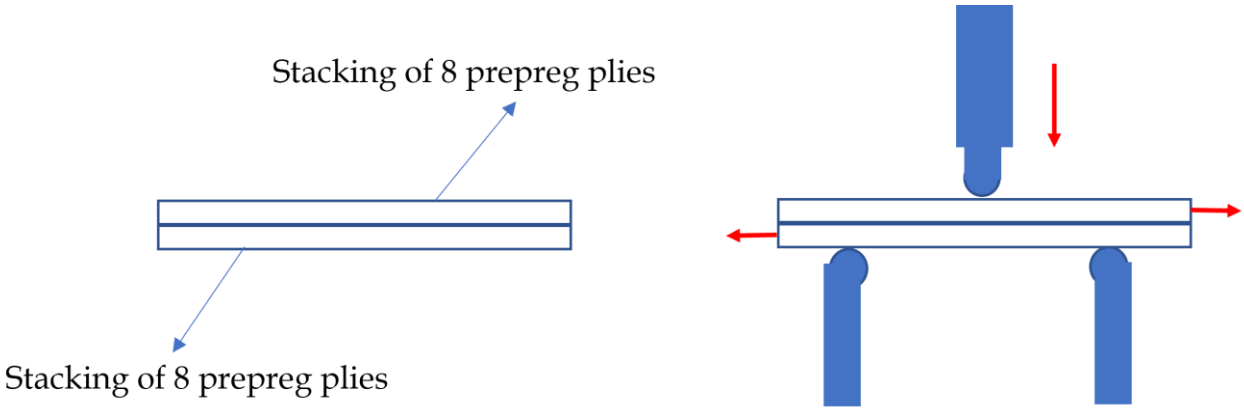

Figure 11 *Side view of the two adherents composed by 8 stacked prepreg plies for mode I fracture toughness configuration (Left); a crosshead pushes down the specimens with an increasing force (Right).*

The obtained results are reported in Figure 12.

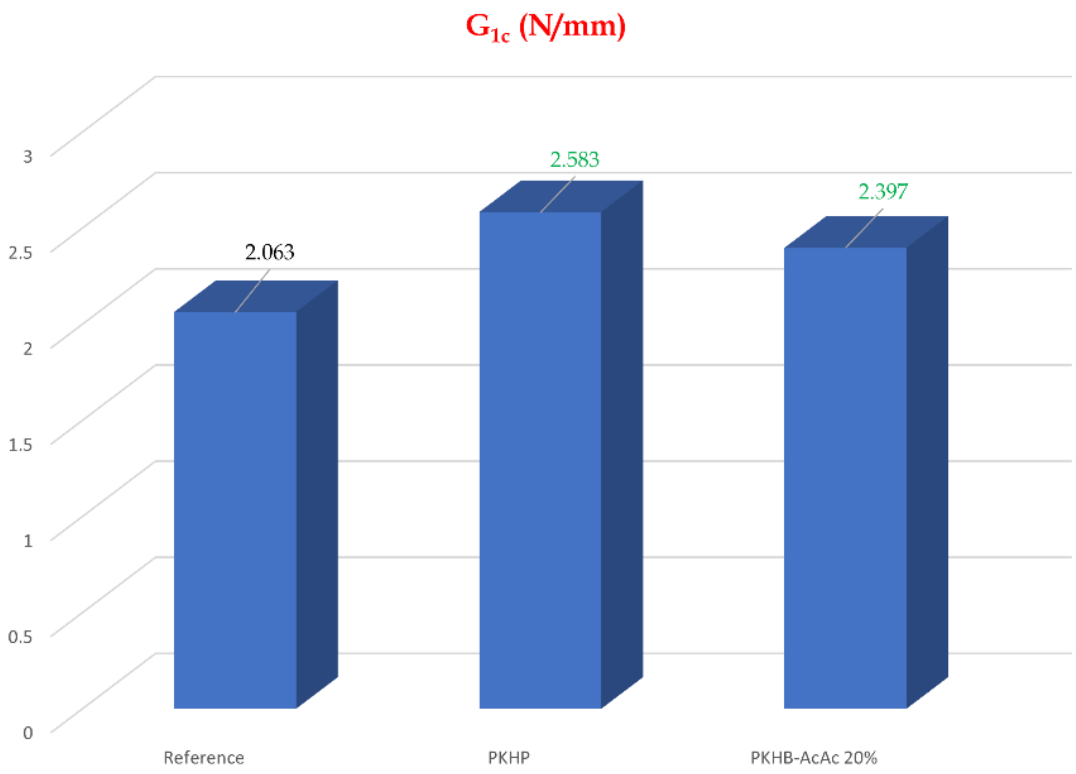

Figure 12 *Results of fracture toughness mode I campaign on DT120.*

Both adhesion promoters demonstrated a considerable increased in mode I (G_{1c} was higher than the reference), although PKHP (25.2%) considerably improved fracture toughness compared to PKHB-AcAc 20% (16.2%).

Analogously, other specimens of the same promoters were prepared to test their behavior in fracture toughness mode II.

The setup of the test for fracture toughness in mode II is quite different from the mode I's one and it is reported in Figure 13.

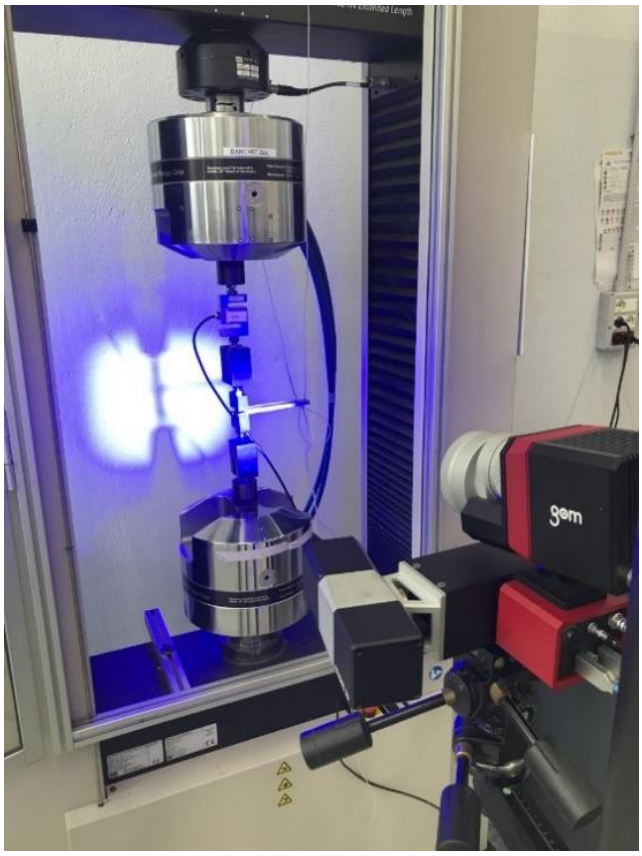

Figure 13 *Setup for the fracture toughness mode II test. The camera records enhanced images of the specimen to detect the front of the propagating crack.*

To better visualize the configuration of the specimens and the forces playing in this test, a schematic representation is reported in Figure 14.

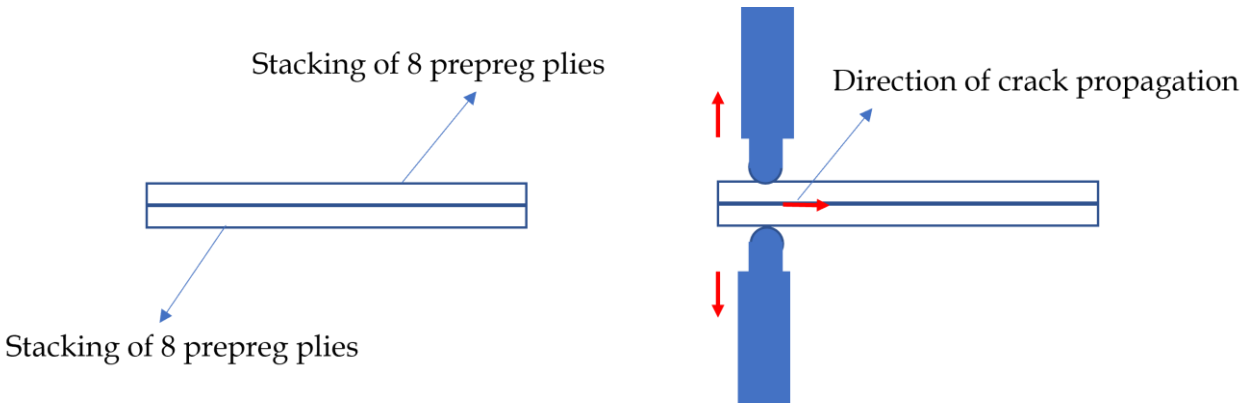

Figure 19 *Side view of the two adherents composed by 8 stacked prepreg plies for mode II fracture toughness configuration (Left); two clamps exert forces in opposite directions to open specimen at the interface of the two adherents (Right).*

The obtained results are reported in Figure 15.

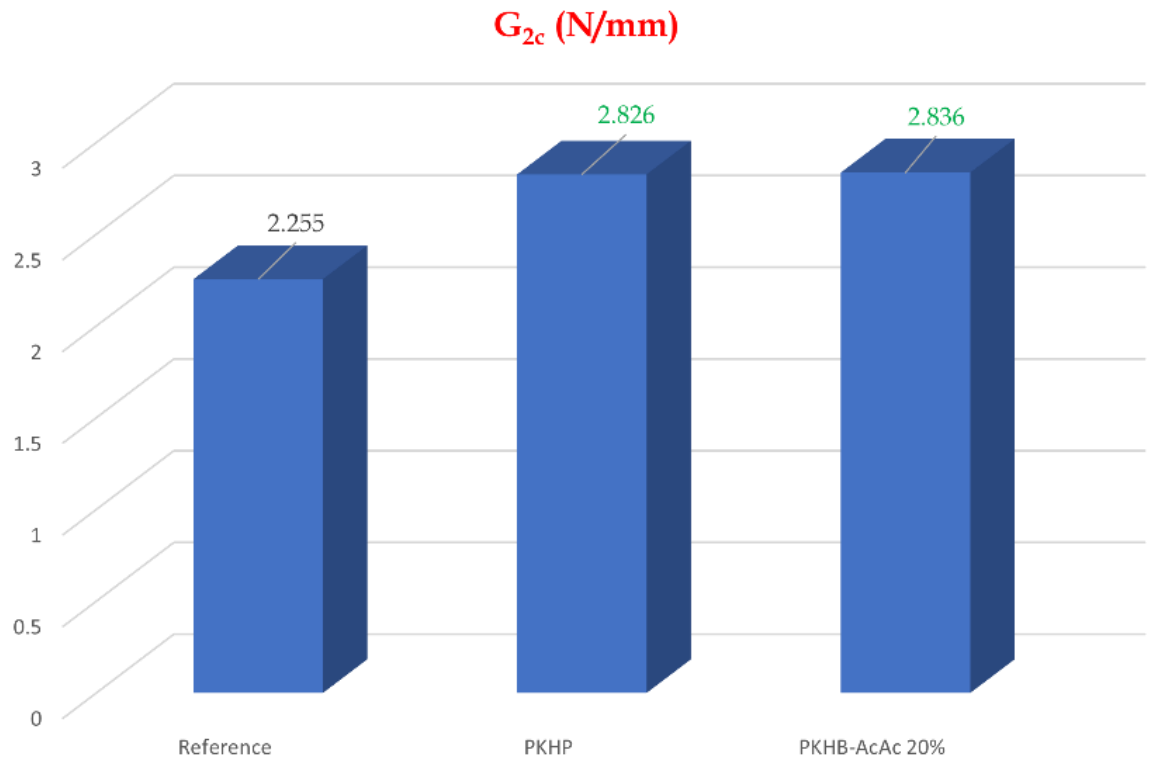

Figure 15 *Results of fracture toughness mode II campaign on DT120.*

Both PKHP (+25.3%) and PKHB-AcAc 20% (+25.8%) exhibit comparable fracture toughness in mode II, demonstrating that the inclusion of a thermoplastic polymer that is highly miscible with the epoxy matrix is the primary cause of the improvement in joint performances. The fact that the improvement was similar shows that the increase in joint performance was caused by the phenoxy resin's physical entanglement rather than the formation *in situ* of a vitrimeric network (topological entanglement).

The improvement in joint performance is sufficient to justify the application of dissolved promoters in critical zones of industrial products.

3.2.5. Mechanical characterization of adhesion promoters as thin films

As previously described, the introduction of phenoxy resin-based adhesion promoters revealed two major drawbacks: first, the use of a solvent implies its evaporation prior to the vacuum bag phase. Solvent residues can be detrimental for the mechanical properties of the object. Additionally, the adhesion promoter's application was not suitable for large scale industrial use, but only for a specialized limited production. Therefore, the focus of the following described campaign was to find a more practical method of applying the

adhesion promoters. Films of two different thickness (100 and 200 µm) were produced with the best candidates emerged from the previous campaigns and applied between the two adherents of DT120 formulation to test their joint performances in single lap shear test configuration. Adhesion promoters were applied between the adherents before the curing cycle.

The obtained results are reported in Figure 16.

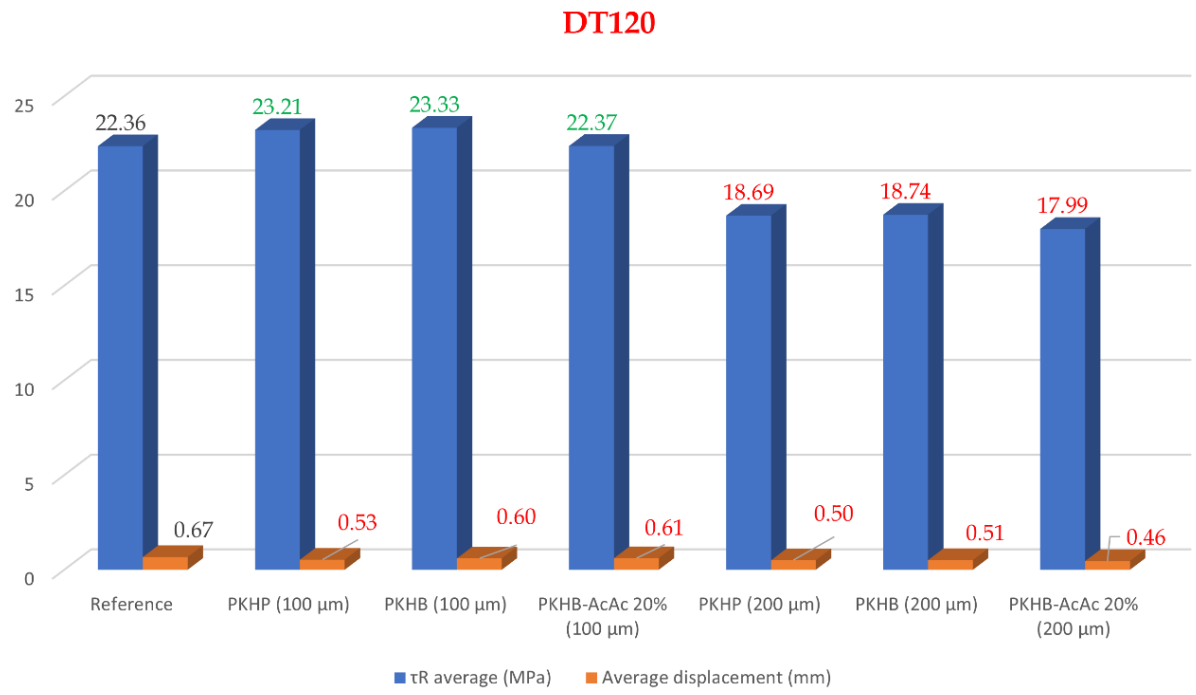

Figure 16 *Results of SLS campaign on DT120 with adhesion promoters as thin films. Red data labels stand for worse values respect with the reference. Green data labels stand for better values respect with the reference.*

Mechanical properties after the addition of promoters in the form of 100 µm films were comparable to those of the reference material. Instead, the mechanical properties after the addition of promoters in the form of 200 µm films were dramatically decreased with respect to those of the reference material.

The explanation for the worsening of the mechanical properties could be ascribable to a limited entanglement of polymeric chains because the promoters were introduced as solid material, hence the curing was not sufficient to allow their permeation in the epoxy matrix. Microscopy images provides evidence for this limited permeation (Figure 17).

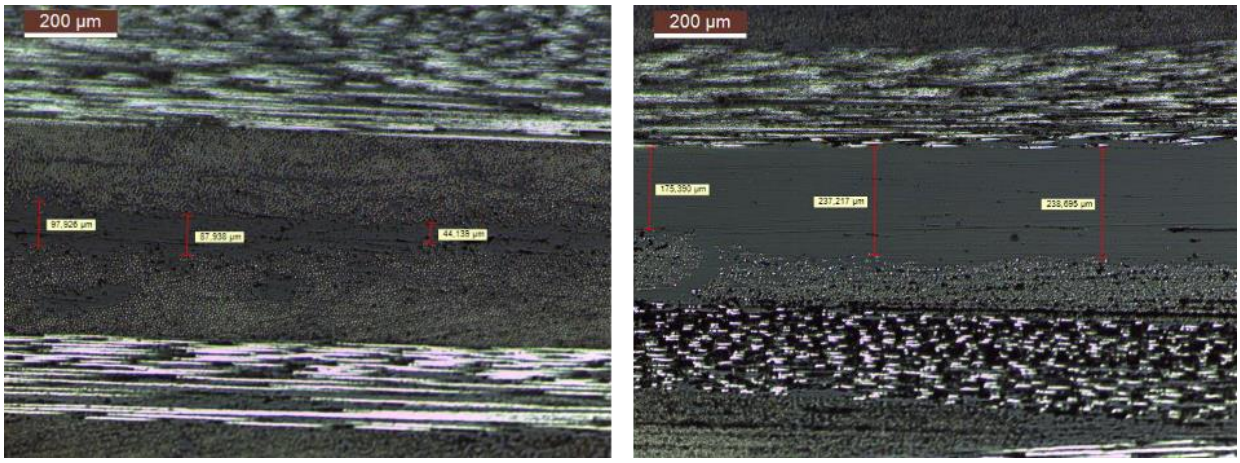

Figure 17 *Microscopy images of a broken DT120 specimens in which a 100 µm (left) and 200 µm (right) films were introduced. Red lines show the thickness of the films after curing.*

The adhesion promoters were found as a separate layer after the curing process; thus, they did not permeate the prepreg resin. This effect is less accentuated in the thinner 100 µm film than in the thicker 200 µm one.

3.3. Conclusions

Phenoxy resins are highly compatible polymers with epoxy resins, thereby they can provide physical entanglement, improving adhesion in multilayer objects. Various phenoxy resins were tested as promoters for a commercial prepreg (DT120). Adhesion promoters were added as dissolved polymer in a suitable solvent. Among the tested promoters, the best results were observed upon the application of PKHP and PKHB-AcAc 20%. Further investigations were performed, therefore the mechanical properties of promoter-added DT120 specimens were tested in the fracture toughness configuration. The results showed that the addition of a polymer capable of arising to a physical entanglement with the epoxy matrix is crucial to enhance the joint performances; in fact, highly promising results in terms of improvement for the two assessed modes (mode I and mode II) were observed. Finally, the addition of adhesion promoters as thin films was investigated. The poor result of the mechanical properties tested by SLS test, with the microscopy images, showed that the introduction of a thin film in the joint area between two adherents did not allow a good permeation of the promoters in the prepreg resin.

3.4. Experimental section

3.4.1. Introduction of PKHP-AcAc 20% as solid promoters for single lap shear test

As composite adhesive, we laminated the following stacking sequence:

- 8 plies of C384 T700 2X2T 12K DT120 40% (3,2 mm)
- Adhesion promoters
- 8 layers of C384 T700 2X2T 12K DT120 40% (3,2 mm)

The adhesion promoter powder is positioned between the two 8-plies stacks as shown in Figure 5. The tested specimen was labelled as following:

- DARC21927: C384 T700 DT120 + PKHP-AcAc 20% + C384 T700 DT120

Curing cycle: 90 min @ 135 °C, 6 bar.

Figure 18 *Pristine specimens with PKHP-AcAc 20%for DT120 prepreg.*

Figure 19 *Broken specimens with PKHP-AcAc 20%for DT120 prepreg.*

3.4.2. Introduction of PKHP, PKHP-AcAc 20%, PKHB and PKHB-AcAc 20% as solution in MEK for single lap shear test

As composite adherent, we laminated the following stacking sequence:

- 8 plies of C384 T700 2X2T 12K DT120 40% (3,2 mm)
- Adhesion promoter
- 8 plies of C384 T700 2X2T 12K DT120 40% (3,2 mm)

The adhesion promoter solution is painted between the two 8-plies stacks as shown in Figure 5.

The tested specimens were labelled as following:

- DARC21929: C384 T700 DT120 + PKHP-AcAc 20% + C384 T700 DT120
- DARC21974: C384 T700 DT120 + PKHP + C384 T700 DT120
- DARC21974: C384 T700 DT120 + PKHB + C384 T700 DT120
- DARC21974: C384 T700 DT120 + PKHB-AcAc 20% + C384 T700 DT120

Curing cycle: 90 min @ 135 °C, 6 bar.

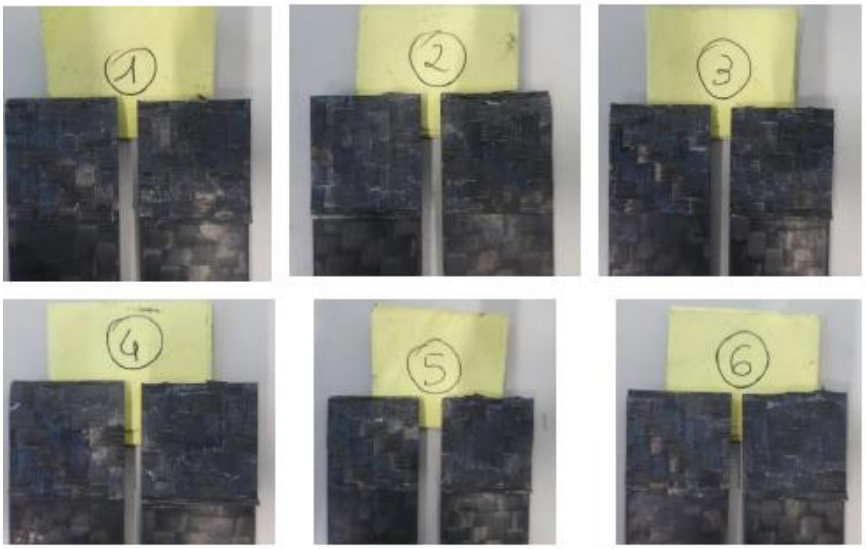

Figure 20 *Broken specimens with PKHB-AcAc 20%for DT120 prepreg.*

3.4.3. Introduction of PKHP and PKHB-AcAc 20% as solution in MEK for fracture toughness test

Specimens were tested according to ASTM D 5528 for mode I and ASTM D 7905 for mode II.

The following stacking sequence was laminated for both the tests:

- 8 plies of C384 T700 2X2T 12K DT120 40% (3,2 mm)
- Adhesion promoter
- 8 plies of C384 T700 2X2T 12K DT120 40% (3,2 mm).

The tested specimens for fracture toughness mode I were labelled as following:

- DARC21B86: C384 T700 2X2T 12K DT120 40% reference
- DARC21B88: C384 T700 2X2T 12K DT120 40% + PKHP
- DARC21B90: C384 T700 2X2T 12K DT120 40% + PKHB-AcAc 20%

The tested specimens for fracture toughness mode II were labelled as following:

- DARC21B87: C384 T700 2X2T 12K DT120 40% reference
- DARC21B89: C384 T700 2X2T 12K DT120 40% + PKHP
- DARC21B91: C384 T700 2X2T 12K DT120 40% + PKHB-AcAc 20%

Curing cycle: 90 min @ 135 °C, 6 bar.

3.4.4. Preparation of the films by compression molding

Films were obtained by compression molding the polymers between Teflon plates, with an appropriate spacer, at 200 °C for 1.5 min under a pressure of 2 ton/m^{-2} (Carver C12, laboratory press).

3.4.5. Introduction of PKHP, PKHB and PKHB-AcAc 20% as 100 µm and 200 µm films for single lap shear stress test

The films were prepared by compression molding at 200 °C.

The following stacking sequence was laminated for all the tests:

- 8 plies of C384 T700 2X2T 12K DT120 40% (3,2 mm)
- Adhesion promoter film
- 8 plies of C384 T700 2X2T 12K DT120 40% (3,2 mm)

The adhesion promoter films are positioned between the two 8-plies stacks as shown in Figure 5.

The 100 µm tested specimens were labelled as following:

- DARC21C61: C384 T700 2X2T 12K DT120 40% + PKHP film 100 µm
- DARC21C62: C384 T700 2X2T 12K DT120 40% + PKHB film 100 µm
- DARC21C63: C384 T700 2X2T 12K DT120 40% + PKHB-AcAc 20% film 100 µm

The 200 µm tested specimens were labelled as following:

- DARC21C64: C384 T700 2X2T 12K DT120 40% + PKHP film 200 µm
- DARC21C65: C384 T700 2X2T 12K DT120 40% + PKHB film 200 µm
- DARC21C66: C384 T700 2X2T 12K DT120 40% + PKHB-AcAc 20% film 200 µm

Curing cycle: 90 min @ 135 °C, 6 bar.

3.4.6. Viscosity profile of ER450 and DT120 prepregs

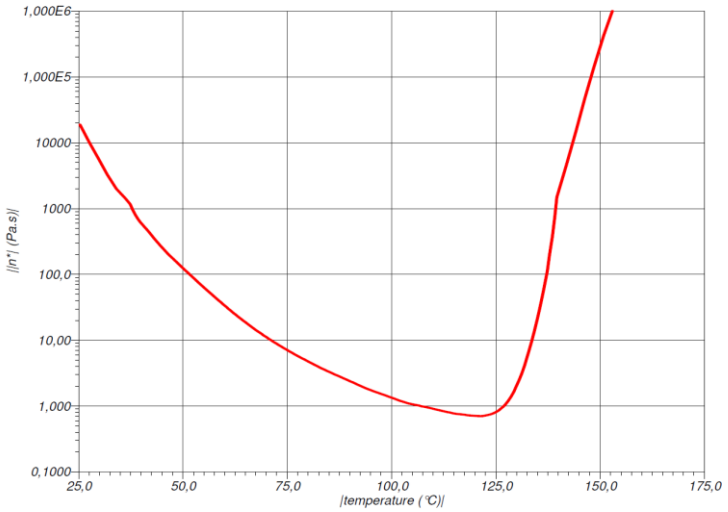

Figure 21 *Viscosity profile for ER450.*

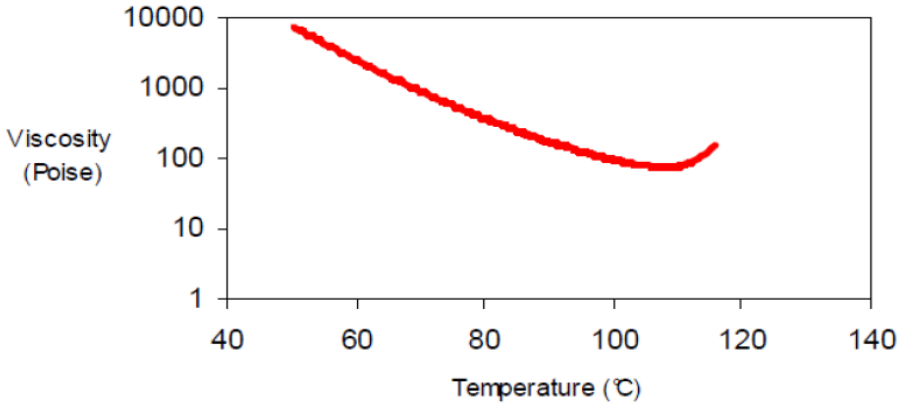

Figure 21 *Viscosity profile for DT120.*

3.4.7. Single lap shear test

Electromechanical testing machine MTS Insight 150 kN, with 250 kN hydraulic grips.

- Position transducer LVDT: 300mm, resolution 0.001 mm
- Load cell: 150 kN, resolution 0.002 kN class 0,5
- Test speed: 2 min.

3.4.8. Fracture toughness test

Electromechanical testing machine MTS Insight 150 kN, with 250 kN hydraulic grips.

- Position transducer LVDT: +/- 300mm, resolution 0.001 mm

Load cell: 150 kN, resolution 0.002 kN class 0.5.

3.5. References

(1) K. K. Chawla, *Composite Materials* **2012**, Springer New York.

(2) P. R. K. Mohan, S. G. Kumar, P. M. Mohite, *Procedia Structural Integrity* **2019**, *14*, 176−183.

(3) Y. J. Kim, S. H. Choi, S. J. Lee, K. S. Jang, *Ind. Eng. Chem. Res.* **2021**, *60*, 6153−6161.

(4) F. Zhihang, H. Michael, S. G. Advani, *Composites: Part A* **2008**, *39*, 540–554.

(5) J. Yang, R. Bai, B. Chen, Z. Suo, *Adv. Funct. Mater.* **2020**, *30*, 1901693.

(6) B.J. Dobraszczyka, M. P. Morgensternb, *J. Cer. Sci.* **2003**, *38*, 229–245.

(7) M. Hayaty, M. H. Beheshty, M. Esfandeh, *Polym. Adv. Technol.* **2011**, *22*, 1001–1006.

(8) M. Hayaty, M. H. Beheshty, M. Esfandeh, *J. Appl. Polym. Sci.* **2011**, *120*, 62–69.

(9) M. Hayaty, M. H. Beheshty, M. Esfandeh, *J Appl Polym. Sci.* **2011**, *120*, 1483–1489.

(10) R. F. Stockel, *American Cyanamid Company* **1969**, *46 (6)*.

(11) K. S. Jang, Y. S. Eom, J. T. Moon, Y. S. Oh, J. D. Nam, *J. Nanosci. Nanotechnol.* **2009**, *9* 7461−7466.

(12) F. Wu, X. Zhou, X. Yu, *RSC Adv.* **2018**, *8*, 8248−8258.

(13) Y. Tanaka, H. Kakiuchi, *J. Appl. Polym. Sci.* **1963**, *7*, 1063−1081.

(14) I. Barabanova, B. V. Lokshin, E. P. Kharitonova, E. S. Afanasyev, A. A. Askadskii, O. E. Philippova, Polymer 2019, 178, 121590.

(15) X. D. Liu, M. Kimura, A. Sudo, T. Endo, *J. Appl. Polym. Sci.* **2010**, *48*, 5298–5305.

(16) N. Poisson, A. Maazouz, H. Sautereau, M. Taha, X. Gambert, *J. Appl. Polym. Sci.* **1998**, *69*, 2487−2497.

(17) T. Guthner, B. Hammer, *J. Appl. Polym. Sci.* **1993**, *50*, 1453–1459.

(18) M. Hesabi, A. Salimi, M. H. Beheshty, *Polym. Test.* **2017**, *59*, 344–354.

(19) J. S. Shim, W. Lee, J. Jang, *Polymer Journal* **1991**, *23*, 903-910.

(20) S. S. Hwang, S. Y. Park, G. C. Kwon, W. J. Choi, *Int. J. Adv. Manuf Technol.* **2018**, *99*, 2743−2753.

Chapter 4

Insulating Vitrimers*

*This work was carried out in the group of Prof. Timothy M. Swager at Massachusetts Institute of Technology (MIT), Cambridge, MA, USA.

4.1. Introduction

Organic polymers are widely used to introduce free volume at the molecular scale, resulting in a lowering of the dielectric constant (ε). Low dielectric constant materials are particularly attractive for the semiconductor and insulating materials industry. A proper design for the synthesis of a dielectric polymers takes account of three main issues:

- minimizing the polarizability of the polymeric backbone avoiding extended π-systems
- incorporation of highly electronegative atoms to localize electrons in σ-bonds
- displaying low water absorption since the introduction of water traces (ε = 78) increases the dielectric constant of the material.[1]

The control of the ε becomes extremely important for those materials which require ε < 2.0. In particular, the control of pore size becomes an issue when the percentage of pores in a network is excessive, weakening the mechanical integrity of the object and thus provoking its collapse. Even the use of a polymeric pore generator,[2] typically introduced in a blend with thermosets, affects the stability of the network, since its overloading can promote the polymer aggregation.

Therefore, the need of a new dielectric material, intrinsically porous due to its peculiar polymeric structure, becomes prominent.

Iptycenes are a class of molecules amenable for the design of advanced materials due to their three-dimensional and noncompliant structure amenable to create interstitial space around the molecules. The simplest member of this class of compounds is triptycene that is based on a [2,2,2]-ring system. To understand how triptycene can define free volume, it can be inscribed into a trigonal prism, thus highlighting the free volume between the molecular structure and the surface of the polyhedron (Figure 1).

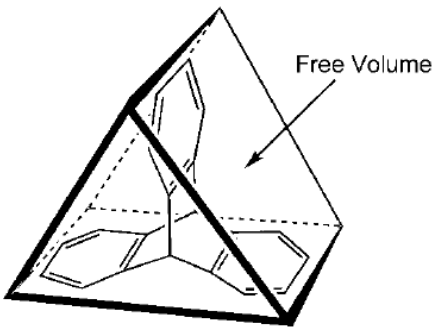

Figure 1 *Triptycene inscribed in a trigonal prism.*[3]

The synthesis of a polymer containing the triptycene unit can result in a low dielectric constant (ε) material due to its rigid and shape-persistent structure, preventing the use of polymeric pore generators.[1,3]

Swager and co-workers introduced a new triptycene-based approach for the lowering of the ε. They synthetized polymers from strained cyclic olefinic monomers *via* ROMP (Figure 2), leading a polymer structure wherein the triptycene orientation is fixed by the orientation of the polymer backbone because of its two-point connection with the main chain.

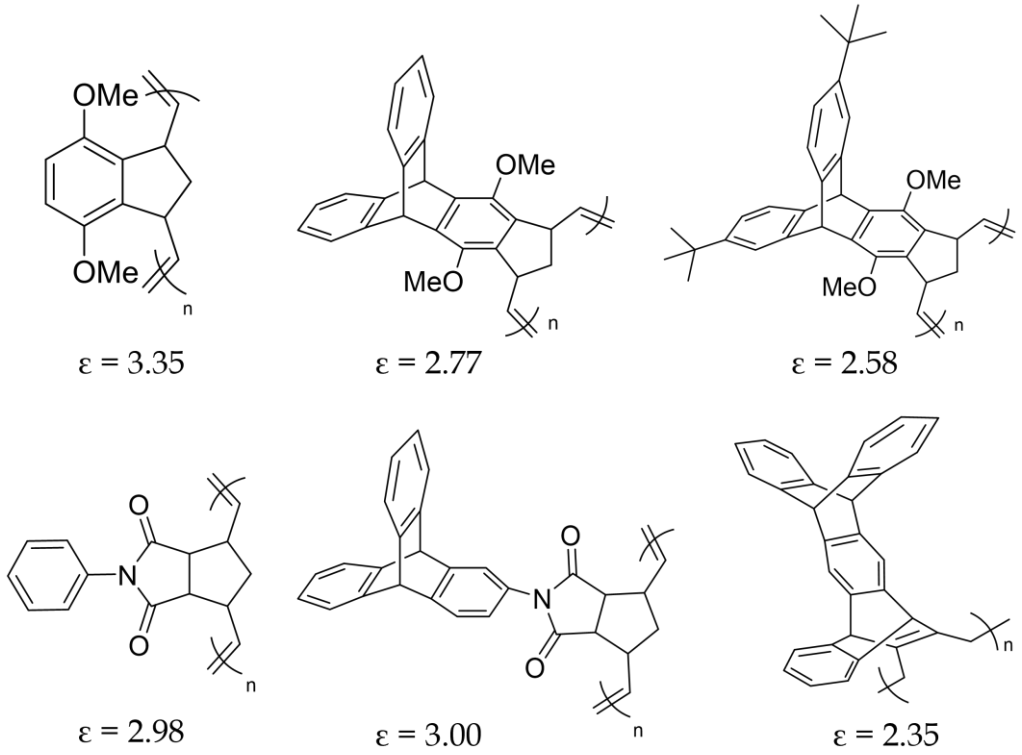

Figure 2 *Polymers derived from strained cyclic olefinic monomers via ROMP. Dielectric constants are lower for polymers in which the triptycene unit is fused to the polymer backbone in a two-point connection. The lowering of the ε can be also obtained by the introduction of bulky functional groups.*[3]

This constrain prevents the free rotation of the triptycene moiety, endowing rigidity and, thereby a greater degree of free volume. It was demonstrated that the incorporation of triptycene into the backbone by the attachment *via* a single bond allows the rotational freedom, permitting a denser packing of the polymeric chains. Therefore, the ring fusion of the triptycenes is essential to create the desired free volume.[3]

The synthesis and the implementation of triptycene-based polymers can find application to address current issues, like the growing demand for renewable sources of energy. For

this purpose, the creation of dynamic covalent network-based insulators to satisfy simultaneously recyclability[4-6] and insulation requirements is aimed to provide a new generation of extruded high voltage cables. Nowadays, they are identified as the best wires to be integrated in the future electricity grid, but they are not recyclable because relying on crosslinked polyethylene (XLPE) as insulating material (Figure 3).

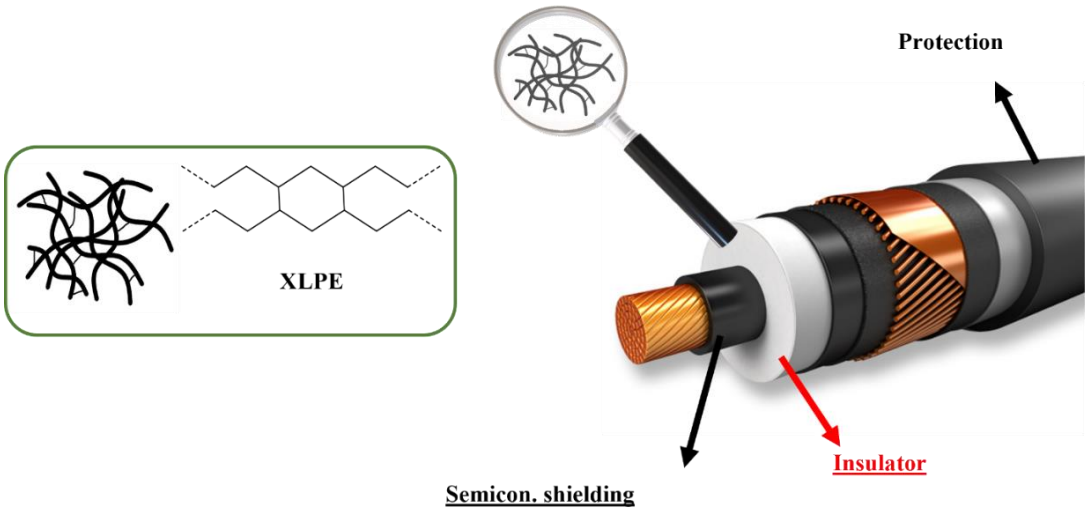

Figure 3 *Composition for current high voltage cables. The insulating material is crosslinked polyethylene (XLPE).*

The use of a new insulating material whose network is reversible can relieve the high voltage cables environmental impact, allowing reprocessing and recycling. Thereby, the mere substitution of the traditionally used thermoset with a vitrimer may ensure the reuse of the same insulator without altering its dielectric properties (Figure 4).

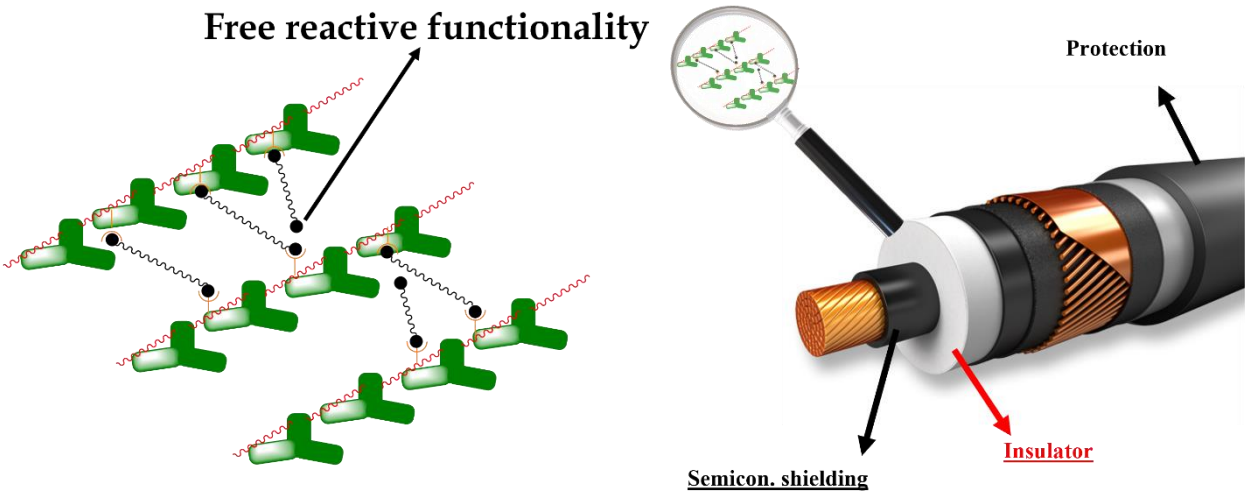

Figure 4 *Schematic representation of a high voltage cable with a covalent dynamic network-based insulator. The polymeric backbone relies on triptycene units.*

The target polymer was a linear polymer, derived from 9,10-benzenoanthracene-1,4-diol and its corresponding diglycidylated homologous. Therefore, this amorphous thermoplastic polymer shows several hydroxy pendant groups, one for every repeating unit (Figure 5).

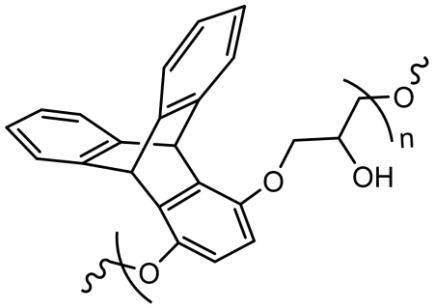

Figure 5 *Chemical structure of the target linear polymer, obtainable from 9,10-benzenoanthracene-1,4-diol and its corresponding diglycidylated homologous, 9,10-benzenoanthracene-1,4-diol diglycidyl ether.*

It was thought to be a good mimic of the phenoxy resin in which the triptycene unit played the same role of the bisphenol A in the phenoxy resin, imparting toughness, chemical and heat resistance, besides free volume. At the same time, the hydroxy groups were amenable for the post-functionalization with acetoacetate (AcAc) units, necessary for the vinylogous transamination.

Due to the challenging effectiveness of the aforementioned polymerization, a more straightforward approach was investigated: the one-pot generation of a dynamic covalent network throughout the polymerization between a multifunctional aminic crosslinker and the triptycene monomer, upon a proper functionalization with acetoacetate functionalities. Being the core of the obtained network, the triptycene units have restricted rotation, introducing free volume and thereby lowering the dielectric constant.

4.2. Results and discussion

4.2.1. Triptycene-based thermoplastics

The triptycene monomers 9,10-benzenoanthracene-1,4-diol **2** with two different hydroxy groups in 1 and 4 position, required to act as nucleophiles in the epoxy ring opening reaction and, its diglycidylated homologous, 9,10-benzenoanthracene-1,4-diol diglycidyl ether **3,** were firstly synthetized.

The two steps synthesis of **2** is sketched in Scheme 1. The first step is a Diels-Alder reaction between anthracene and 1,4-benzoquinone, previously purified by sublimation to obtain

bright yellow crystals. The solid product, triptycene benzoquinone **1**, collected by filtration, is transformed into its hydroquinone form **2** by an acid-catalyzed enolization (Scheme 1).[7]

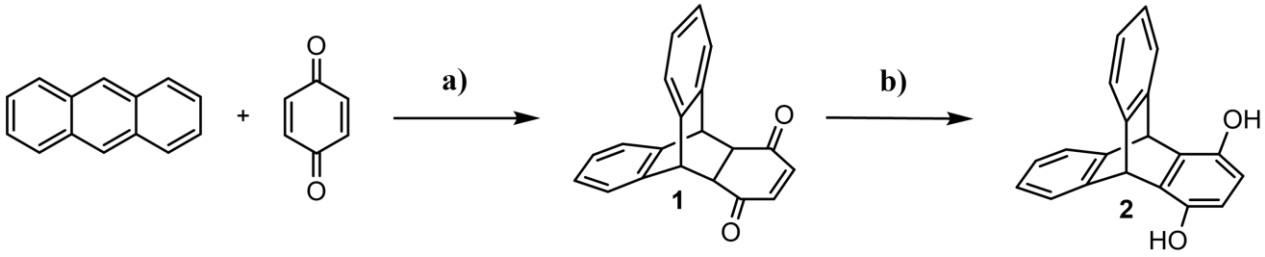

Scheme 2 *Synthesis of 9,10-benzenoanthracene-1,4-diol (**2**): a) 110 °C, 6 h, 70%; b) acetic acid, HBr cat., 115 °C, 3 h, 82%.*

The synthesis of **3** starting from **2** requires the use of a large excess of epichlorohydrin (20 equivalents), exploiting the catalytic action of benzyltriethylammonium chloride (Scheme 2a). This salt polarized the oxygen-hydrogen bond of the hydroxy group, thus increasing its reactivity toward the nucleophilic substitution on the carbon bearing the chlorine atom. A post treatment with an aqueous solution of sodium hydroxide is required to promote the intramolecular reaction between the hydroxy functionality generated by the direct nucleophilic attack on the epoxy ring, to restore the desired epoxy rings. After extractions with ethyl acetate to eliminate the excess of epichlorohydrin, the undesired monodiglycidylated is removed by column chromatography.[8] This procedure gave **3** in just 30%yield. To increase the yield of **3**, the reaction conditions were changed: longer reaction time, no use of the catalyst and no final basic treatment (Scheme 2b).

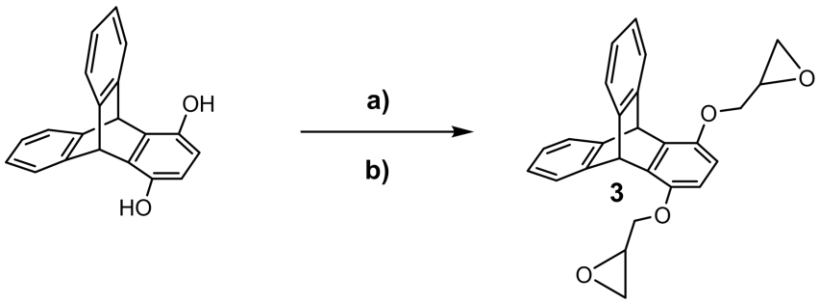

Scheme 3 *Synthesis of 9,10-benzenoanthracene-1,4-diol diglycidyl ether (3): a) epichlorohydrin (20 eq.), benzyltriethylammonium chloride cat., 90 °C, 16 h. Post treatment with NaOH (aq), 30 min, 30 °C. Yield: 30%; b) epichlorohydrin (20 eq.), 100 °C, 48 h, quantitative yield.*

The modified synthesis affords the pure product in quantitative yield after a recrystallization in ethanol, as shown by the NMR of the recrystallized crude (Figure 6).

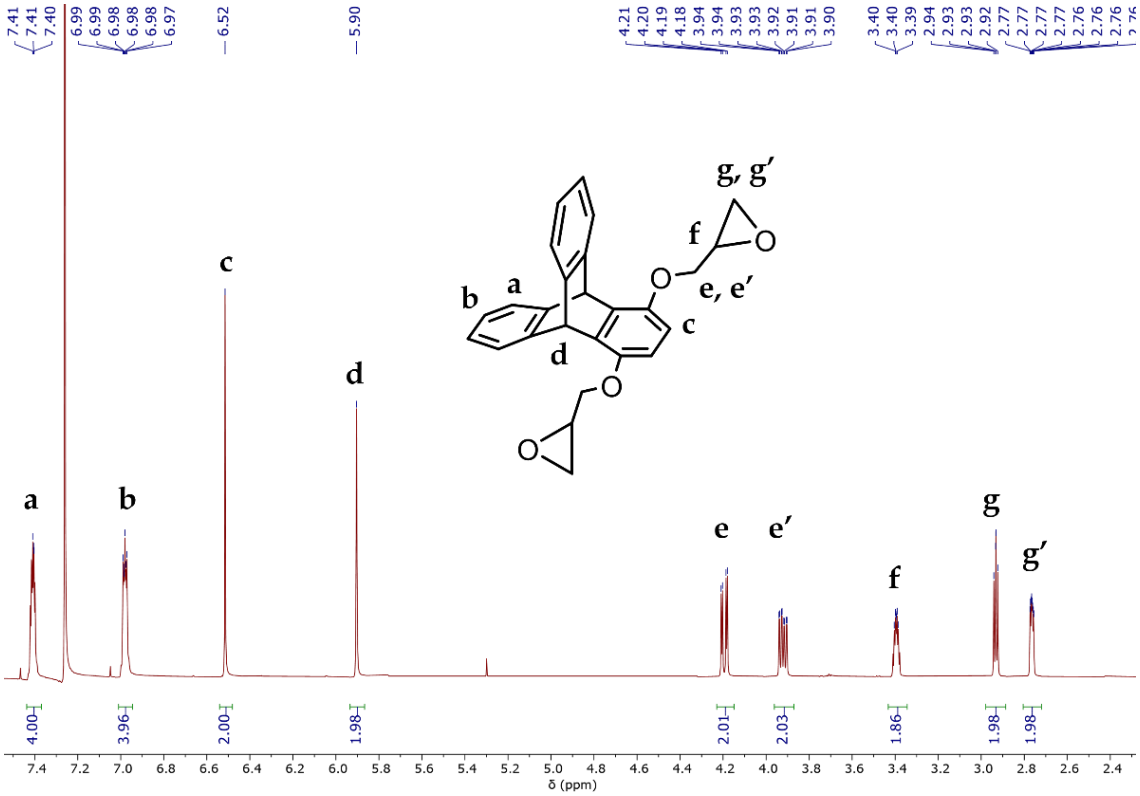

Figure 6 *^{1}H NMR ($CDCl_3$) spectrum of 9,10-benzenoanthracene-1,4-diol diglycidyl ether* ***3****.*

The monomers **2** and **3** showed high melting points, thus excluding the possibility to conduct the reaction in bulk. Dioxane, a good solvent for the epoxy ring opening polymerization, was excluded since it does not solubilize the phosphonium catalyst. Alternatively, dimethylformamide (DMF) was selected because it can solubilize the catalyst and ensure high reaction temperatures (Scheme 3).

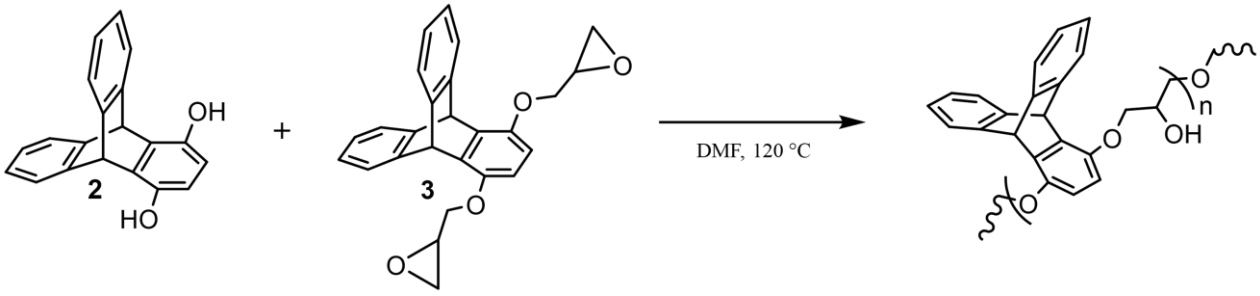

Scheme 4 *Schematic representation for the synthesis of the linear polymer. Tested reaction conditions are reported in Table 1.*

The polymerization reactions were made in dry DMF and air-free conditions, varying bases/catalysts, time reaction and temperature (Table 1). These conditions were required because the monomers are sensitive towards moisture and atmospheric oxygen. The overall monomers concentration was equal to 0.01 g/mL. At the end, addition of water

led to the precipitation of the polymer, collected by filtration after centrifugation. The crudes were dissolved in tetrahydrofuran and GPC runs were performed (Table 1).
The reactions that were conducted without base or catalyst or with an organic base as catalyst, like 1,8-diazabicyclo[5.4.0]undec-7-ene (DBU) and 1,5,7-triazabicyclo [4.4.0] dec-5-ene (TBD) did not give any significant result in terms of molecular weight (entries 3, 6, 8, Table 1). Oligomerization was observed using potassium carbonate as base (entries 5, 10, Table 1) or triphenyl butyl phosphonium bromide (TBPB) as catalyst (entries 1 ,2, Table 1).[9] Despite the longer time for the reactions with TBPB as catalyst, the molecular weights achieved with K_2CO_3 and TBPB were approximatively the same, hence the polymerization with K_2CO_3 was further investigated, trying to repeat the same reaction in presence of 18-Crown-6 to better solubilize the base in DMF (entry 10).

Table 1 *Summary of polymerization trials between monomers* ***2*** *and* ***3****.*

Entry	Solvent	Base/cat.	T (°C)	Time (h)	M_n[a] (kDa)	M_w[a] (kDa)	PDI
1	DMF	TBPB	120	72	1.741	1.820	1.04
2	DMF	TBPB	120	7 days	1.008	1.111	1.10
3	DMF	/	120	48	0.683	0.706	1.03
4	DMF	TBPB	120	48	0.703	0.737	1.05
5	DMF	K_2CO_3	120	48	1.050	1.545	1.47
6	DMF	DBU	120	48	0.773	0.860	1.11
7	DMF	TBPB	120	48	0.670	0.688	1.03
8	DMF	TBD	120	48	0.436	0.756	1.73
9	DMF	t-BuOK	120	72	0.873	0.953	1.09
10	DMF	K_2CO_3 [b]	120	48	1.203	1.701	1.41

[a] Relative to polystyrene standards (GPC). [b] 18-Crown-6r used to solubilize the base.

The NMR spectrum (relative to K_2CO_3 promoted polymerization) confirmed the shift and the broadening of the peaks respect to the monomers. Moreover, the disappearance of the diagnostic peaks of the diglycidylated monomer in the aliphatic area was observed, as indication of the epoxy rings opening (Figure 7).

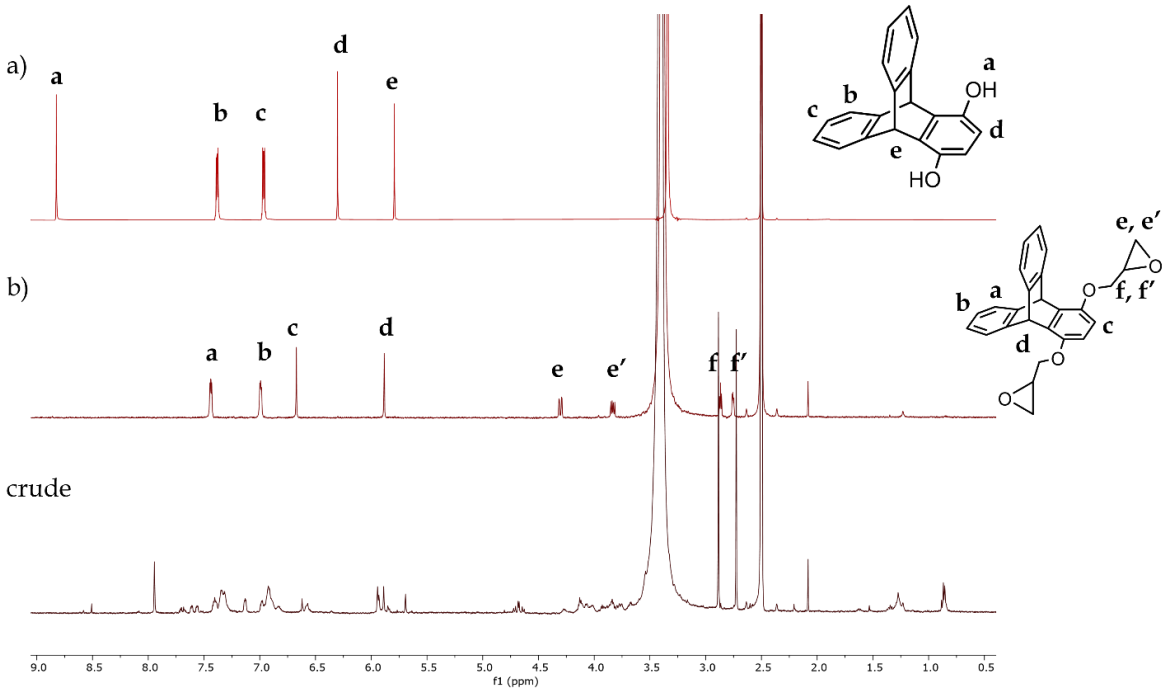

Figure 7 *^{1}H NMR (DMSO-d_6) a) spectrum of* ***2****, b) spectrum of* ***3****, c) spectrum of crude.*

Considering the very low M_w of the polymeric chains, two different polymerization procedures were implemented.

The first one aimed to prevent the possible side reaction of 9,10-benzenoanthracene-1,4-diol **2**. It is known that hydroquinones can form the corresponding quinone form, when deprotonated and in presence of atmospheric oxygen, following a radical oxidation pathway in which an electron can resonate in the aromatic ring (Scheme 4).

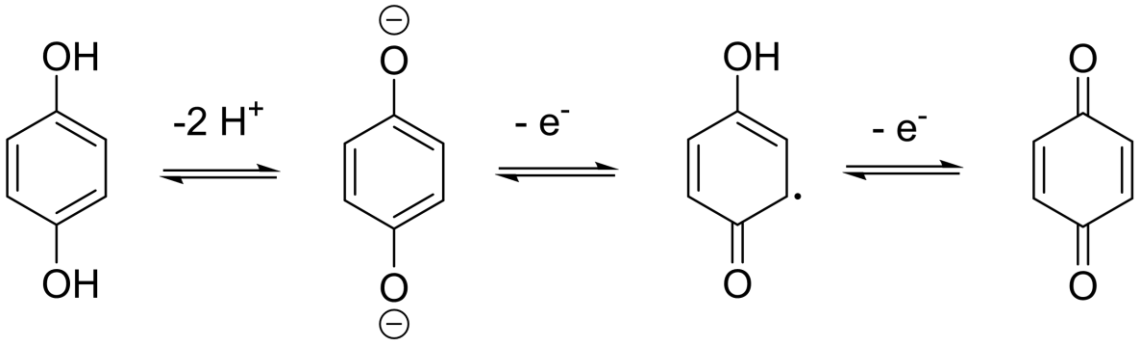

Scheme 4 *Oxidation pathway for hydroquinone molecules. This radical mechanism generated the oxidated quinone species.*

This oxidated form cannot act as nucleophile, hence the concentration of the nucleophilic hydroquinone in solution decreases, hampering the polymerization. To prevent the occurrence of this collateral reaction, bisphenol A was used instead of 9,10-benzenoanthracene-1,4-diol because it has not a hydroquinone unit (Scheme 5).

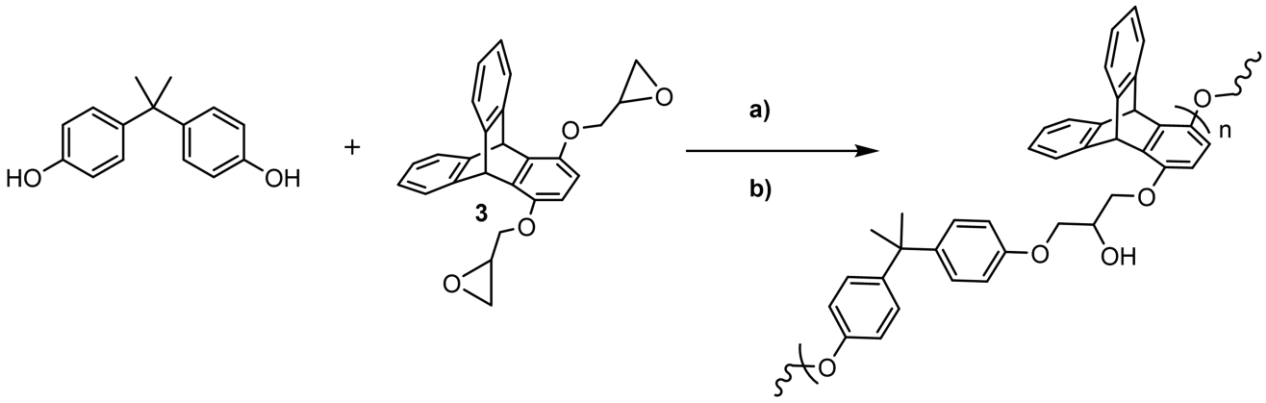

Scheme 5 *Schematic representation for the synthesis of the linear polymer: a) K_2CO_3 (3 eq.), DMF, 120 °C, 72 h; b) TBD cat., DMF, 120 °C, 48 h.*

The following polymerization trials, reported in Table 2, were performed by reacting bisphenol A, using the best conditions found for the previous polymerization attempts (K_2CO_3 as base). Additionally, the use of 1,5,7-triazabicyclo [4.4.0] dec-5-ene (TBD) as catalyst was also investigated. The polymerization with bisphenol A in presence of K_2CO_3 was the best result achieved up to that point, demonstrating a slight improvement but not so significant in terms of molecular weight (entry 1, Table 2).

Table 2 *Summary of polymerization trials between bisphenol A and* ***3****.*

Entry	Solvent	Base/cat.	T (°C)	Time (h)	M_n (kDa)	M_w (kDa)	PDI
1	DMF	K_2CO_3	120	72	1.790	2.501	1.40
2	DMF	TBD	120	48	0.449	0.759	1.69

[a] Relative to polystyrene standards (GPC).

The second approach was based on different triptycene-based monomer, obtained by the reaction of 9,10-benzenoanthracene-1,4-diol with ethylene carbonate. The product was a triptycene derivative **4** with two ethylenic spacers, ending with aliphatic hydroxyl groups.[10]

The rationale of this approach was to prevent the oxidation of hydroquinone and to distance the hydroxyl groups from the triptycene skeleton, preventing any steric hindrance effect in the nucleophilic substitution (Scheme 6).

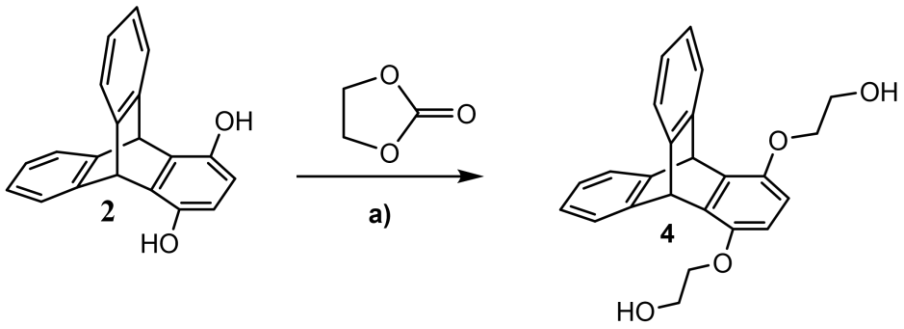

Scheme 6 *Synthesis of triptycene-1,4-hydroquinone-bis(2-hydroxyethyl) ether (4): a) K_2CO_3, DMF, 165 °C, 16 h.*

The obtained product **4** was characterized by NMR spectroscopy (Figure 8).

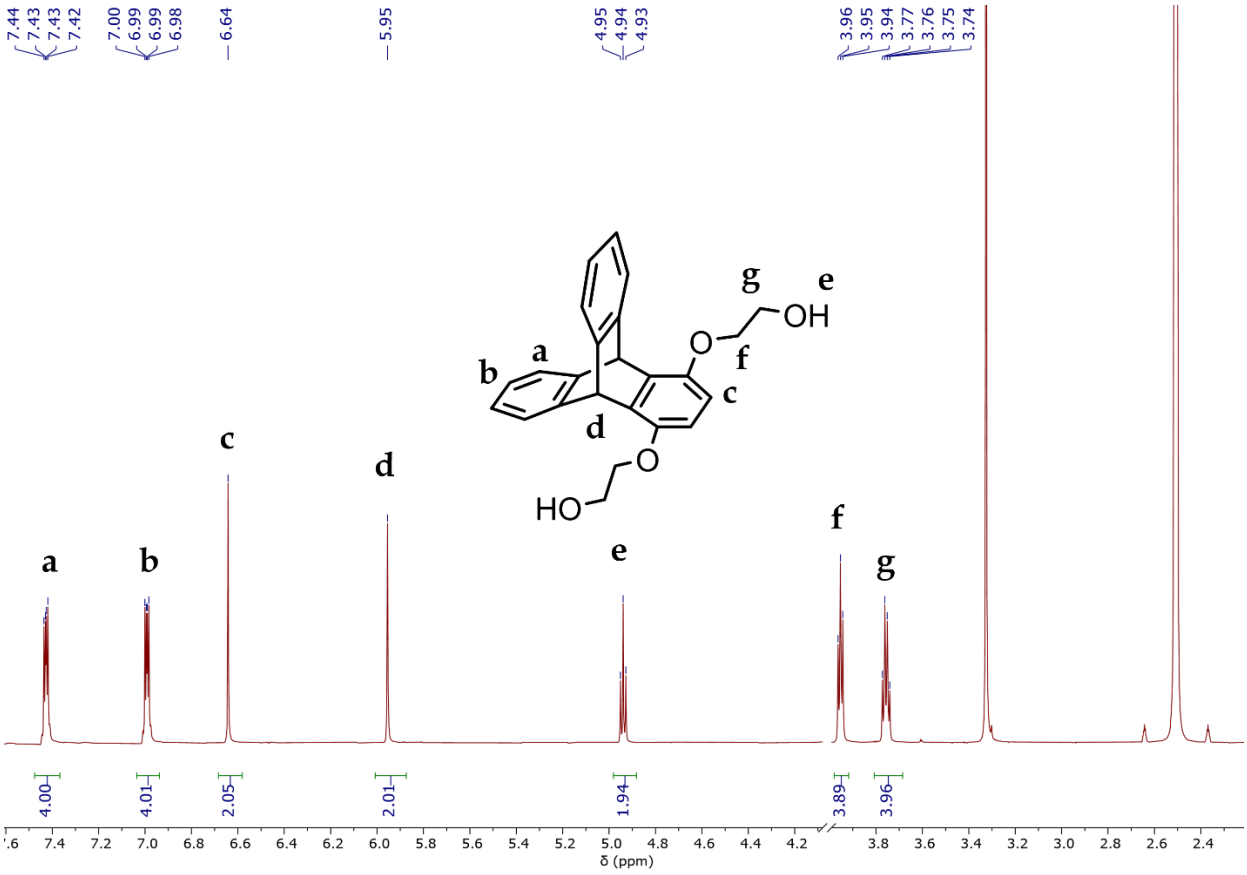

Figure 8 *^{1}H NMR (DMSO-d_6) spectrum of 9,10-benzenoanthracene-1,4-hydroquinone-bis(2-hydroxyethyl) ether **4**.*

The subsequent polymerization experiments were carried out by reacting **3** with 1,4-hydroquinone-bis(2-hydroxyethyl) ether **4**, using K_2CO_3 and TBD even in this case (Scheme 7).

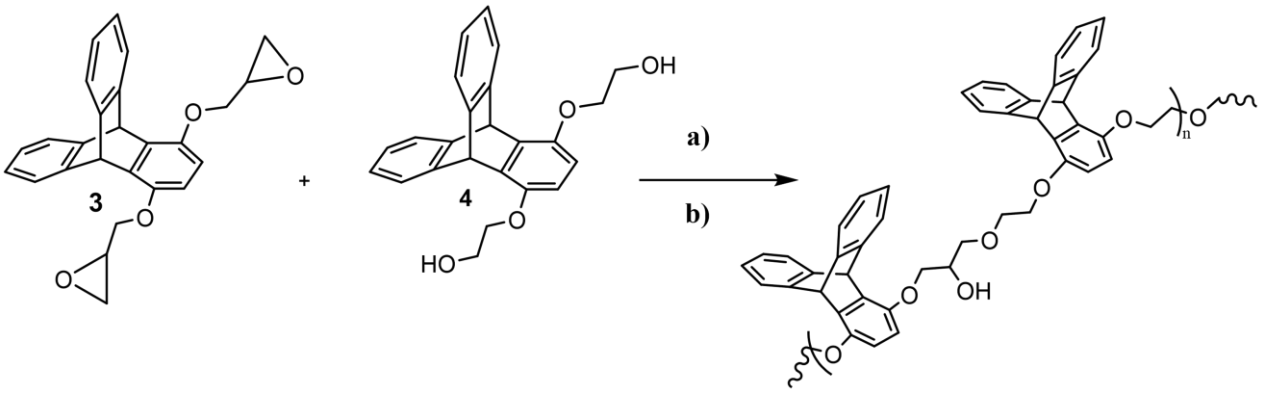

Scheme 7 *Schematic representation for the synthesis of the linear polymer: a) K_2CO_3 (3 eq.), DMF, 120 °C, 48 h; b) TBD cat., DMF, 120 °C, 48 h.*

Also in this case the reactions showed no evidence of polymerization (Table 3).

Table 3 *Summary of polymerization trials between **3** and **4**.*

Entry	Solvent	Base/cat.	T (°C)	Time (h)	M_n (kDa)	M_w (kDa)	PDI
1	DMF	K_2CO_3	120	48	0.391	0.445	1.13
2	DMF	TBD	120	48	0.377	0.406	1.08

[a] Relative to polystyrene standards (GPC).

At this point a completely different approach was undertaken, by changing the nucleophile to overcome the above described issues. Primary and secondary amines were chosen as nucleophilic co-monomers for the ring opening of epoxides in **3 (**Scheme 8**)**.

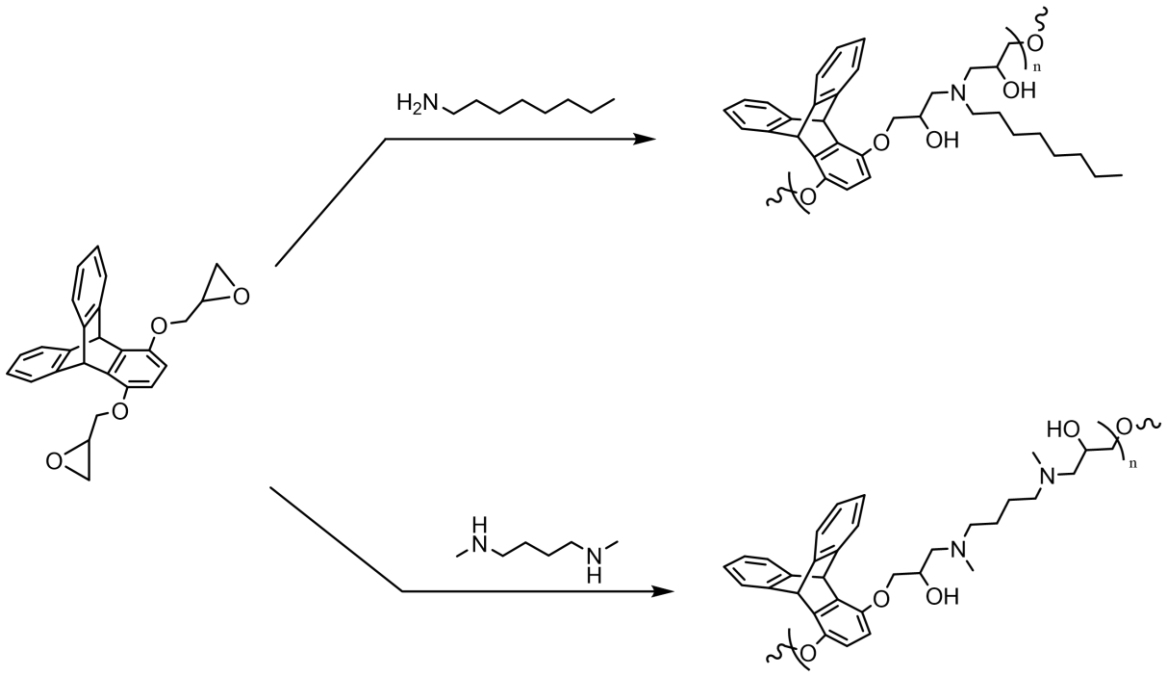

Scheme 8 *Polymerization experiments between 3 and octylamine and N, N'-dimethyl-1,3-propanediamine.*

Monomer **3** was reacted with different amines in presence of imidazole, a good catalyst for the epoxy ring-opening polymerization.

Table 4 *Summary of polymerization trials between* ***3*** *and different amines.*

Entry	Solvent	Base/cat.	T (°C)	Time (h)	M_n[a] (kDa)	M_w[a] (kDa)	PDI	[conc.] (g/mL)
1[b]	DMF	Imidazole	120	35	3.508	4.057	1.16	0.4
2[b]	DMF	Imidazole	120	60	4.318	5.250	1.22	0.2
3[c]	DMF	Imidazole	120	60	0.799	0.935	1.18	0.2

[a] Relative to polystyrene standards (GPC). [b] Octylamine as reagent. [c] N, N'-dimethyl-1,3-propanediamine as reagent.

The first reaction (entry 1, Table 4) involved octylamine, which has two active hydrogen atoms, hence every amine can react with two different epoxy groups. The overall concentration of the monomers in DMF was higher (0.4 g/mL) than the concentration used for the polymerization with **2** (0.01 g/mL), but it did not allow a complete solubilization of the reagents. The crude was analyzed by GPC, showing a clear increase of the average molecular weight. A second attempt performed by halving the overall concentration (0.2 g/mL) and extending the time reaction (60 hours) (entry 2, Table 4) confirmed that a better solubilization of the monomer led to an enhanced effectiveness of the polymerization. To understand the reason why the growth of the chain is limited, N, N'-dimethyl-1,3-propanediamine was used as reagent. Being a secondary amine, N, N'-dimethyl-1,3-propanediamine did not allow the attachment on the same nitrogen by two different triptycene moieties, excluding from the possible explanation steric effects (entry 3, Table 4). The measured molecular weight was lower than the one obtained by the reaction with octylamine, thus excluding that the limited growth of the polymer was a matter of steric hindrance.

4.2.2. Triptycene-based crosslinked polymers as potential vitrimers

A different strategy was chosen considering the poor results from the previously discussed polymerization experiments. A new vitrimeric network starting from the reaction between two multifunctionalized monomers that allows to achieve a crosslinked network in one step was identified as target polymer. A suitable triptycene-based monomer, such as the diacetoacetylated triptycene, had to be synthesized first. The first

synthetic effort was the acetoacetylation of 9,10-benzenoanthracene-1,4-diol to obtain a suitable raw material for vinylogous urethane-based vitrimers.

According to a literature procedure,[11] the hydroquinone triptycene was reacted with 2,2,6-trimethyl-1,3-dioxin-4-one (TMDO): it undergoes a *retro*-Diels Alder reaction at elevated temperature, thus releasing a reactive acetylketene and acetone, removed by distillation. The reactive acetylketene can react with the hydroquinone giving the final product (Scheme 9a).

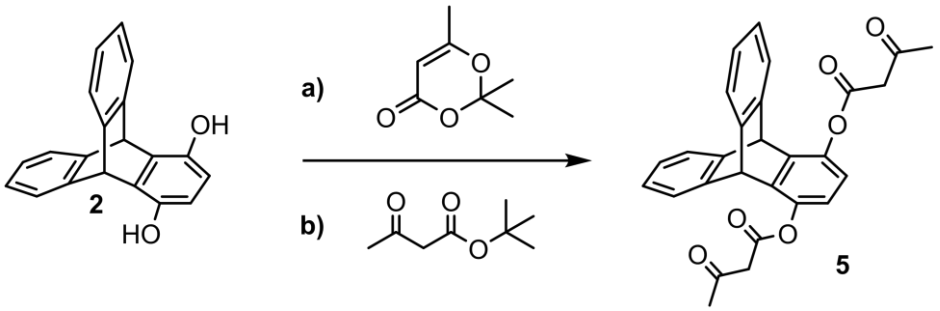

Scheme 9 *Synthesis of 9,10-benzenoanthracene-1,4-diol diacetylacetate (5): a) TMDO (10 eq.), xylene, 135 °C. 16 h; b) t-BuAcAc (20 eq.), 110 °C, 48 h, 90 %.*

The black-colored crude, containing the monofunctionalized product, suggested the occurrence of side reactions. For these reasons, the acetoacetylation was made using *tert*-butylacetoacetate (*t*-BuAcAc), after some attempts to optimize the reaction conditions, changing solvent, temperature, and molar ratio (Table 4).

Table 4 *Summary of acetoacetylation trials with t-BuAcAc.*

Entry	Solvent	Base/cat.	T (°C)	Time (h)	Molar ratio [a]	Result
1	Toluene	DMAP	110	16	1:20:0.2	Mono
2	Toluene	/	80	16	1:2.1	None
3	Toluene	/	80	16	1:20	Mono
4	Bulk	/	80	16	1:20	Mono
5	Bulk	K_2CO_3	80	16	1:20:3	None
6	Toluene	/	110 °C	48	1:20	Difunct.

[a] Relative to triptycene:*t*-BuAcAc:base/catalyst.

Using a large excess of *t*-BuAcAc (entry 1,3, Table 4), or leading the reaction in bulk overnight (entry 4,5, Table 4) was not sufficiently to achieve the difunctionalized product.

Finally, the best attempt was made in dry toluene for 48 hours at 110 °C, with a large excess of *t*-BuAcAc (1:20) (Scheme 9b). The obtained product (Figure 9) was amenable to react with a multifunctionalized amine to give a vitrimeric network in one step synthesis.

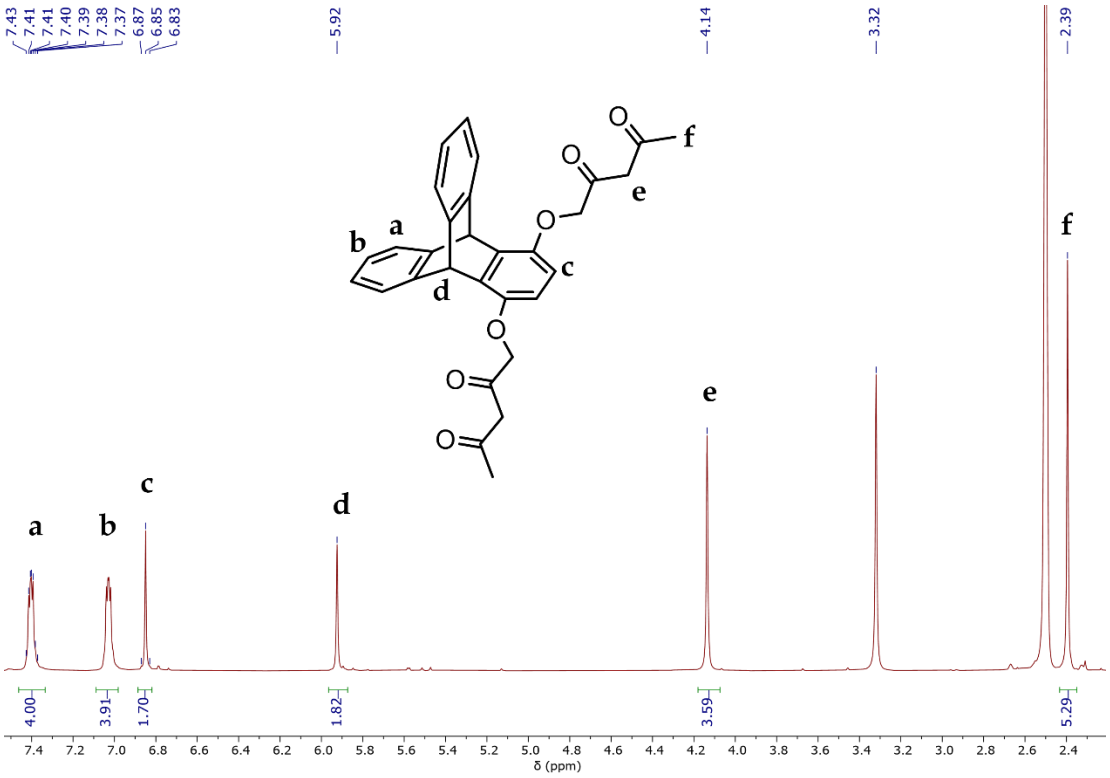

Figure 9 *^{1}H NMR (DMSO-d6) spectrum of 9,10-benzenoanthracene-1,4-diol diacetylacetate 5.*

Aromatic acetoacetates can undergo condensation and substitution reactions with aliphatic primary amines; indeed, the nucleophilic attack can either occur at the keto group, giving a vinylogous urethane, or at the ester unit, producing a vinylogous urea, after the nucleophilic attack of a second amine. Due to the significantly lower electrophilicity of the conjugated C=O ester bond of the vinylogous urethane, the substitution reaction by a free amine functionality is prevented, while the C=C bond enables dynamic covalent exchange reactions. Thus, mixtures of vinylogous urethane/urea compounds and pendant free amines could be obtained. Moreover, experiments showed that the ratio of the emerging vinylogous urethane (VUT) and vinylogous urea (VUA) products can be adjusted by the solvent and/or acetic acid as a catalyst (Figure 10): the latter can protonate the keto group of the acetoacetate and increase the electrophilicity, which shift the ratio to the vinylogous urethane products, allowing a selective conversion.[11]

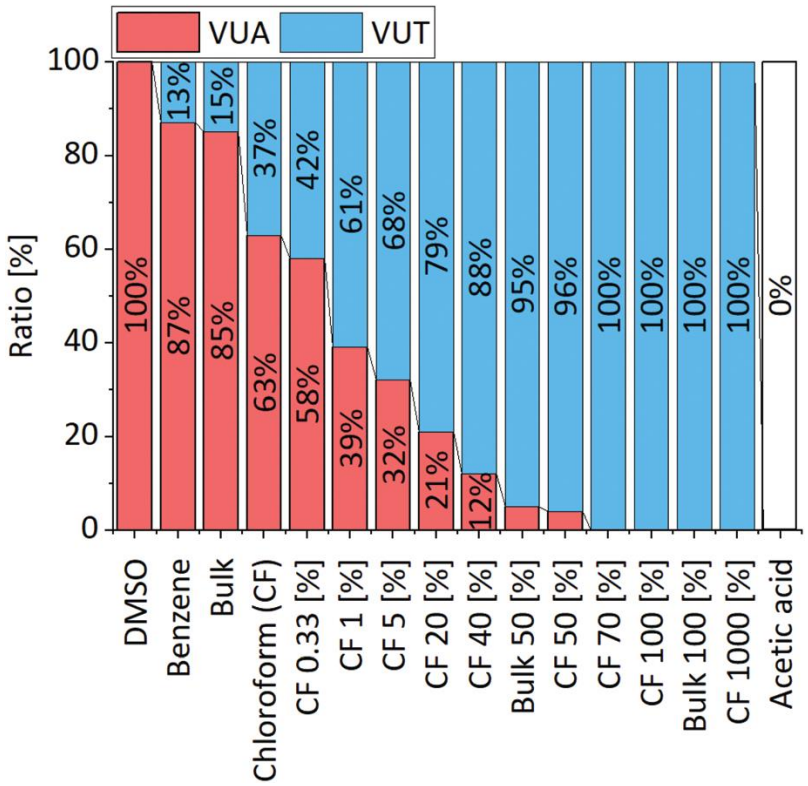

Figure 10 *Ratio of the vinylogous urethane (VUA) and vinylogous urea (VUT) moieties, resulting from the condensation and substitution reactions of acetoacetylated monomers with amines. The ratio can be shifted to a selective formation of either the vinylogous urethane or the vinylogous urea compound.*[11]

Two distinct crosslinked networks were obtained, mixing tris(2-aminoethyl) amine (TREN) and the diacetoacetylated triptycene **5** in different molar ratio. The two monomers were dissolved in chloroform in presence of acetic acid (70 mol%), according to a literature procedure.[11] The reaction was carried out at 40 °C, until the gelification.

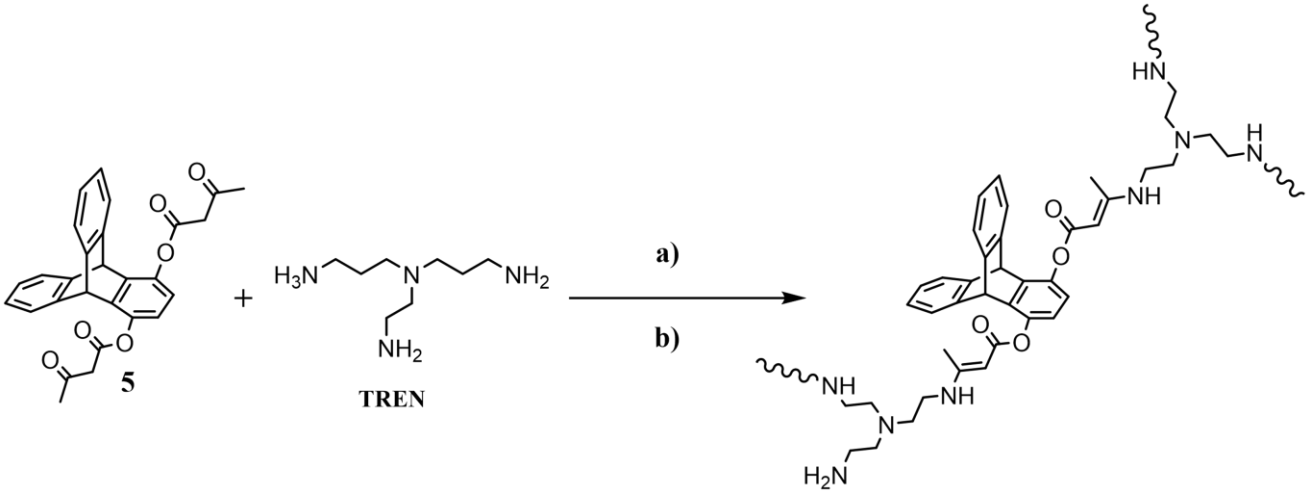

Scheme 10 *Synthesis of the vitrimer: a) TREN (1.1 eq.), acetic acid cat., chloroform, 40 °C, 24 h; b) TREN (2.2 eq.), acetic acid, chloroform, 40 °C, 60 h.*

The vitrimer was post-cured for 24 hours at 100 °C *in vacuo*. The equimolar reaction was thought to ensure sufficient amine groups for the transamination reactions, but the gel content (37%) showed a not full conversion of the acetoacetate moieties (Scheme 10a). This result was also confirmed by FT-IR: the two bands relative to the stretching of the acetoacetate carbonyl groups (1760 cm^{-1} and 1713 cm^{-1}) are still present in the vitrimer spectrum which simultaneously shows the typical bands for the stretching the C=O ester band (1660 cm^{-1}) and the C=C band (1586 cm^{-1}) (Figure 11).

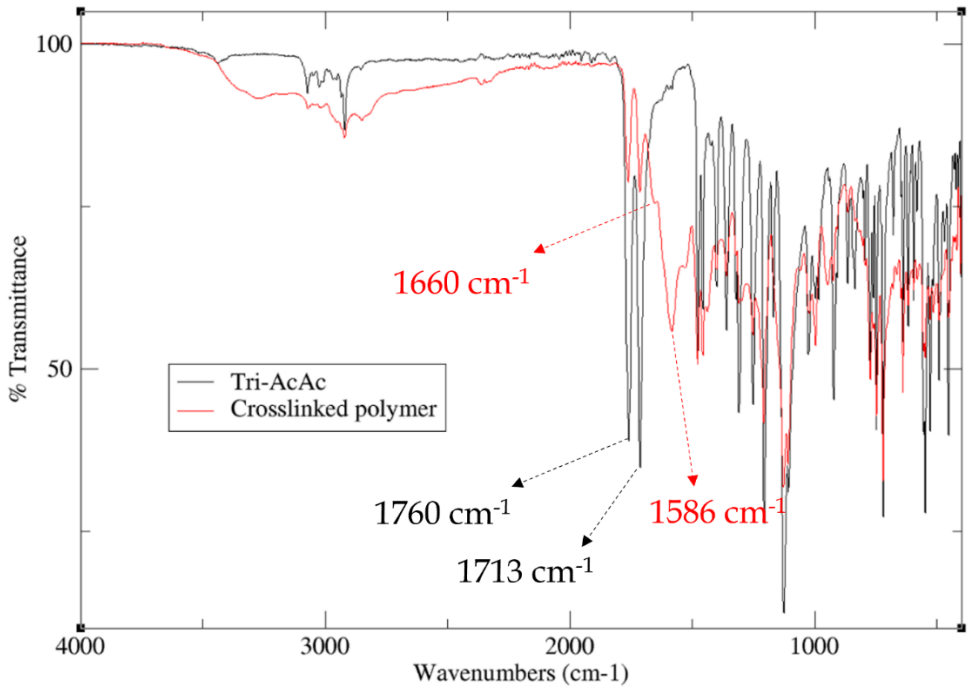

Figure 11 *FT-IR of the vitrimer cured with TREN in molar ratio 1:1.1. The bands relative to the stretching of the acetoacetate functionality are still present in the spectrum of the product (red line).*

To overcome the incomplete conversion of the acetoacetate groups, a reaction with an excess of TREN (2.2 eq) was performed (Scheme 10b). The obtained product exhibited a more crosslinked network, confirmed by the increased value of gel content (74%) and by the disappearance of the stretching bands relative to the AcAc moieties (Figure 12).

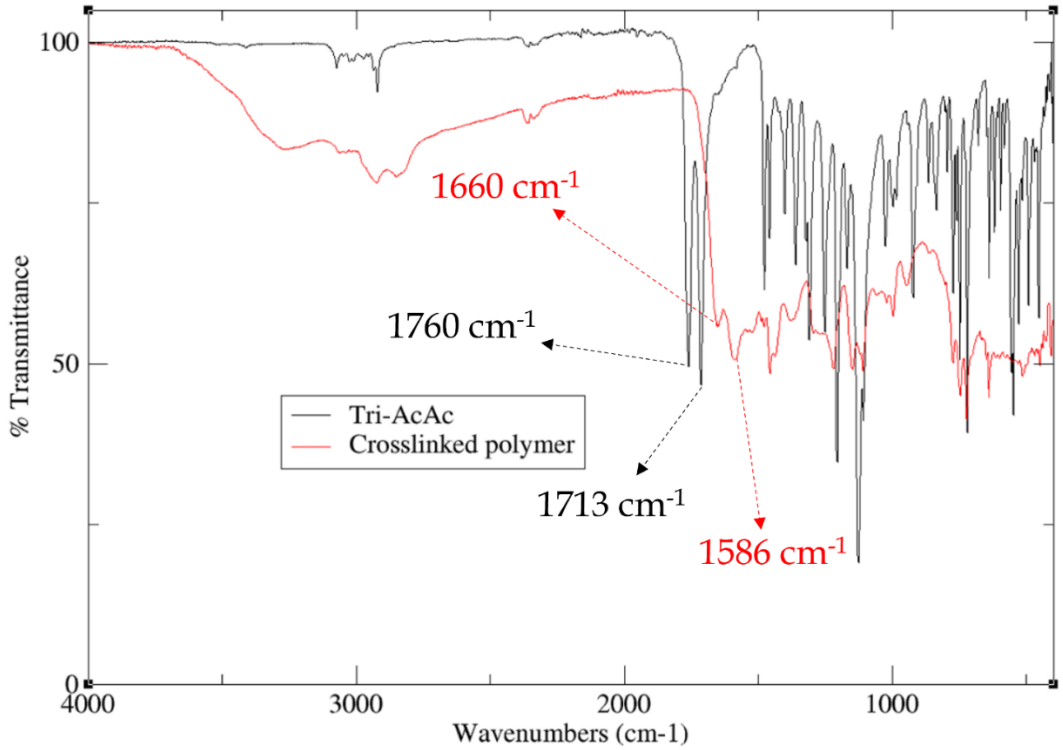

Figure 12 *FT-IR vitrimer cured with TREN in molar ratio 1:2.2.*

The glass transition (T_g) of this latter vitrimer was measured by differential scanning calorimetry (DSC), giving as value 85 °C.

Finally, a new approach for the recycling of a vitrimeric crosslinked polymer was investigated. The mixture was heated at 80 °C in acetonitrile with a large excess of *n*-butylamine to enable the exchange reactions with the monofunctionalized amine.[12] After 20 hours, the vitrimer was completely dissolved, suggesting the occurrence of the chemical recycling. To assess the presence of the vinylogous bands also in the crude, relative to the new formed vinylogous urethane moiety generated by the reaction with *n*-butylamine, a FT-IR was recorded. The spectrum showed the two characteristics bands at 1655 cm^{-1} and 1552 cm^{-1} (Figure 13).

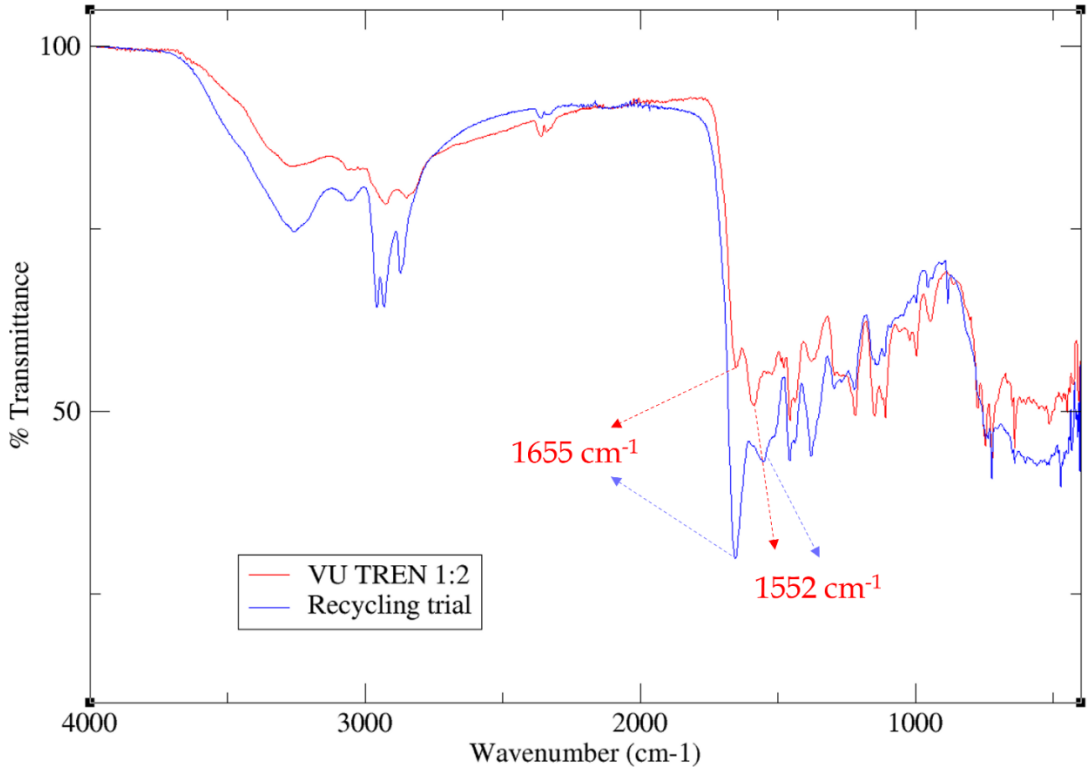

Figure 13 *FT-IR comparison before and after the reaction of the vitrimer with n-butylamine. The presence of the stretching bands relative to vinylogous urethane moiety confirmed the occurrence of the transamination exchange reaction with n-butylamine.*

Moreover, an NMR spectrum of the crude was recorded; it showed several peaks in the aromatic area, suggesting the presence in solution of triptycene moieties, a further proof of the depolymerization.

4.3. Conclusions

The replacement of crosslinked polyethylene is becoming a prominent issue to relieve the environmental footprint due to the end-life high voltage cables disposal. Therefore, the design of a new vitrimer which intrinsically presenting high free volume was identified as the best solution to address this problem. As building blocks, triptycene-based molecules were chosen thanks to the ability to create interstitial space around them.

The purpose was the development of a vinylogous transamination-based CAN, attainable by the reaction between aminic crosslinkers and acetoacetylated amorphous thermoplastics.

Several routes were explored to generate triptycene-based phenoxy resins, in which the triptycene unit ideally replaces the bisphenol A. The synthetic attempts concerned the

reactions between the diglycidylated triptycene with the hydroquinone homologous or a primary amine. The trials showed the formation of just oligomers even varying the conditions in terms of temperature, base/catalyst, and time.

For this purpose, a more straightforward approach was also studied, thus avoiding the challenging synthesis of the linear polymer and its functionalization. The 9,10-benzenoanthracene-1,4-diol was properly acetoacetylated, becoming a suitable raw material for the reaction with TREN, to generate a vinylogous urethane-based vitrimer.

Finally, future outlooks will be the assessment of the mechanical and rheological behavior and, meanwhile the measurement of the insulating properties to study if the generated vitrimer presents a lower dielectric constant than the currently used insulators, becoming suitable for the integration in a real system.

4.4. Experimental section

4.4.1. Monomer synthesis

Triptycene benzoquinone (1)

Anthracene (2.00 g, 0.011 mol) and 1,4-benzoquinone (1.22 g, 0.011 mol) were dissolved in 20 mL of toluene under reflux for 6 hours. The precipitated triptycene benzoquinone was filtered and washed with toluene and dried in a vacuum overnight (1.1059 g, 0.0039 mol, 70%).

^{1}H NMR (DMSO-d_6, 500 MHz): δ (ppm) = 7.48 (dd, J = 5.3, 3.2 Hz, 2H), 7.17 (ddd, J = 8.1, 5.4, 3.2 Hz, 4H), 7.07 (dd, J = 5.4, 3.2 Hz, 2H), 6.43 (s, 2H), 4.84 (s, 2H), 3.17 (s, 2H).

9,10-benzenoanthracene-1,4-diol (2)

Triptycene benzoquinone (1.1059 g, 0.0038 mol) was added to 14 ml of glacial acetic acid and was heated under reflux. 0.5 ml of 40% hydrobromic acid was slowly added to the reaction and the reaction was left to stir under reflux condition for 3 h and left to cool to room temperature, precipitating triptycene hydroquinone that is filtered and dried in the vacuum oven overnight (0.8932 g, 0.0031 mol, 82%).

^{1}H NMR (DMSO-d_6, 500 MHz): δ (ppm) = 8.82 (s, 2H), 7.38 (dd, J = 5.3, 3.2 Hz, 4H), 6.97 (dd, J = 5.4, 3.1 Hz, 4H), 6.30 (s, 2H), 5.79 (s, 2H).

MS: m/z: calculated for [M+H]+ = 287.11, experimental for [M+H]+ = 287.09.

9,10-benzenoanthracene-1,4-diol diglycidyl ether (3)

9,10-benzenoanthracene-1,4-diol (0.500 g, 0.00175 mol) and epichlorohydrin (2.744 mL, 0.035 mol) were added to a dried flask and the reaction was heated at 90 °C for 48 hours. Ethyl acetate was added to the reaction and washed with deionized water to remove the excess of epichlorohydrin. Organic phases were combined and dried with Na_2SO_4. Ethyl acetate was removed under vacuum and the pure product was collected as white solid after recrystallization in ethanol (0.6833 g, 0.0017 mol, 98%).
^{1}H NMR ($CDCl_3$, 500 MHz): δ (ppm) = 7.44 – 7.38 (m, 4H), 7.01 – 6.95 (m, 4H), 6.52 (s, 2H), 5.90 (s, 2H), 4.19 (dd, J = 11.3, 3.1 Hz, 2H), 3.92 (ddd, J = 11.3, 5.8, 1.3 Hz, 2H), 3.39 (dt, J = 4.3, 3.0 Hz, 2H), 2.93 (dd, J = 4.9, 4.1 Hz, 2H), 2.76 (ddd, J = 4.9, 2.7, 1.1 Hz, 2H).
MS: m/z: calculated for $[M+H]^+$ = 375.17, experimental for $[M+H]^+$ = 375.16.

9,10-benzenoanthracene-1,4-hydroquinone-bis(2-hydroxyethyl) ether (4)

9,10-benzenoanthracene-1,4-diol (0.1 g, 0.000349 mol) and K_2CO_3 (4.82 mg, 0.0000349 mol) were dissolved in 1 mL of DMF, and the reaction was led at reflux under argon. 0.092 mL (0.00105 mol) of ethylene carbonate in 0.5 mL of DMF were added into the flask drop by drop (about 1 h). After that, the reaction mixture was stirred at reflux overnight. A fine precipitate was obtained by pouring the reaction mixture into water. The solid was filtered and washed completely with water. A fine white solid was obtained after recrystallization from methanol and dried in the oven overnight (0.1163 g, 0.00031 mol, 89%).
^{1}H NMR (DMSO-d_6, 400 MHz): δ (ppm) = 7.42 (dd, J = 5.4, 3.2 Hz, 1H), 6.98 (dd, J = 5.4, 3.1 Hz, 1H), 6.63 (s, 2H), 5.95 (s, 2H), 4.93 (t, J = 5.7 Hz, 2H), 3.95 (t, J = 5.0 Hz, 4H), 3.75 (d, J = 5.2 Hz, 4H).
MS: m/z: calculated for $[M+H]^+$ = 399.16, experimental for $[M+H]^+$ = 399.15.

9,10-benzenoanthracene-1,4-diol diacetylacetate (5)

9,10-benzenoanthracene-1,4-diol (0.100 g, 0.000349 mol) was dissolved in 8 mL of dry toluene. After complete dissolution, tert-butylacetoacetate (1.157 mL, 0.00698 mol) was

added. The reaction was led under reflux for 48 hours. The excess of t-BuAcAc was removed under reduced pressure and the pure white product was collected after a trituration in hexane (0.146 g, 0.00032 mol, 92%).

^{1}H NMR (DMSO-d_6, 400 MHz): δ (ppm) = 7.40 (dd, J = 5.3, 3.2 Hz, 4H), 7.03 (dd, J = 5.4, 3.2 Hz, 4H), 6.85 (s, 2H), 5.92 (s, 2H), 4.14 (s, 4H), 2.39 (s, 6H).

MS: m/z: calculated for $[M+H]^+$ = 455.15, experimental for $[M+H]^+$ = 455.16.

4.4.2. Polymer synthesis

Linear polymer between 9,10-benzenoanthracene-1,4-diol (2) and 9,10-benzenoanthracene-1,4-diol diglycidyl ether (3) (synthetic general procedure)

In a dried Schlenk tube, 9,10-benzenoanthracene-1,4-diol, 9,10-benzenoanthracene-1,4-diol diglycidyl ether and the base/catalyst were dissolved in dry DMF (if K_2CO_3 was used as base, 18-Crown-6 ether was added in catalytic amount). The solution was degassed and then the reaction was led for 48/72 hours or 7 days at 120 °C. Afterwards, the crude was extracted with DCM and the organic layers were washed with acidic water. In some cases, when a fine precipitated was observed after precipitation in water, the solid was collected by filtration.

Linear polymer between 9,10-benzenoanthracene-1,4-diol diglycidyl ether (3) and primary amine (synthetic general procedure)

9,10-benzenoanthracene-1,4-diol diglycidyl ether, the primary amine and imidazole (catalytic amount) were dissolved in DMF. The reaction was led at 120 °C until the observation of the increase of the viscosity. Afterwards, the crude was extracted with DCM and the organic layers were washed with acidic water. The solvent was removed under reduced pressure.

Vitrimer synthesis (synthetic general procedure)

The acetoacetylated monomer was dissolved in chloroform (0.3 M) and acetic acid was added to the solution (70 mol%). Afterwards, TREN was added to the solution and stirred until gelation at 40 °C. The gel was filled onto a Teflon sheet and cured under for 24 hours at 100 °C *in vacuo*.

4.4.3. Gel fraction

A certain amount of the vitrimeric network was dispersed in acetone to have a total concentration of 1.71 mg/mL. The suspension was heated at 55 °C for 24 hours. The solid residual was collected by filtration and dried at 100 °C *in vacuo*.

4.4.4. Differential scanning calorimetry (DSC)

To determine the glass transition temperature (Tg) of the crosslinked polymer, Perkin Elmer model DSC6000 was used. 4 mg of the polymer was weighted into an aluminum pan. The measurement was performed under nitrogen flow (20 mL min^{-1}) in the temperature range between -50 °C and 250 °C. The thermal properties were analyzed using DSC data of the second and third heating curves.

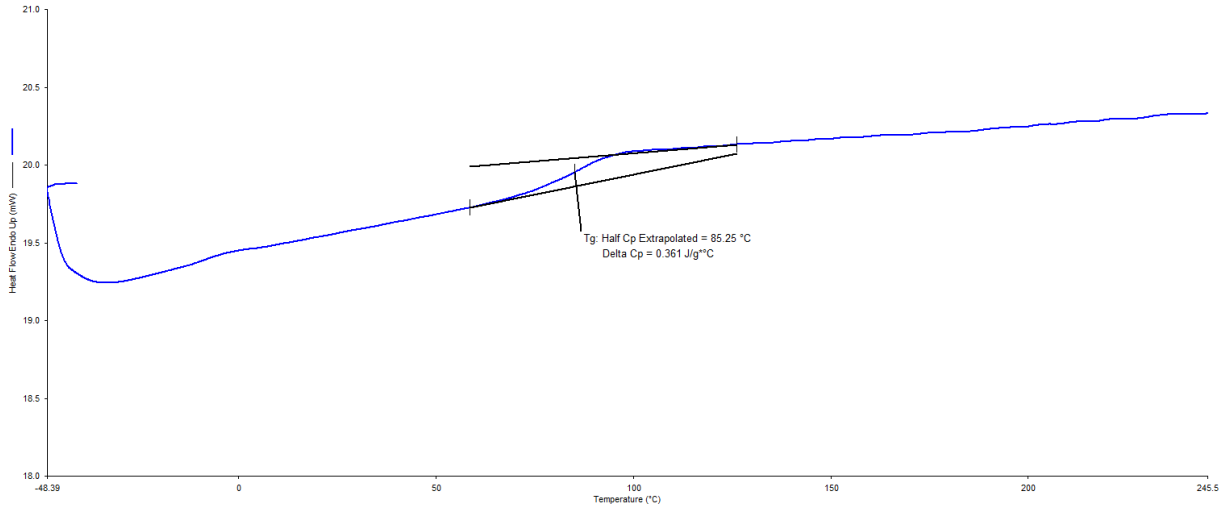

Figure 14 *DSC of the vitrimer cured with TREN in molar ratio 1:2.2.*

4.5. References

(1) T. M. Long, T. M. Swager, *J. Am. Chem. Soc.* **2003**, *125*, 14113-14119.

(2) C. V. Nguyen, K. R. Carter, C. J. Hawker, J. L. Hedrick, R. L. Jaffe, R. D. Miller, J. F. Remenar, H.W. Rhee, Philip M. Rice, M. F. Toney, M. Trollsås, and D. Y. Yoon, *Chem. Mater.* **1999**, *11*, 3080-3085.

(3) T. M. Swager, *Acc. Chem. Res.* **2008**, *41*, 1181-1189.

(4) R. J. Wojtecki, M. A. Meador, S. J. Rowan, *Nat. Mater.* **2011**, *10*, 14−27.

(5) Z. P. Zhang, M. Z. Rong, M. Q. Zhang, *Prog. Polym. Sci.* **2018**, *80*, 39−93.

(6) D. J. Fortman, J. P. Brutman, G. X. De Hoe, R. L. Snyder, W. R: Dichtel, M. A. Hillmeyer. *ACS Sustainable Chem. Eng.* **2018**, *6*, 11145−11159.

(7) L. C. H. Moh, J. B. Goods, Y. K., T. M. Swager, *J. Membrane Sci.* **2018**, *549*, 236–243.

(8) M. Fache, B. Boutevin, S. Caillol, *Green Chem*. **2016**, *18*, 712-725.

(9) W. C. Shih, C. C. M. Ma, *J. Appl. Polym. Sci*. **1999**, *73*, 2369–2376.

(10) Y. Liu, S. R. Turner, G. Wilkes, *Macromolecules* **2011**, *44*, 4049–4056.

(11) P. Haida, G. Signorato, V. Abetz, *Polym. Chem.* **2022**, *13*, 946-958.

(12) J. Zhao, Z. Zhang, L. Cheng, R. Bai, D. Zhao, Y. Wang, W. Yu, X.Yan, *J. Am. Chem. Soc.* **2022**, *144*, 872−882.

Chapter 5

Synthesis and Spectroscopic Characterization of a Supramolecular Complex as Fluorescent Probe for Self–reporting Polymers

5.1. Introduction

The use of polymeric composites[1] as structural materials has exponentially grown in the recent decades because of their light-weight combined with excellent mechanical properties. However, they experience stresses during their lifetime, which can result in micro damages (e.g., low-speed impacts). The growth of these microscopic fractures induces the catastrophic failure of the material.

Therefore, the nondestructive detection of internal stress in composites becomes the focus for the prevention of structural failures, contributing to reach a longer service life. Self-reporting polymers, able to carry out autonomous diagnostic functions, are the best solution to address this problem. They can highlight the damage or the exposure to excessive stress through signals of various nature.[2-17]

Most of the options proposed in literature are based on mechanochemistry, where a mechanical stress is used as stimulus to promote chemical reactions in polymers. An example of this type of application is given by the system showed in Figure 1 in which the spiropyran, the mechanophore, undergoes a reversible reaction of heterocyclic ring opening after the application of a tensile force. Therefore, the molecular skeleton changes and, consequently, the emission wavelength varies, resulting in a color change, from colorless (spiropyran) to purple (merocyanine).[18]

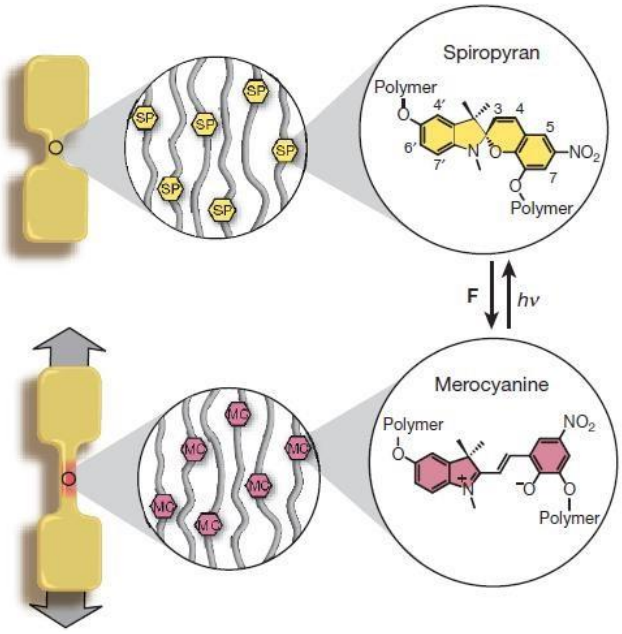

Figure 1 *Conversion between spiropyran form (colorless) and merocyanine form (purple) after the application of a tensile force.*[18]

The most recent damage-reporting strategies are based on supramolecular mechanoluminophores, which transduce the localized stress in the material into a detectable fluorescence signal. The turning on of the fluorescence, upon dissociation of the complex, represents an efficient, sensitive, simple, nondestructive, and real time reporting tool to detect high-strain regions. Moreover, to have a fluorescence response triggered by a strain, it is sufficient to have a very low concentration of the probe crosslinked into the material. Since it is a tiny amount, it does not modify any mechanical performances of the matrix.

Among the examples of mechanoluminophores reported in literature, a self-diagnostic poly(dimethylsiloxane) (PDMS) elastomer, containing a supramolecular probe based on nonfluorescent complex, has been studied by our research group (Figure 2).[19] The high-strain affected regions provide an easily detectable turning on of the fluorescence due to the mechanical-induced dissociation of the supramolecular complex.

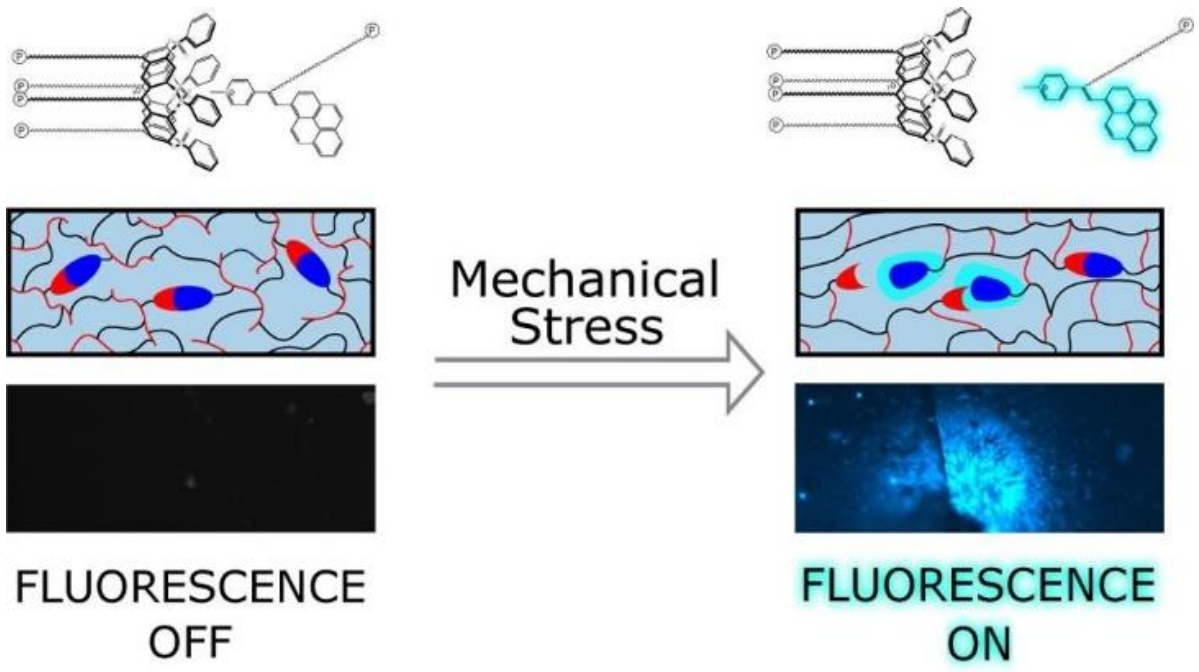

Figure 2 *Schematic representation of the self-reporting polymer based on a tetraphosphonate cavitand-pyrene complex.*[19]

As demonstration of the versatility of this approach, the incorporation of a cucurbit[8]uril (CB[8]) based ternary complex as an additive in carbon fiber epoxy composite material was reported. The complex comprises a fluorescent guest and a quencher, held in spatial proximity by the host molecule. The mechanical stress is responsible for the turn on of the fluorescence due to the mechanical-induced release of

one of the two guest molecules from the host, hence the distance between fluorophore and quencher is no longer optimal to establish a proper quenching energy transfer interaction (Figure 3).[20]

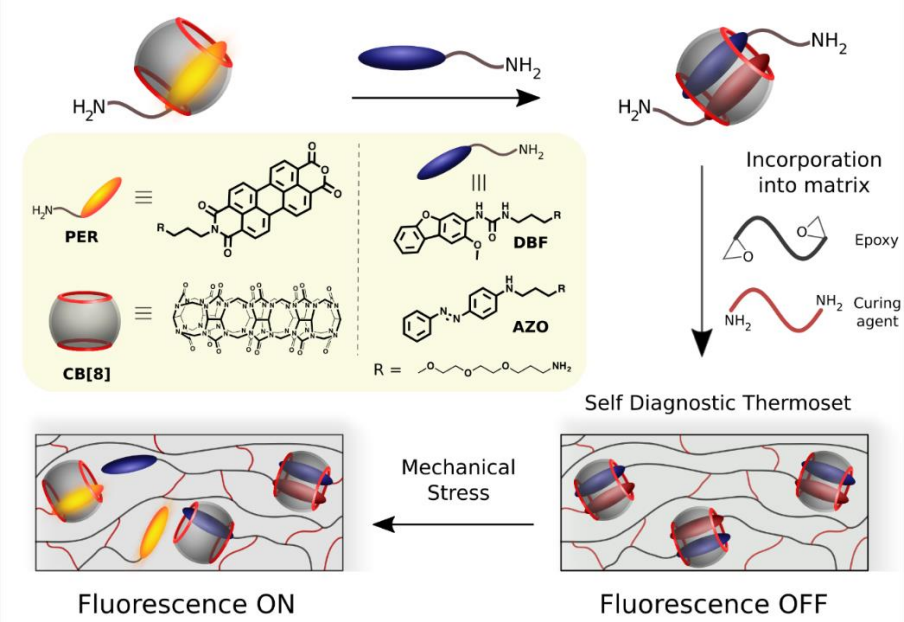

Figure 3 *Schematic representation of the working principle and components of the damage reporting carbon fiber-epoxy resin composites.*[20]

The purpose of this study is to introduce self-diagnostic properties in a polyurethane matrix. A phenyl tetraphosphonate cavitand in which one of the aliphatic chains at the lower rim has a terminal -OH group was used as host (Scheme 1, right). The guest was an N – methylated pyridinium salt conjugated to a pyrene, functionalized with a ω-hydroxy alkyl chain (Scheme 1, left). Upon complexation, the emission of the guest is quenched through an electron-transfer process between the electron-poor methylpyridinium moiety of the guest and the electron-rich cavity of the cavitand.[21] The complex was pre-formed in solution and covalently attached to a polyurethane matrix to investigate its mechanoresponsive behavior.

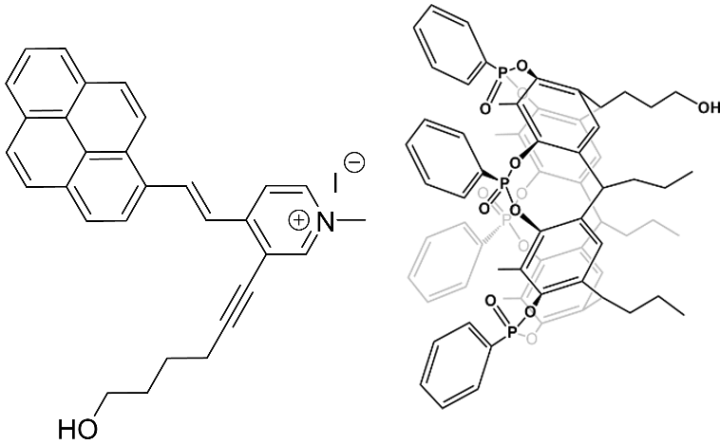

Scheme 1 *Host-guest complex of N-methyl pyridinium salt (guest, left) and phenyl tetraphosphonate cavitand mono -OH,* ***CavPOPh (mono -OH)*** *(host, right).*

5.2. Results and discussion

5.2.1. Synthesis of guest and host molecules

The first part of the thesis deals with the synthesis and the characterization of the N–methylpyridinium salt, **PyPyr-OH**.

It was prepared following a three steps synthesis, as shown in Scheme 2.

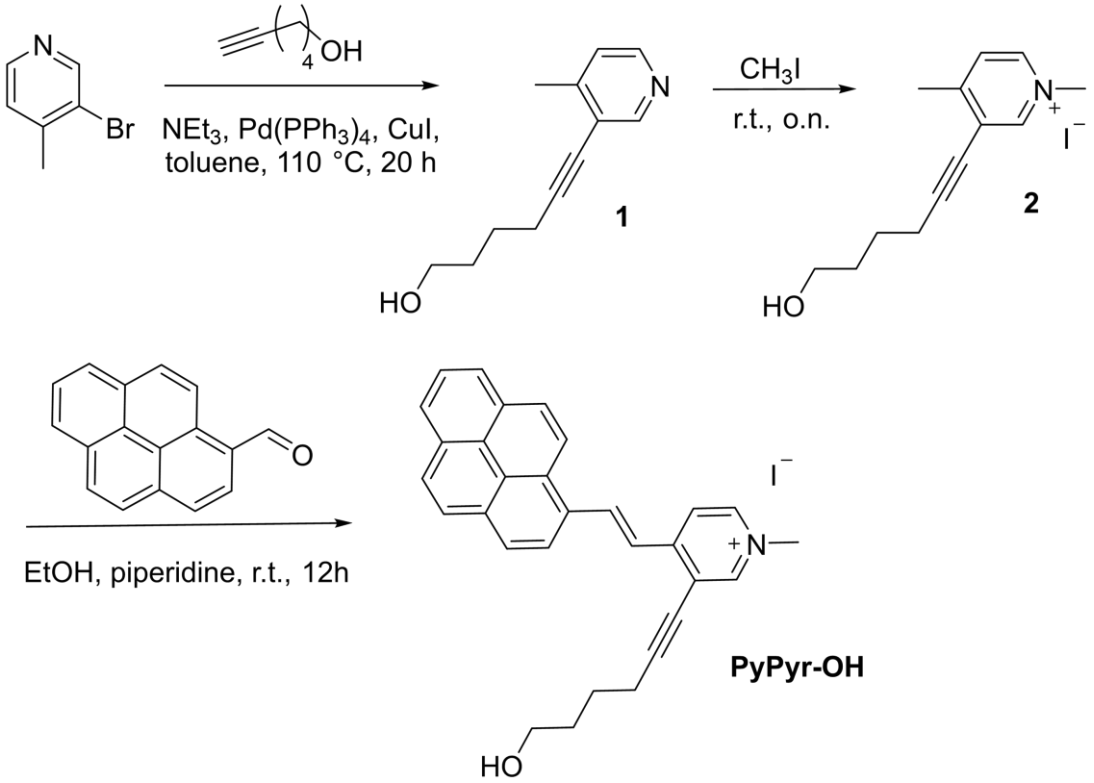

Scheme 2 *Synthetic scheme of* ***PyPyr-OH****.*

In the first step, the 6-(4-methylpyridin-3-yl)hex-5-yn-1-ol intermediate (**1**) was obtained *via* a Sonogashira coupling between 3-Bromo-4-methylpyridine and 5-Hexyn-1-ol. The reaction was carried out by solubilizing both reagents together in dry toluene with NEt_3, a non-nucleophilic base needed to allow the deprotonation of the terminal alkyne. Then $Pd(PPh_3)_4$ and CuI were added to catalyze the coupling cycle. The reaction mixture was stirred for 20 hours at 110 °C. The crude was then purified over a silica gel chromatography to obtain the target product as a dark brown oil. The product **1** was obtained pure with a 75% yield.

In the second step,[22] the pyridine nitrogen acted as nucleophile in a nucleophilic substitution reaction using two equivalents of CH_3I as electrophile. After stirring the reaction mixture overnight at room temperature, the unreacted CH_3I is removed under vacuum. The 3-(6-hydroxyhex-1-yn-1-yl)-1,4-dimethylpyridin-1-ium iodide (**2**) was obtained quantitatively.

The final step involved the reaction between **2** and pyrene-1-carbaldehyde.[23] The reaction was conducted mixing the reagents in absolute EtOH under inert atmosphere in presence of a catalytic amount of piperidine and stirring for 12 hours at 80 °C. The non-nucleophilic base deprotonated the methyl group in the position 4, obtaining a primary carbanion stabilized by the resonance of the pyridinium electron-poor ring. The carbanion acted as a nucleophile, reacting with the electrophilic aldehyde function of pyrene-1-carbaldehyde. The crude was purified by filtration and the product was obtained with 65% yield. In these conditions, the ^1H NMR spectrum showed an unexpected pattern of signals. (Figure 4, Top).

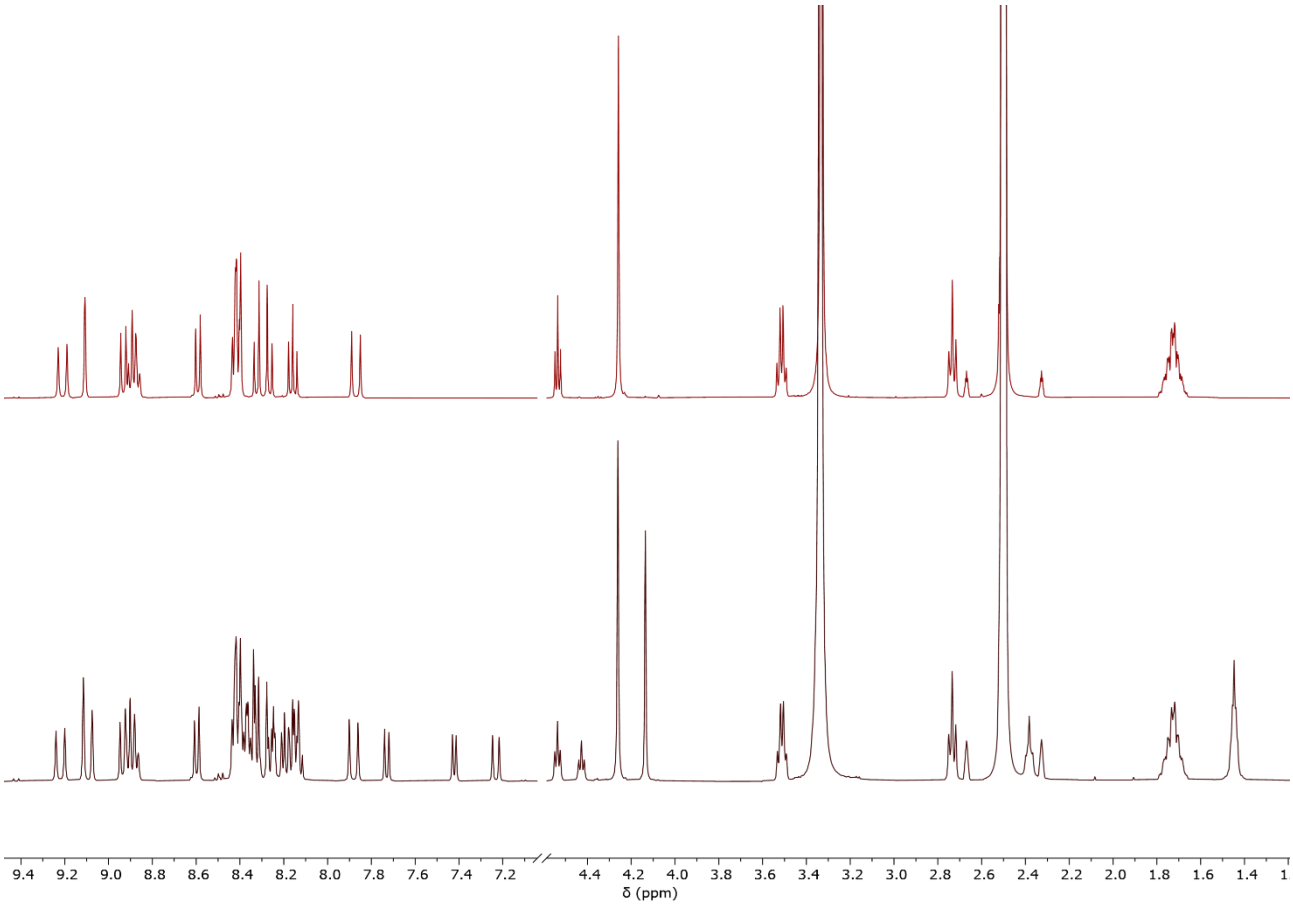

Figure 4 *Comparison between ^{1}H NMR spectra of* ***PyPyr-OH*** *kept in the dark (Top) and exposed to the light (Bottom).*

The observed splitting of the signals can be explained with the occurrence of the **PyPyr-OH** photoisomerization, indeed the light exposure led to the formation of both the thermodynamic product (*trans* isomer) and the kinetic product (*cis* isomer). To prevent the light-promoted isomerization, the reaction was performed in the dark at room temperature and the corresponding ^{1}H NMR spectrum presented a different pattern (Figure 4, Bottom). The assignment of the peaks is described below (Figure 5).

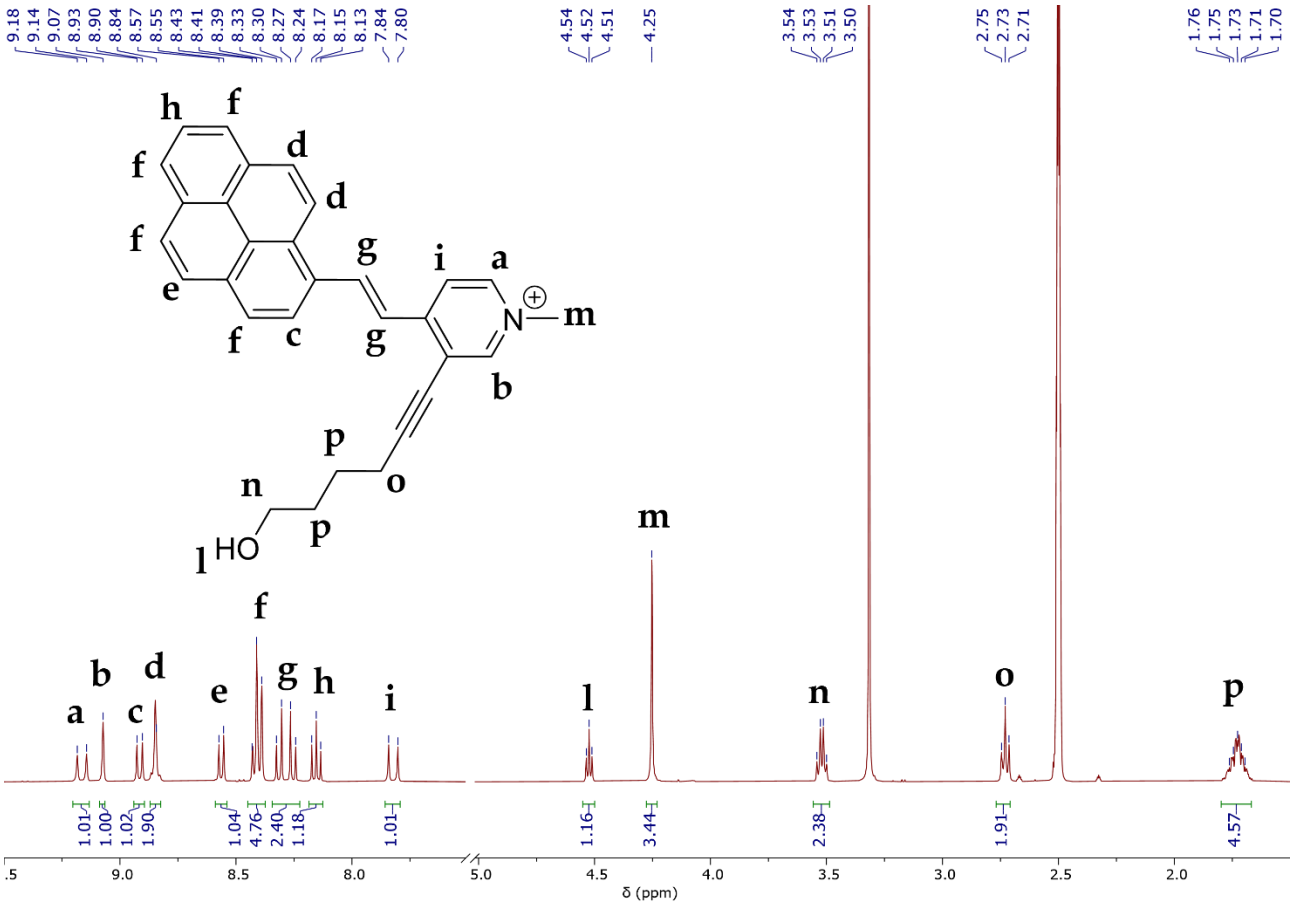

Figure 5 *^{1}H NMR (DMSO–d_6) spectrum of* ***PyPyr-OH****.*

The two doublets at 8.31 ppm and 8.25 ppm are relative to the -CHs of the double bond as diagnostic signals. The pyrene moiety can be distinguished from the triplet at 8.43 ppm and a series of doublets of the aromatic -CHs in the range between 8.40 ppm and 9.00 ppm. The N–methyl pyridine portion is characterized by four signals: (i) the singlet at 9.07 ppm is assigned to the aromatic -CH between the nitrogen and the chain; (ii) the doublet at 9.16 ppm of the -CH in ortho position with respect to N; (iii) the doublet at 7.82 ppm of the -CH in *meta* position with respect to N; (iv) the singlet at 4.25 ppm of the -CH_3. Finally, the chain with the terminal -OH give rise to four peaks: (i) the triplet at 4.52 ppm of the -OH proton; (ii) the quadruplet at 3.52 ppm of the -CH_2 adjacent to the -OH; (iii) the multiplet at 1.76 – 1.70 ppm of the two following -CH_2; (iv) the triplet at 2.73 ppm of the -CH_2 adjacent to the alkyne.

The host **CavPOPh (mono -OH)** was previously synthetized according to the following synthetic scheme (Scheme 3).

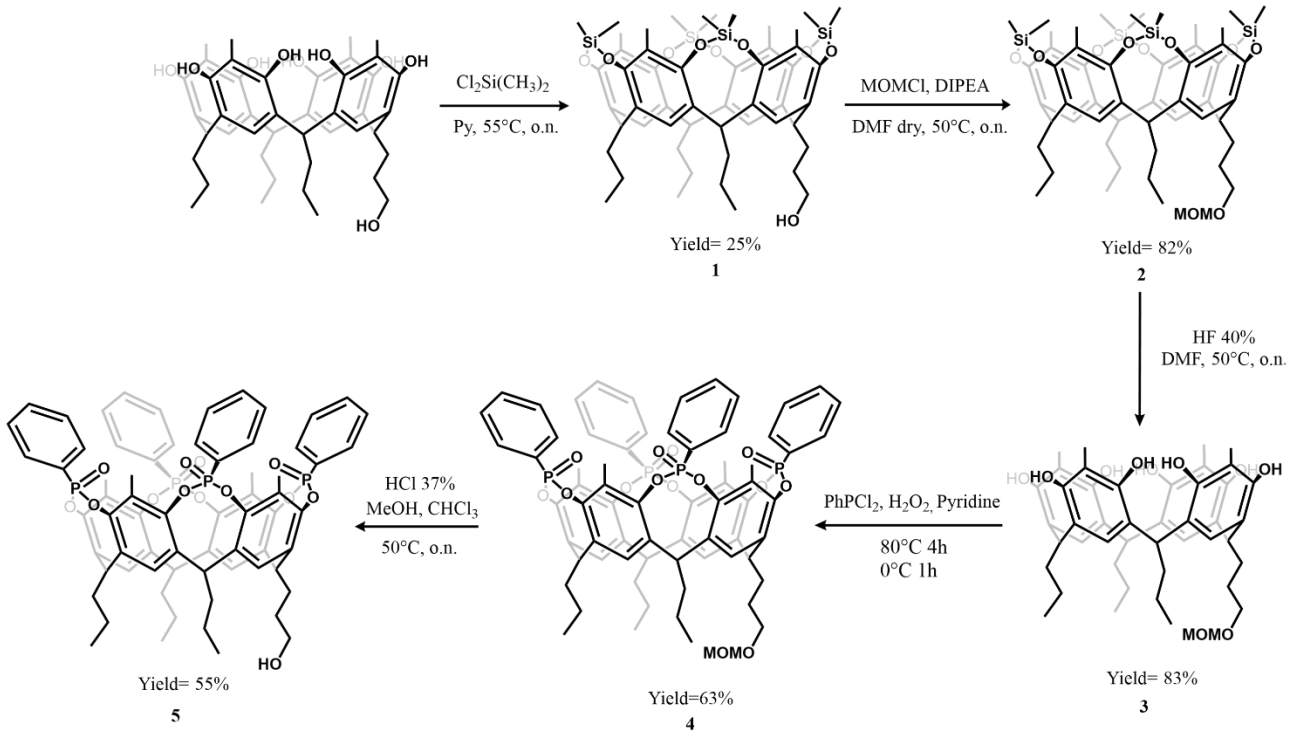

Scheme 3 *Synthetic scheme of* ***CavPOPh (mono -OH)****.*

The complexation of **PyPyr-OH** with mono -OH phenyl tetraphosphonate cavitand was monitored through a ^{31}P NMR titration (Figure 6).

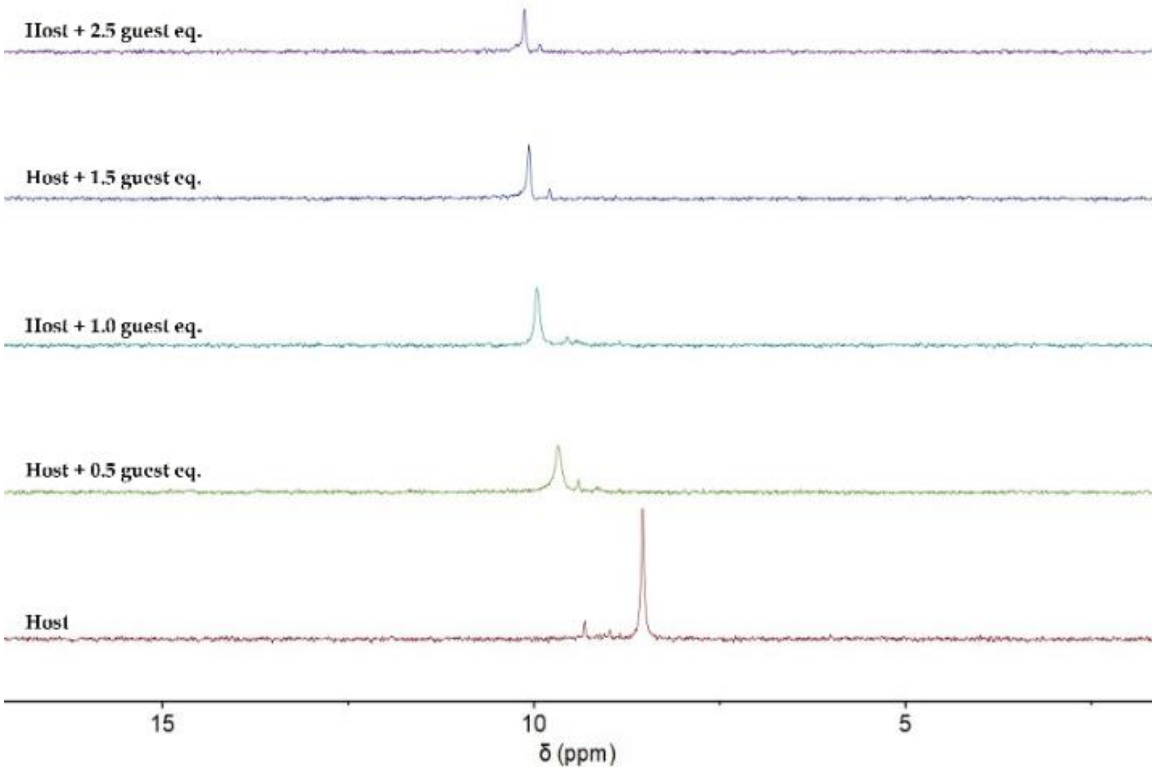

Figure 6 *^{31}P NMR titration of mono -OH phenyl tetraphosphonate cavitand with* ***PyPyr-OH*** *(methanol–d_4).*

Consecutive additions of aliquots of guest **PyPyr-OH** to the cavitand led to a progressive downfield shift of the signal associated to the ^{31}P of the inward facing phosphonate groups, indicating the complexation of the methyl-pyridinium moiety by the tetraphosphonate cavitand.

5.2.2. Spectroscopic characterization of the supramolecular probe in solution

The photophysical behavior of the supramolecular complex was investigated.

First, **PyPyr-OH** and **CavPOPh (mono -OH)** stock solutions were prepared. Since fluorescence is a very sensitive technique, the concentration used to perform the measurements were in the order of µM, thus preventing the undesired inner filter, a re-absorption of the emitted light in highly concentrated samples. The solvents suitable for the solubilization of the host and the guest are DMSO and MeOH. The choice fell on MeOH because DMSO was able to solvate the cationic guest, disfavoring the complexation.

Therefore, a stock solution of **PyPyr-OH** in MeOH with a concentration of 4.0 µM was prepared. The solution of **CavPOPh (mono –OH)** was made up to the mark with the 4.0 µM solution of **PyPyr-OH** to keep constant the concentration of the guest, thus avoiding dilution effect throughout the titration. The final concentration of **CavPOPh (mono –OH)** was $0.315x10^{-3}$ M. The titration was performed by adding to a quartz cuvette, containing 2 mL of 4.0 µM solution of guest, increasing equivalents of host.

Then, the absorption titration was performed (Figure 7). The spectrum of **PyPyr-OH** shows two absorption maxima, at 325 and at 450 nm respectively, typical of molecules presenting pyrene moieties. From the titration spectra, the maximum at 325 nm remains constant upon each addition of host equivalents, while the one at 450 nm has a slight hypsochromic shift.

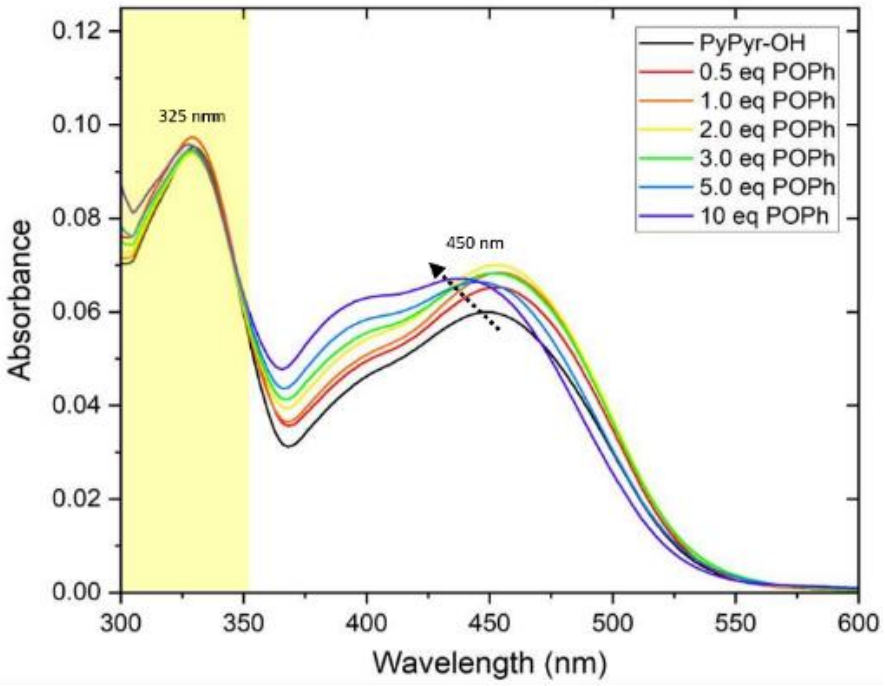

Figure 7 *Absorption titration of* ***PyPyr-OH*** *with* ***CavPOPh (mono -OH)***.

Exciting both at 325 and at 450 nm, the fluorescence emission was observed at around 610 nm. Since the absorption at 325 nm remained constant during the titration, the latter was chosen as excitation wavelength.

At the same time, a fluorescence emission titration was performed (Figure 8). **PyPyr-OH** had an emission wavelength at about 610 nm and it was possible to notice an evident quenching of the band of the guest by increasing the amount of added host.

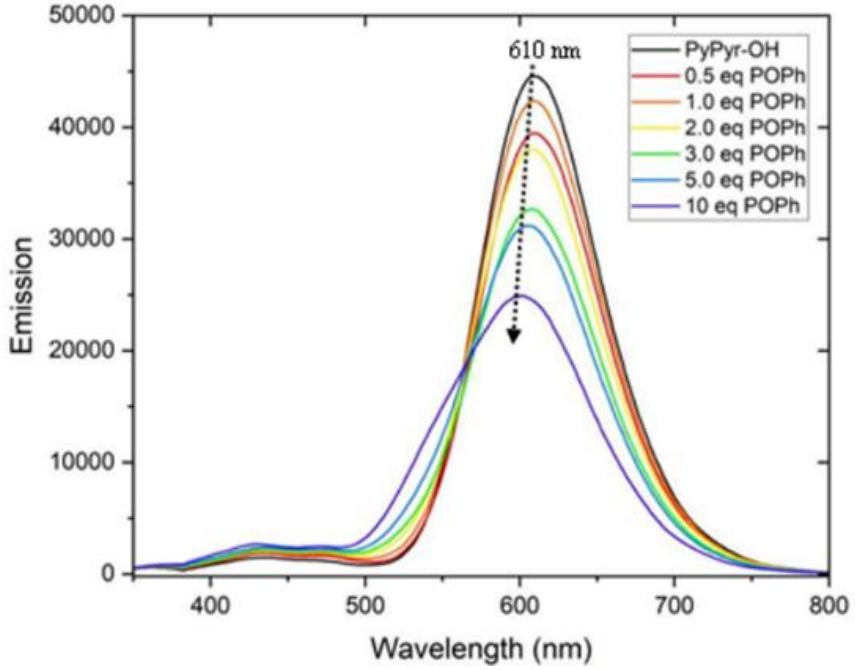

Figure 8 *Fluorescence emission titration of* ***PyPyr-OH*** *with mono-OH phenyl tetraphosphonate cavitand using* λ_{exc} *= 325 nm.*

The absorption and emission spectra were immediately recorded after adding the corresponding host equivalent. Since the emission spectrum relative to the addition of 1.0 equivalent of host showed higher emission than 0.5 equivalents one, a kinetic study of the complex formed by **PyPyr-OH** and the cavitand was performed to assess the time needed to reach the stabilization.

Using the same procedure described above, guest and host stock solutions were prepared. The measurements were performed on a sample containing 1 equivalent of **PyPyr-OH** and 5 equivalents of the cavitand immediately after adding the host, after 1 hour and after 24 hours.

The kinetic analysis of the absorption spectra showed that the system had the same identical trend after one hour and after 24 hours (Figure 9): this means that the complex took at least one hour to stabilize itself.

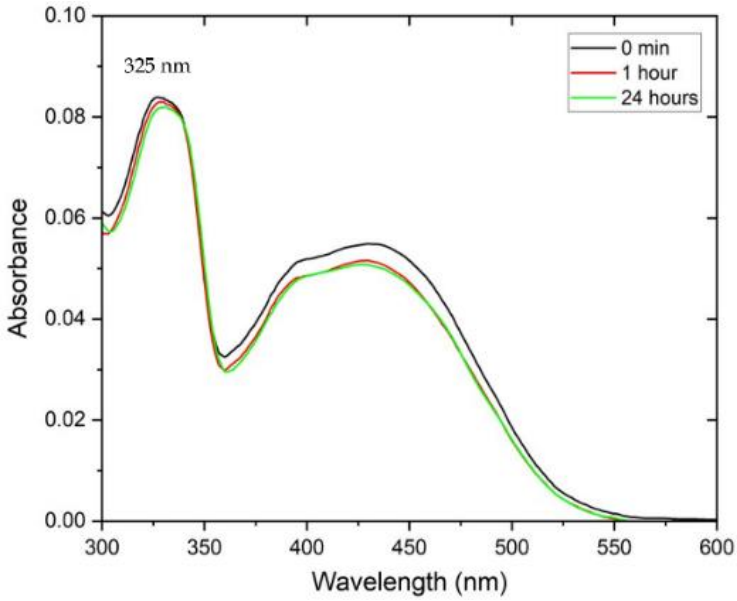

Figure 9 *Absorption spectra of* ***PyPyr-OH*** *with 5 equivalents of* ***CavPOPh (mono-OH)*** *immediately recorded after adding the host (black line), after 1 hour (red line) and after 24 hours (green line).*

Considering the time stabilization, a set of vials, each containing the diluted guest solution (4 µM) and increasing host equivalents, was prepared in advance; absorption and emission titration spectra were recorded 24 hours after.

The UV–Vis absorption spectra display the same two maxima at 325 nm and 450 nm, like the previous titration. Performing the absorption measurements 24 hours after adding host equivalents, the spectra had an absorbance value at 325 nm which was double the value recorded immediately after the addition. Meanwhile, the maximum at 450 nm showed the same slight hypsochromic effect throughout the complexation (Figure 10).

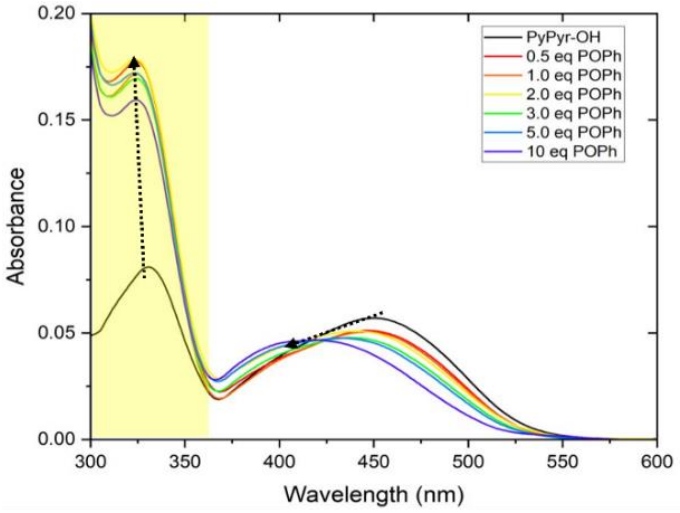

Figure 10 *Absorption titration of* ***PyPyr-OH*** *with* ***CavPOPh (mono -OH)*** *collected 24 hours after adding the corresponding host equivalents.*

An odd behavior was also observed on the fluorescence emission spectra. Indeed, the appearance of a new emission maximum at about 370 nm had no explanation (Figure 11). During the analysis, different interference sources were studied: (i) an effect from the solvent was investigated by performing again the same titration but using HPLC grade methanol to exclude the presence of some emissive impurities; (ii) an effect from the cavitand was examined by recording the fluorescence emission spectrum of the host. None of the previous assumptions provided an answer to the formation of the emission peak at 350 nm. Meanwhile, the other maximum at about 610 nm had the same trend of the previous titration and a quenching by increasing the host equivalents was observed again.

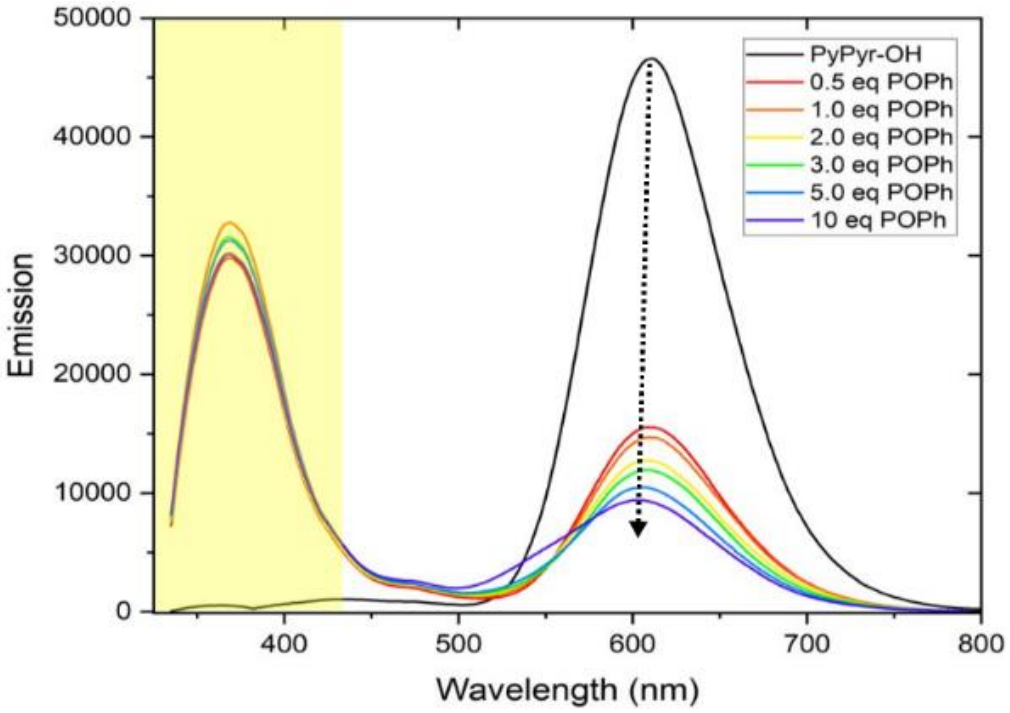

Figure 11 *Emission titration of* ***PyPyr-OH*** *with mono -OH phenyl tetraphosphonate cavitand using* λ_{exc} *= 325 nm registered 24 hours after adding the corresponding host equivalents.*

To complete the investigation on this supramolecular system, a lifetime measurement was performed (Figure 12). When complexed within a cavity, the value of the fluorescence lifetime of a molecule increases because, in a restricted area, nonradiative relaxation is less likely. The registered spectra showed an increased lifetime (τ = 1.48 ns for **PyPyr-OH** with 1.0 host equivalents) that confirmed the complexation of **PyPyr-OH** within the cavity of the host.

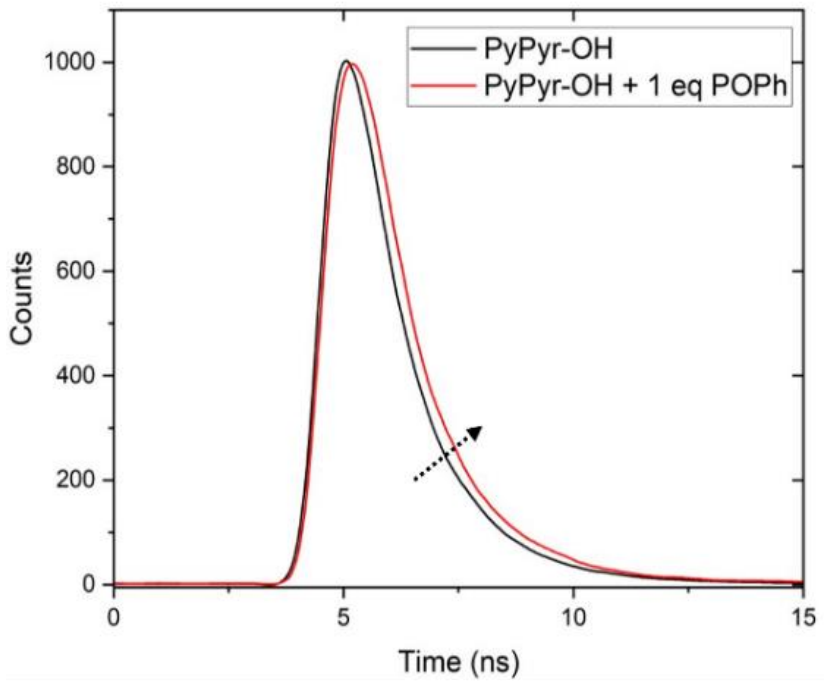

Figure 12 *Lifetime titration of* ***PyPyr-OH*** *with mono -OH phenyl tetraphosphonate cavitand registered 24 hours after adding the corresponding host equivalents.*

The target probe was based on **PyPyr-OH** and the mono -OH phenyl tetraphosphonate cavitand, necessary to crosslink with the polyurethane matrix. To verify that the functionalization was pivotal to make the polymeric matrix stress sensitive, it was necessary to develop a reference system, with an analogous photophysical behavior, but that did not possess terminal -OH groups, hence not connected to the polymeric matrix. The chosen guest for this purpose is **PyPyr**,[19] i.e., a **PyPyr-OH** homologous without the terminal -OH and the corresponding cavitand without -OH (Scheme 4).[21]

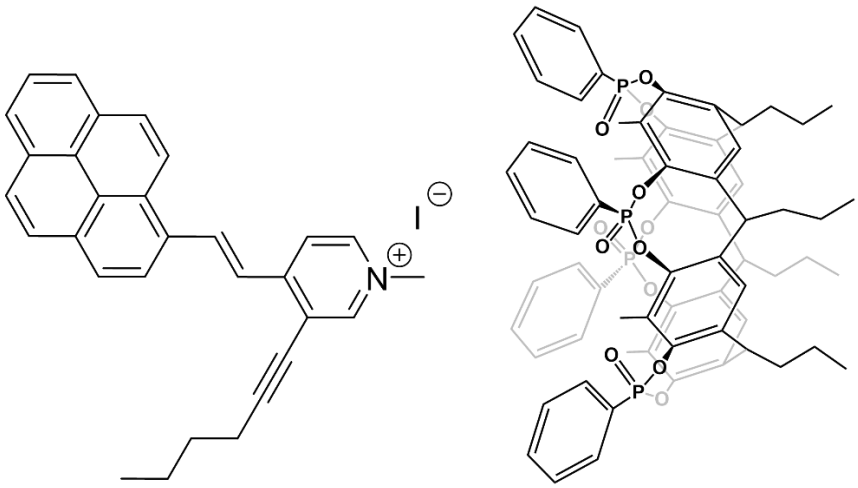

Scheme 4 *Host-guest complex of N-methyl pyridinium salt (guest, left) and phenyl tetraphosphonate cavitand CavPOPh (host, right).*

Therefore, stock solutions with the same procedure described above were prepared and the titration was performed using a 4 μM methanol solution of **PyPyr**. The recorded spectra displayed the same identical behavior of **PyPyr-OH**, with an emission maximum at the same wavelength (i.e., 610 nm), showing both quenching by increasing the host equivalents and the appearance of the band at 350 nm (Figure 13).

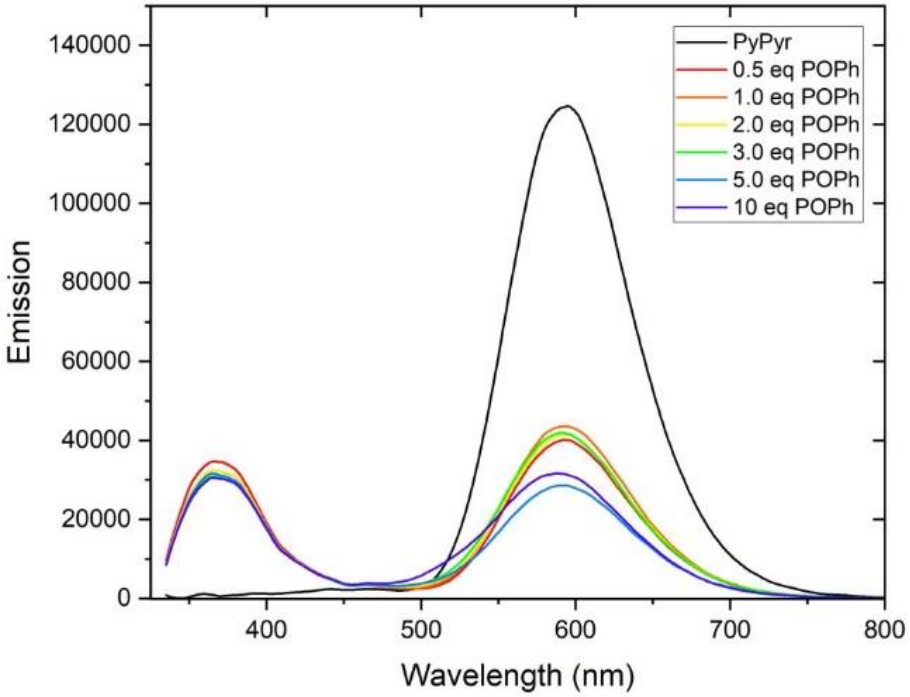

Figure 13 *Emission titration of* ***PyPyr*** *with CavPOPh (mono -OH) using* λ_{exc} *= 325 nm registered 24 hours after adding the corresponding host equivalents.*

5.2.3. Spectroscopic characterization of the supramolecular probe in matrix

The spectroscopic characterization of the complex described above was preparatory to investigate the probe once integrated in a polymeric matrix. Therefore, the pre-formed host-guest complex was introduced into a commercial polyurethane matrix by dispersion of a relevant solution in THF.

First, the complex was dissolved in the minimum amount of dry THF, and the solution was homogenized into the polyol component of the polyurethane (PC 224 GLASS MR). The solvent was then removed under vacuum at room temperature. After the evaporation of THF, the isocyanate component (G124) was added to the suspension and rapidly homogenized. Any trace of air inside the polyurethane was removed under vacuum before pouring the matrix into the mold.

The commercial polyurethane matrix used for these studies was a rigid polymer formed by reaction of a polyol (PC 224 GLASS MR) and an isocyanate (G124). This polyurethane has a glass transition, T_g, between 80 °C and 86 °C and a maximum strain of the 5-7%. Moreover, it possesses a window of transparency above 450 nm, verified by recording the transmittance spectrum of pristine polyurethane (Figure 14).

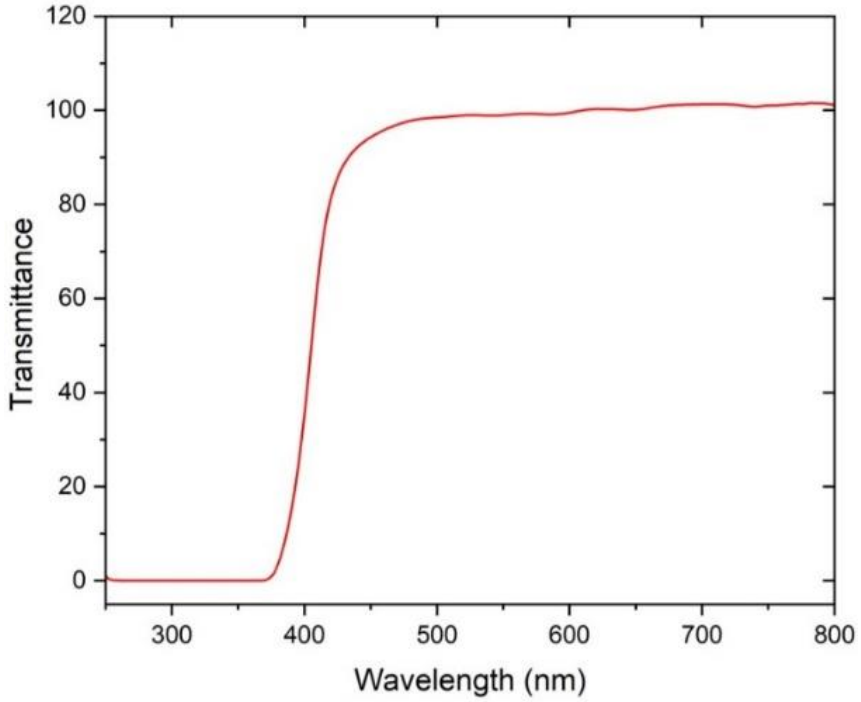

Figure 14 *Transmittance spectrum of polyurethane matrix composed by PC 224.*

To prevent any change in the mechanical properties of the polyurethane, a 0.0005% of the supramolecular probe was added as cross-linking probe to the matrix.

To verify if the target system displayed the same behavior (i.e., fluorescence emission quenching upon complexation) when integrated within the matrix, preliminary studies in cuvettes of the supramolecular complex in the polymerized polyurethane were performed. Three cuvettes containing: (i) the 0.0005 % of target complex, (ii) the reference complex and (iii) the **PyPyr-OH** guest are prepared.

The procedure to prepare the samples was the same described above: (i) the probe under investigation was dissolved in the minimum amount of dry THF and homogenized to the polyol component, (ii) all solvent traces were removed under vacuum; (iii) the isocyanate component was added to the suspension and quickly homogenized; (iv) any trace of air was removed under vacuum and the polyurethane thus obtained was poured into UV grade PMMA disposable cuvettes.

Then absorption (Figure 15) and fluorescence emission spectra (Figure 16) were recorded.

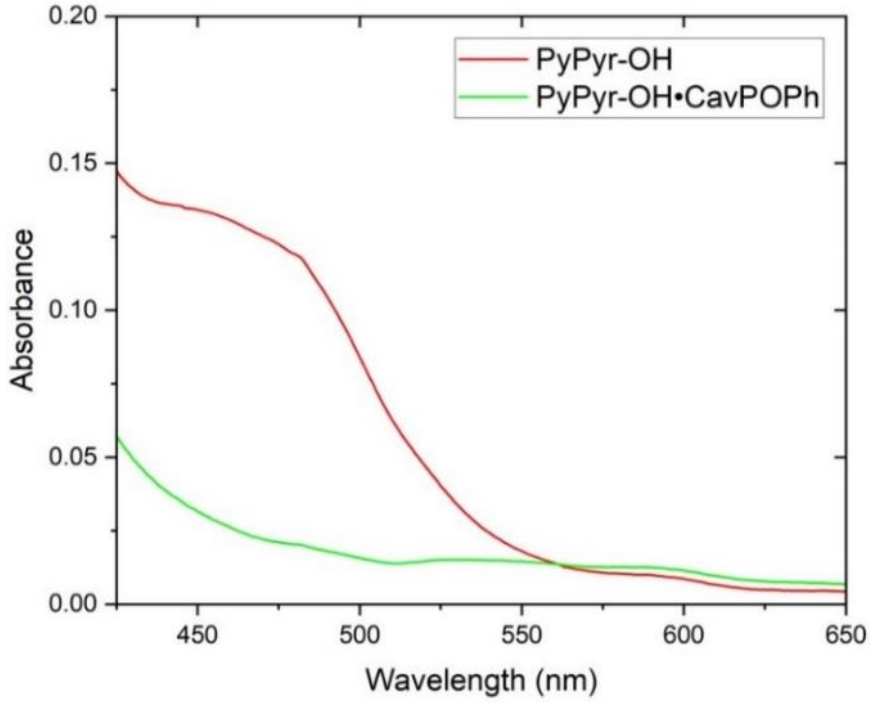

Figure 15 *Absorption spectra of polyurethane with* ***PyPyr-OH*** *(red line) and* ***PyPyr-OH•CavPOPh (mono - OH)*** *(green line).*

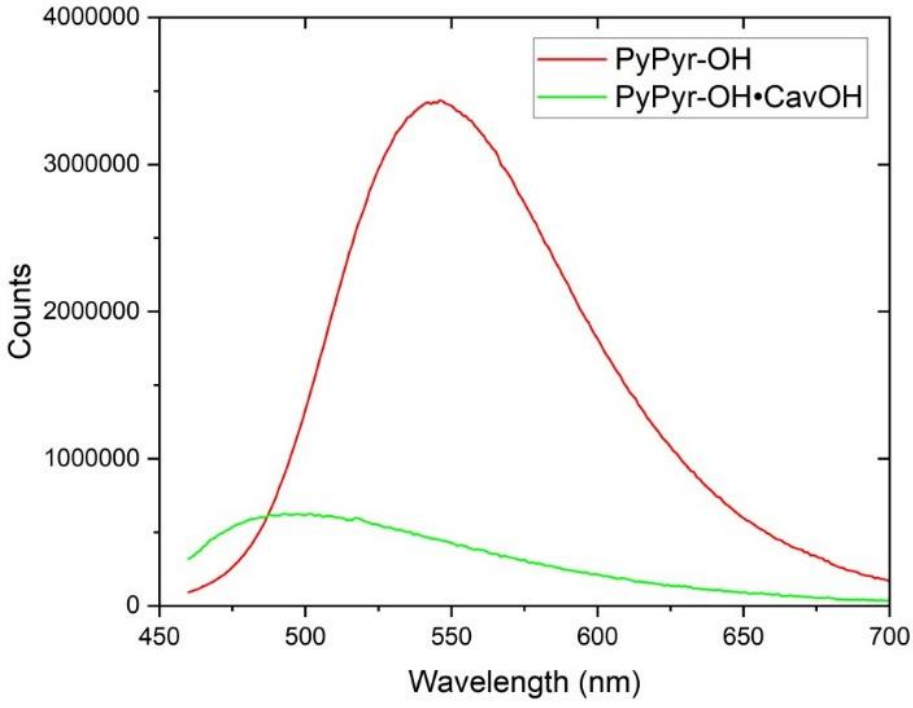

Figure 16 *Fluorescence emission spectra of polyurethane with* ***PyPyr-OH*** *(red line) and* ***PyPyr-OH*** *with mono - OH phenyl tetraphosphonate cavitand (green line),* λ_{exc} *= 450 nm.*

The spectra confirmed the strong fluorescence of the guest and its quenching upon complexation.

Once the behavior of the target was proved even within the matrix, loaded polyurethane specimens were prepared and stress tests were performed.

Four types of specimens were obtained: (i) a pristine polyurethane used to test the mechanical properties of the matrix, (ii) **PyPyr-OH** dispersed in the PU, (iii) the target crosslinked complex and (iv) the reference complex dispersed in the matrix, but not crosslinked.

Figure 17 *Integer specimens of polyurethane matrix containing* ***PyPyr-OH*** *(left) and* ***PyPyr-OH•CavPOPh (mono -OH)*** *(right).*

From the picture above (Figure 17) it is possible to observe that the specimen containing the guest presented a more evident yellowish color than the supramolecular complex–dispersed one. This color difference was due to the quenching of the fluorescence emission intensity when the guest was complexed.

The procedure to make the samples was the same described above: (i) the probe under investigation was dissolved in the minimum amount of dry THF and homogenized into the polyol, (ii) all solvent traces were removed under vacuum; (iii) the isocyanate was added to the suspension and quickly homogenized (iv) any trace of air was removed under vacuum and the polyurethane thus obtained was poured into Teflon mold to obtain dog-bone specimens.

To verify the behavior of the probe, the purpose was to study the fluorescence emission on three types of specimens (Figure 18): (i) an integer one; (ii) an elongated one, to

understand if it was possible to detect early-stage damages; (iii) a broken one to observe the fluorescence after the break.

Figure 18 *Specimens of polyurethane containing* ***PyPyr-OH****: (from left to right) integer, elongated at 2.5 % and broken.*

First, mechanical properties of the polyurethane matrix were tested on several pristine specimens through tensile test. The specimens reached an elongation of 5 % of the whole length before rupture. Knowing that, elongated specimens with an extension of 2.5 %, i.e., a 50 % of the maximum elongation before the break, were obtained.

After the mechanical tests were carried out, fluorescence emission studies were performed on every sample with a two photons microscope. For every specimen two different areas were investigated to verify that the probe was well homogenized within the matrix and make a qualitatively comparison of the behavior on different regions of different specimens. First, two different areas in the center of the integer specimen containing **PyPyr-OH** only were investigated as control experiment (Figure 19). From the images collected it was possible to observe that the guest was well homogenized within the whole matrix and possessed a high fluorescence emission with an intensity of about 4000 counts.

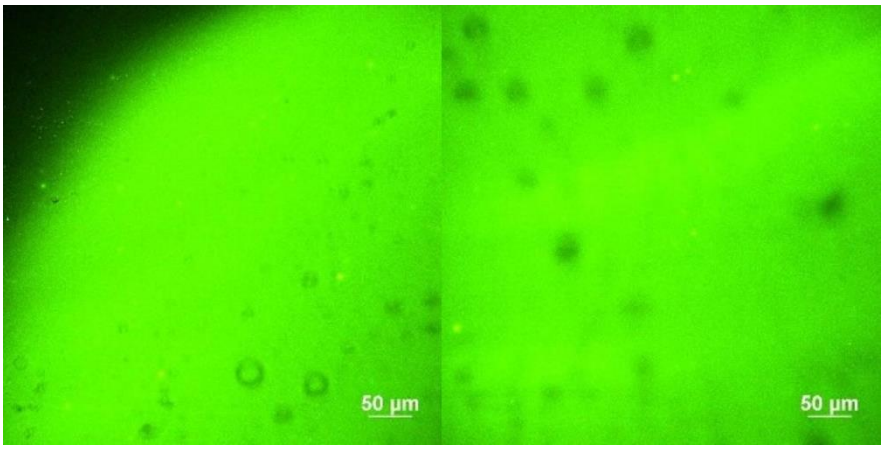

Figure 19 *Images of area 1 (left, edge) and area 2 (right) of pristine specimen containing* ***PyPyr-OH*** *collected at the surface by two photons microscope.*

Then, two different areas in the center of the elongated specimen containing **PyPyr-OH** only were investigated (Figure 20). From a comparison with the images regarding the pristine specimen, it was possible to observe that a mechanical stress did not affect the fluorescence of the guest dispersed in the polyurethane matrix, as predicted.

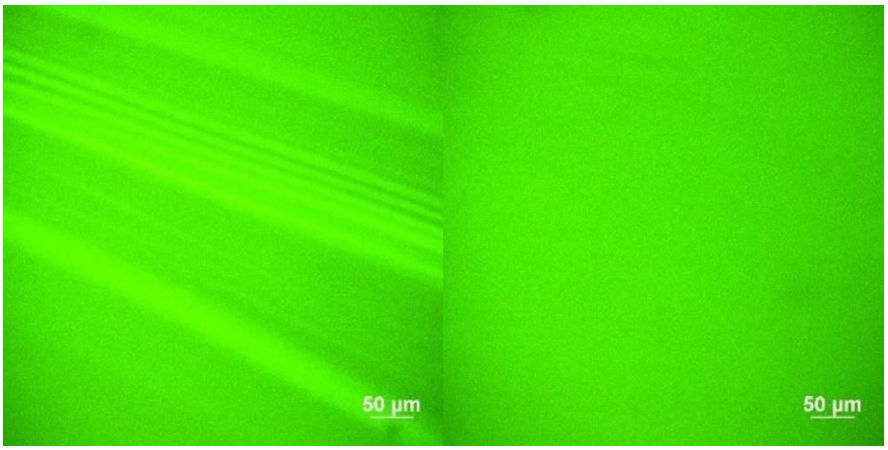

Figure 20 *Images of area 1 (left) and area 2 (right) of elongated specimen containing* ***PyPyr-OH*** *collected at the surface by two photons microscope.*

After the investigation of the specimens containing only the guest, the samples with the reference complex (Scheme 4) were studied and images regarding a pristine and a broken specimen were collected. It was noticeable that the fluorescence emission was much lower than that one containing the guest (Figure 21). Moreover, the fluorescence emission did not change after a mechanical stress, according to the fact that this system was not chemically linked to the matrix and hence it was not stress sensitive.

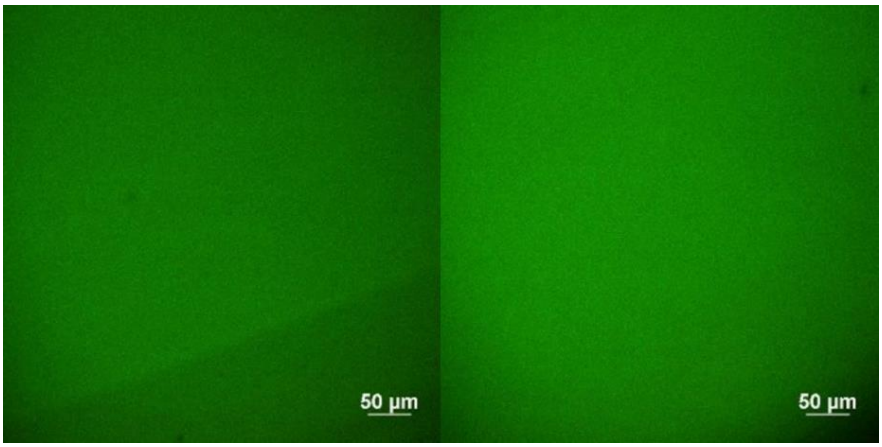

Figure 21 *Images of pristine (left) and broken (right) specimen containing the reference probe collected at the surface by two photons microscope.*

Finally, the samples with the target complex were studied. First, images related to a pristine specimen were collected. Once again, it was noticeable that the fluorescence emission was much lower than that of the guest only sample.

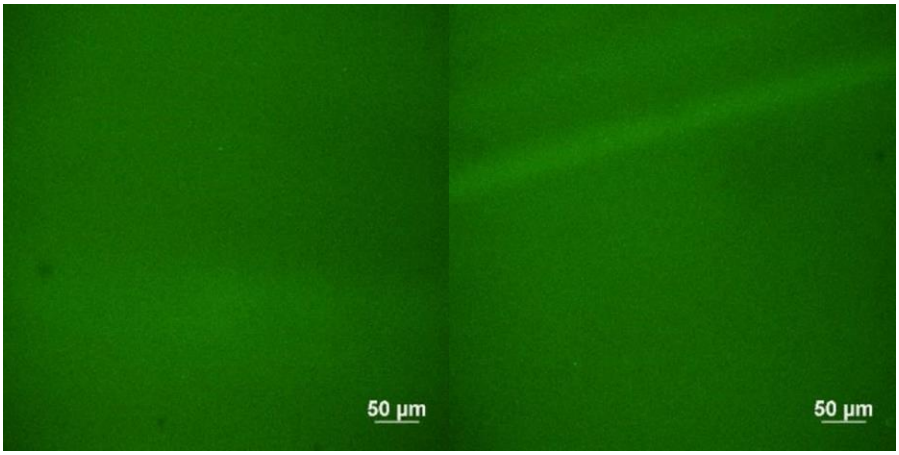

Figure 22 *Images of area 1 (left) and area 2 (right) of pristine specimen containing* ***PyPyr-OH•CavPOPh (mono -OH)*** *collected at the surface by two photons microscope.*

Then, images regarding the elongated and the broken specimen containing the complex are investigated (Figure 23). From a comparison with the images regarding the pristine specimen, it was not possible to observe a significant enhancement of the fluorescence. The two possible explanations are: (i) this specific polyurethane matrix is too rigid to allow the mechanically induced decomplexation of the guest from the cavity; (ii) alternatively, but less likely, the polymeric chains were flexible enough to dissipate the mechanical stress without inducing the dissociation of the supramolecular complex.

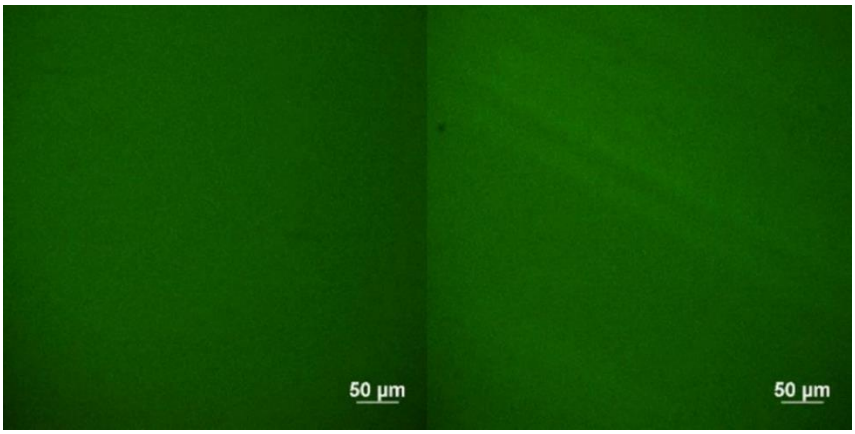

Figure 23 *Images of elongated (left) and broken (right) specimen containing* ***PyPyr-OH•CavPOPh (mono -OH)*** *collected at the surface by two photons microscope.*

Future investigations will focus on the explanation of this phenomenon, to confirm the trend or understand the reason why this probe did not show the desired behavior (e.g., trying with a less rigid matrix).

5.3. Conclusions

The introduction of a nonemissive supramolecular unit, designed for the nondestructive and noninvasive detection of micro–damages, in a commercial polyurethane matrix was studied. The implemented system was based on a fluorescent N-methyl pyridinium salt conjugated to a pyrene unit (**PyPyr-OH**) and a tetraphosphonate cavitand, **CavPOPh (mono -OH)**. Once confirmed the complexation of **PyPyr-OH** by **CavPOPh (mono -OH)**, in solution, through spectroscopic techniques (^{31}P NMR, UV-Vis absorption, fluorescence emission measurements), the probe was added in the polyurethane matrix, as crosslinked probe. Tensile tests were carried out on the dog-bone specimens to evaluate how the fluorescent response of the probe changed as stress level increased. As expected, the fluorescence of **PyPyr-OH** was quenched in the specimens containing the complex, but it did not show a significant emission enhancement after a mechanical stress application. The rigidity of the polyurethane matrix used, which did not allow for the efficient transfer of mechanical stress to the probe, was one possible explanation for the failure of probe activation. Future work will focus on testing the probe in less rigid polyurethane matrix.

5.4. Experimental section

5.4.1. Guest synthesis

6-(4-methylpyridin-3-yl)hex-5-yn-1-ol intermediate (1)

A Schlenk tube, previously dried, was loaded with 3-bromo-4-methylpyridine (0.13 mL, 1.16 mmol), 5-hexyn-1-ol (0.19 mL, 1.74 mmol), toluene dry and NEt_3. The solution was degassed and then loaded with CuI (0.00884 g, 0.0464 mmol) and $Pd(PPh_3)_4$ (0.05362 g, 0.0464 mmol). The reaction was stirred for 20 hours at 110 °C and monitored by TLC (DCM/Acetone = 1:1). Toluene and NEt_3 were evaporated under vacuum at room temperature. Silica gel column chromatography (from DCM to DCM/Acetone = 1:1) was done to purify the product. A dark brown oil (0.16445 g, 0.87 mmol, 75%) was recovered.

^{1}H NMR ($(CD_3)_2CO$-d_6, 400 MHz): δ (ppm) = 8.47 (s, 1H), 8.33 (d, *J* = 5.0 Hz, 1H), 7.23 (d, *J* = 4.9 Hz, 1H), 5.15 (s, 1H), 3.60 (bs, 2H), 2.55 – 2.39 (m, 2H), 2.39 (s, 3H), 1.71 (s, 4H).

MS: m/z: calculated for $[M+H]^+$ = 190.12, experimental for $[M+H]^+$ = 190.52.

3-(6-hydroxyhex-1-yn-1-yl)-1,4-dimethylpyridin-1-ium iodide (2)

A one-necked flask was loaded with 6-(4-methylpyridin-3-yl)hex-5-yn-1-ol (0.16445 g, 0.87 mmol) and placed in an ice bath. CH_3I (0.11 mL, 1.74 mmol) was added to the flask. The reaction was stirred overnight at room temperature. CH_3I was removed under vacuum at room temperature. A dark brown oil was recovered (0.17365 g, 0.85 mmol, 98%).

^{1}H NMR (DMSO-d_6, 400 MHz,): δ (ppm) = 9.05 (s, 1H), 8.77 (d, *J* = 6.3 Hz, 1H), 8.02 (d, *J* = 6.3 Hz, 1H), 4.46 (t, *J* = 5.1 Hz, 1H), 4.23 (s, 3H), 3.45 (q, *J* = 5.3 Hz, 2H), 2.60 (m, 5H), 1.61 (m, 4H).

MS: m/z: calculated for $[M+H]^+$ = 204.14, experimental for $[M+H]^+$ = 204.20.

(E)-3-(6-hydroxyhex-1-yn-1-yl)-1-methyl-4-(2-(pyren-1-yl)vinyl)pyridin-1-ium iodide (PyPyr-OH)

To a solution of 3-(6-hydroxyhex-1-yn-1-yl)-1,4-dimethylpyridin-1-ium iodide (0.3037 g, 0.92 mmol) and pyrene-1-carbaldehyde (0.3167 g, 1.37 mmol) in 15 mL of EtOH 100% under inert atmosphere 5/6 drops of dry piperidine were added to the system and an orange precipitate immediately started to occur. The mixture was stirred for 12 h at

room temperature. The suspension was cooled down and the orange precipitate was recovered by filtration, washed with cold ethanol and DCM. An orange solid was recovered (0.3258 g, 0.596 mmol, 65%).

^{1}H NMR (DMSO-d_6, 400 MHz,): δ (ppm) = 9.16 (d, *J* = 16.0 Hz, 1H), 9.07 (s, 1H), 8.92 (d, J = 9.4 Hz, 1H), 8.84 (bs, 2H), 8.56 (d, J = 8.2 Hz, 1H), 8.43 - 8.39 (m, 4H), 8.31 (d, *J* = 8.9 Hz, 1H), 8.25 (d, *J* = 8.9 Hz, 1H), 8.15 (t, *J* = 7.6 Hz, 1H), 7.82 (d, J = 15.9 Hz, 1H), 4.52 (t, *J* = 5.0 Hz, 1H), 4.25 (s, 3H), 3.52 (q, *J* = 5.7 Hz, 2H), 2.73 (t, *J* = 6.5 Hz, 2H), 1.80–1.67 (m, 4H).

MS: m/z: calculated for $[M+H]^+$ = 416.20, experimental for $[M+H]^+$ = 416.14.

5.4.2. Titration in solution

Titration of PyPyr-OH with CavPOPh (mono-OH)

A stock solution of **PyPyr-OH** was prepared from 5 mg of solid that were dissolved in 10 mL of MeOH. From this mother solution, 217 µL were taken and transferred in a 50 mL flask.

This was filled with MeOH obtaining a final concentration of 4.0 µM.

The solution of **CavPOPh (mono-OH)** was prepared in a 5 mL flask with 1.92 mg of host (PM = 1217.16 g/mol) dissolved in diluted solution of **PyPyr-OH**.

The titration was done by adding to the quartz cuvette, containing 2 mL of diluted solution of guest (4.0 µM), increasing equivalents of host (1 eq = 25.4 µL).

Furthermore, a titration was also done by preparing in advance a set of vials each containing 2 mL of the diluted guest solution and increasing host equivalents to assess the stabilization time for the system. The spectra were recorded after 24 hours.

5.4.3. Spectroscopic characterization in matrix

Preparation of samples for matrix fluorescence measurement in cuvette (general procedure)

A sample was prepared from 3 g of PC 224 GLASS MR (resin), 1.95 g of G124 (hardener) and a solution of dry THF containing the system under investigation. The quantity of the latter must be the 0.0005% of the total weight of the matrix (4.95 g).

For every sample a vial was loaded with 3 g of PC 224 GLASS MR and the solution of dry THF. The formed suspension was then homogenized, and the solvent was removed under vacuum. When all dry THF was evaporated, 1.95 g of GS124 were added and

homogenized to the other components. Disposable cuvettes UV grade PMMA were used to collect absorption and fluorescence emission spectra.

Added systems:

- Guest **PyPyr-OH**, 49.50 µL of a solution 0.92 mM (dry THF)
- Complex **PyPyr-OH**:CavPOPh (mono-OH), 0.33 mg dissolved in the minimum amount of dry THF (~ 50 µL)
- Complex **PyPyr**:CavPOPh (C_3) 0.34 mg dissolved in the minimum amount of dry THF (~ 50 µL).

5.4.4. Preparation of specimens for matrix fluorescence measurement (general procedure)

A sample was prepared from 7.27 g of PC 224 GLASS MR (resin), 4.73 g of G124 (hardener) and a solution of dry THF containing the system under investigation. The quantity of the latter must be the 0.0005% of the total weight of the matrix (12 g).

For every sample, a vial was loaded with 7.27 g of PC 224 GLASS MR and the solution in dry THF. The formed suspension was then homogenized, and the solvent was removed under vacuum. When all dry THF was evaporated, 4.73 g of GS124 were added and homogenized to the other components. A Teflon mold was used to obtain the specimens used for tensile tests and emission fluorescence measurements.

Added systems:

- Guest **PyPyr-OH**, 120 µL of a solution 0.92 mM (dry THF)
- Complex **PyPyr-OH**:CavPOPh (mono-OH), 0.949 mg dissolved in the minimum amount of dry THF (~ 100 µL)
- Complex **PyPyr**:CavPOPh (C_3) 0.832 mg dissolved in the minimum amount of dry THF (~ 100 µL)

5.4.5. Tensile tests of PC224 GLASS MR/G124 (dog bone specimens)

Specimen dimensions: 25 mm x 1.5 mm (width x thikness).

Crosshead speed: 1.0 mm/min

5.5. References

(1) R. M. Wang, S. R. Zheng, Y. P. Zheng, *Polymer Matrix Composites and Technology* **2011**, pp. 1-548.

(2) F. Ciardelli, G. Ruggeri, A. Pucci, *Chem. Soc. Rev.* **2013**, *42 (3)*, 857-870.

(3) J. M. Clough, A. Balan, R. P. Sijbesma, *Topics Curr. Chem.* **2015**, *Vol. 369*, pp. 209-238.

(4) R. Klajn, *Chem. Soc. Rev.* **2014**, *43 (1)*, 148-184.

(5) Z. S. Kean, S. L. Craig, *Polymer* **2012**, *53 (5)*, 1035-1048.

(6) G. R. Gossweiler, C. L. Brown, G. B. Hewage, E. Saphiro-Gheiler, W. J. Trautman, G. W. Welshofer, S. L. Craig, *ACS Appl. Mater. Interfaces* **2015**, *7 (40)*, 22431-22435.

(7) Z. Chen, J. A. M. Mercer, X. Zhu, J. A. H. Romaniuk, R. Pfattner, L. Cegelski, T. J. Martinez, N. Z. Burns, Y. Xia, *Science* **2017**, *357 (6350)*, 475−479.

(8) H. Zhang, F. Gao, X. Cao, Y. Li, Y. Xu, W. Weng, R. Boulatov, *Angew. Chem. Int. Ed.* **2016**, *55 (9)*, 3040−3044.

(9) T. Matsuda, R. Kawakami, R. Namba, T. Nakajima, J. P. Gong, *Science* **2019**, *363 (6426)*, 504−508.

(10) K. Imato, A. Irie, T. Kosuge, T. Ohishi, M. Nishihara, A. Takahara, H. Otsuka, *Angew. Chem. Int. Ed* **2015**, *54 (21)*, 6168−6172.

(11) M. E. McFadden, M. J. Robb, *J. Am. Chem. Soc.* **2021**, *143 (21)*, 7925−7929.

(12) H. Zhang, F. Gao, X. Cao, Y. Li, Y. Xu, W. Weng, R. Boulatov, *Angew. Chem. Int. Ed.* **2016**, *55 (9)*, 3040−3044.

(13) M. J. Robb, T. A. Kim, A. J. Halmes, S. R. White, N. R. Sottos, J. S. Moore, *J. Am. Chem. Soc.* **2016**, *138 (38)*, 12328−12331.

(14) T. Sumi, R. Goseki, H. Otsuka, *Chem. Commun.* **2017**, *53 (87)*, 11885−11888.

(15) H. Qian, N. S. Purwanto, D. G. Ivanoff, A. J. Halmes, N. R. Sottos, J. S. Moore, *Polymeric Materials Chem* **2021**, *7 (4)*, 1080−1091.

(16) T. Yamakado, S. Saito, *J. Am. Chem. Soc.* **2022**, *144 (6)*, 2804−2815.

(17) A. Piermattei, S. Karthikeyan, R. P. Sijbesma, *Nat. Chem.* **2009**, *1 (2)*, 133−137.

(18) D. A. Davis, A. H., J. Y., L. D. Cremar, D. Van Gough, S. L. Potisek, M. T. Ong, P. V. Braun, T. J. Martinez, S. R. White, J. S. Moore, N. R. Sottos, *Nature* **2009**, *459*, 68-72.

(19) A. E. Früh, F. Artoni, R. Brighenti, E. Dalcanale, *Chem. Mater.* **2017**, *29*, 7450-7457.

(20) A. D. Das, G. Mannoni, A. E. Früh, D. Orsi, R. Pinalli, E. Dalcanale, *ACS Appl. Polym. Mater.* **2019**, *1*, 2990-2997.

(21) E. Biavardi, G. Battistini, M. Montalti, R. M. Yebeutchou, L. Prodi, E. Dalcanale, *Chem. Commun.* **2008**, 1638-1640.

(22) R. Ling, M. Yoshida, P. S. Mariano, *J. Org. Chem.* **1996**, *61*, 4439-4449.

(23) L. M. M. Mouterde, F. Allais, *Front. Chem.* **2018**, 6:426.

Chapter 6

Encapsulation of Trimethine Cyanine in Cucurbit[8]uril: Solution versus Solid-State Inclusion Behavior*

*The content of this chapter has been published in Chem. Eur. J. **2022**, *28*, e202200185. Crystallographic characterization was carried out by the group of Professor Geremia (UNITS).

6.1. Introduction

Cyanines are widely used organic fluorescent dyes whose attractiveness is due to their favorable optical properties such as high molar extinction coefficient, suitable fluorescence quantum yield and narrow absorption/emission bands.[1] These molecules belong to the polymethine class of dyes and present a planar, conjugated chain of sp^2-hybridized carbon atoms with an odd number of methine groups and an even number of π electrons between the two nitrogen-containing heterocyclic rings.[2,3] According to the number of carbon atoms of the chain, these dyes are usually referred to as monomethine (Cy1), trimethine (Cy3), pentamethine (Cy5), and heptamethine cyanines (Cy7). The tunability of their fluorescence profiles from UV-Vis to near-infrared (NIR) by changing the polymethine chain length or by inserting functional groups on the heterocycles, together with their outstanding biocompatibility and low toxicity, makes cyanines suitable probes for medicinal and biological imaging.[4,5] In the early 1990's, cyanine dyes with increased water solubility and reduced fluorescence quenching by dye-dye interactions became commercially available in the succinimidyl ester form. These ready availability and improved properties kick-started their widespread use as labelling agents for nucleic acids. Being highly sensitive to microenvironmental factors such as hydrogen bonding and viscosity-dependent C-C bond rotational motion,[6,7] cyanines are also promising candidates for the development of molecular fluorescent probes for the visualization of viscosity in living biosystems.[8] Rapid photobleaching and the tendency to form aggregates in aqueous solutions are common drawbacks for the use of these dyes in the above mentioned applications.[9-11] Encapsulation of fluorescent molecules in nanoparticles or macromolecules can drastically change their local microenvironments, subsequently affecting their stability and spectral properties.[12] In particular, host-guest complexation by water-soluble macrocyclic receptors is a powerful tool to fine-tune the absorption and emission behavior of the dyes.[13] For example, cyclodextrins have been shown to dramatically alter the microenvironment of cyanines, leading to the disruption of aggregates in favor of the formation of dimers and inhibiting their photodegradation.[14-16] The formation of a rotaxane by the threading of a α-cyclodextrin by the heptamethine chain of a Cy7 was found to increase both chemical stability and water-solubility of the dye.[17] In addition, cucurbit[7]uril (CB[7]), a synthetic

macrocycle characterized by a toroidal, hydrophobic cavity constituted by seven glycoluril units bound together by 14 methylene bridges, has been demonstrated to effectively complex monomeric Cy1 and Cy3 dyes thereby disrupting their J- and H-aggregates, respectively.[9,18] The same macrocycle was exploited to alter the photophysical properties of a different Cy3 guest[19] and a linear cyanine dye (LDP)[20] in aqueous solution. Moreover, Cy3-conjugated CB[7] (Cy3-CB[7]) found several application as live cell imaging probes, both alone[21,22] and as component of high affinity host-guest Forster resonance energy transfer (FRET) pairs.[23-25] If CB[7] has been well exploited in combination with cyanines, interactions between these dyes and cucurbit[8]uril (CB[8]) are far less investigated. Bearing an additional glycoluril unit (Figure 1), CB[8] has a larger portal diameter (6.9 Å) and inner cavity volume (479 Å^3) than CB[7].[26] These features allow for additional binding modes as well as various stoichiometries, ranging from the simplest 1:1 binary complexes[27] to discrete (n:n) host:guest oligomers.[28] Depending on the guests structures, 2:1,[29] 1:2 homoternary,[30] 1:1:1 heteroternary[31] and 2:2 quaternary[32] complexation modes are possible. The binding mode of CB[8] complexes have a strong impact on their spectral properties, in particular on fluorescence emission.[33]

6.2. Results and discussion

We investigated the interaction of a model indocyanine trimethine dye, namely 1-methyl-2-[3-(1-methyl-3,3-dimethylindolin-2-ylidene)prop-l-enyl]-3,3-dimethyl-3*H*-iodolium iodide (Cy3), with CB[8] (Figure 1).

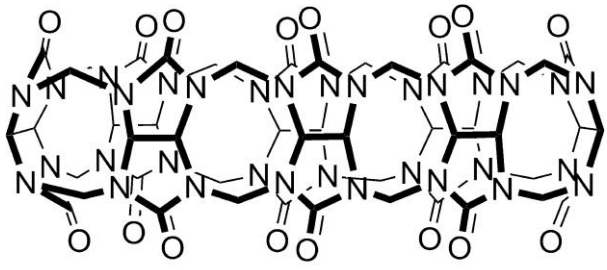

CB[8]

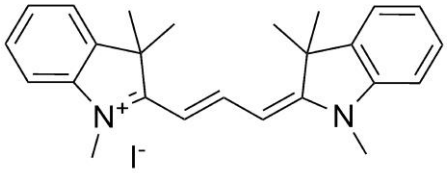

Cy3

Figure 1 *Structures of CB[8] and the cyanine dye Cy3 involved in this study.*

The dye was synthesized following a two-step procedure reported in the literature (Scheme 1).[34]

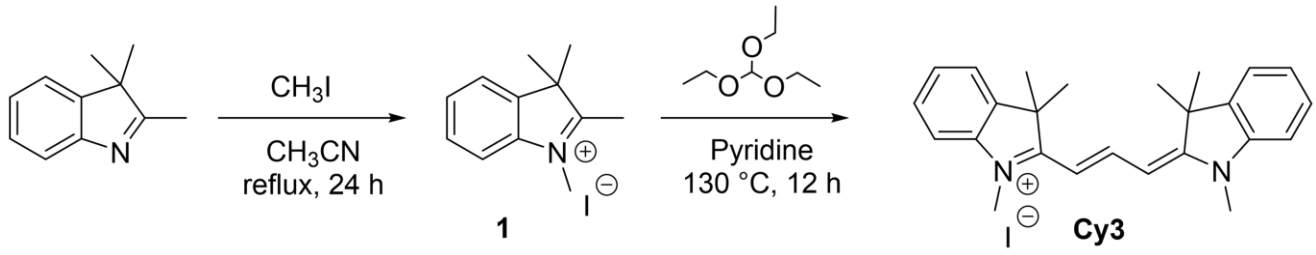

Scheme 5 *Synthesis of Cy3.*

Briefly, 1-methyl-2,3,3–trimethyl-3H-indolium iodide was synthesized by refluxing 2,3,3-trimethyl-3H-indole with iodomethane at 130 °C for 6 h. Subsequently, the red product was reacted with triethylorthoformate in pyridine to give dye Cy3 which was purified by recrystallization in ethanol. CB[8] was prepared by acid-catalyzed condensation of glycoluril with formaldehyde and purified accordingly to a well-established protocol based on repeated precipitations.[35] The binding interaction between Cy3 and CB[8] was firstly monitored via matrix-assisted laser desorption ionization time-of-flight (MALDI-TOF) spectrometry, confirming the presence of a binary complex in aqueous solution. Furthermore, ^{1}H NMR spectra in D_2O were performed to characterize the system. Figure 2 shows the difference between the ^{1}H NMR spectrum of Cy3 at 0.1 mM and the spectra obtained after addition of CB[8]. A sizable upfield shift was observed for the aromatic protons ($H_{1,2,3,4}$) upon addition of 0.4 equiv. of CB[8] (Figure 2b), while slight upfield shifts were also seen for the signals of the polymethine chain ($H_{7,8}$). Therefore, the largest perturbation was observed for the protons in the aromatic region, thus suggesting an asymmetric binding of the longer Cy3 molecule with respect to the depth of the CB[8] cavity. Indeed, symmetric 1:1 binding should expose the aromatic protons outside the macro-ring. On the other hand, it was notable that the spectrum still shows symmetric signals for the Cy3 molecule. This can be rationalized in terms of fast exchange between complexed and uncomplexed Cy3 molecules. Additionally, when the ^{1}H NMR spectrum was recorded with one equivalent of CB[8] (Figure 2c), the signals of Cy3 were significantly broadened and were barely visible. A similar absence of sharp signals was also observed by Scherman and co-workers in other CB[8] complexes.[36]

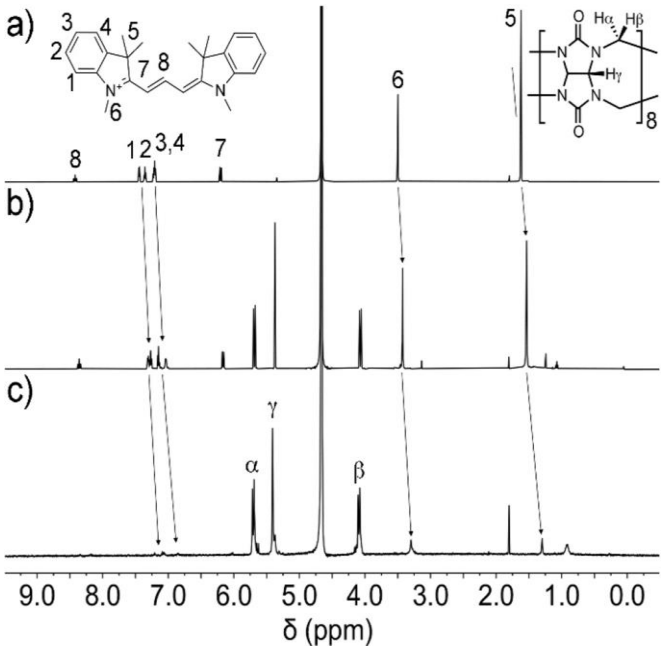

Figure 2 *^{1}H NMR (600 MHz, D_2O): addition of increasing amounts of CB[8] to Cy3: (a) Cy3 at 0.1 mM; (b) addition of 0.4 equiv. of CB[8]; (c) addition of 1 eq. of CB[8].*

This was attributed to the formation of a supramolecular polymer in solution. Isothermal titration calorimetry (ITC) experiments were performed to investigate the binding strength, stoichiometry, and thermodynamic parameters for the host-guest complexation of Cy3 by CB[8]. Figure 3 shows a typical ITC titration experiment with Cy3 and CB[8]. A 27 injection experiment was carried out at T = 25 °C where the cell contains a 0.1 mM aqueous solution of CB[8], and Cy3 is in the syringe at a concentration of 1.0 mM. The observed exothermic binding curve has a sharp inflection point at a molar ratio of one indicating the formation of a 1:1 assembly in aqueous solution. A second and less pronounced binding event is present when 0.5 equivalents of guest are added to the host solution, suggesting the coexistence of a 2:1 host-guest complex. The data fitting of the titration with a "two sequential binding sites" model gave an association constant $K_{a,1}$ = 3.9×10^7 M^{-1} with a ΔH_1 of -5.1 kcal mol^{-1} for the first binding of the guest and a $K_{a,2}$ of 1.4×10^5 M^{-1} plus a ΔH_2 of -0.7 kcal mol^{-1} for the interaction with the second host. The corresponding calculated thermodynamic parameters ΔG_1 and $T\Delta S_1$ are -10.4 kcal mol^{-1} and 5.3 kcal mol^{-1}, respectively, while ΔG_2 = -5.6 kcal mol^{-1} and $T\Delta S_2$ = 4.9 kcal mol^{-1}, making the two binding processes both enthalpy and entropy driven.

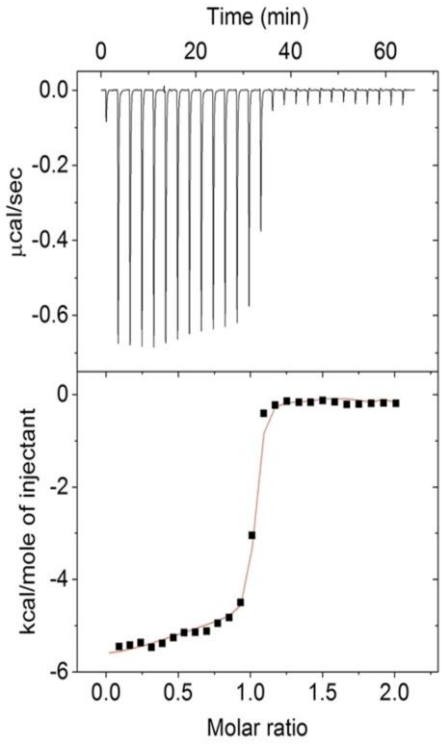

Figure 3 *Isothermal calorimetric data obtained in the titration experiment of a CB[8] solution by adding aliquots of the Cy3 guest; [CB[8]]=0.1 mM, [Cy3]=1.0 mM.*

These thermodynamic values are in agreement with the displacement of high energy water molecules from the cavity by the guest, which is known to be one of the main driving forces of CB[8] complexation.[37] The spectroscopic behavior of the dye upon addition of CB[8] was studied in aqueous solution at a concentration of 1 µM to minimize dye self-aggregation and any effect of inner filter. As shown in Figure 4a, free Cy3 shows two UV absorption maxima, one at 540 nm (main band) and another at 510 nm (vibronic band). Upon addition of CB[8] a red shift is observed in the λ_{max} along with a decrease in the absorption coefficient. A precise isosbestic point is observed at 545 nm only at low CB[8]/Cy3 ratio, suggesting that at higher CB[8] content the equilibrium is not between two unique species. This spectral shift is in line with a change in the microenvironment of the dye caused by its inclusion in the hydrophobic cavity of CB[8], as already reported in literature for the tetrafluoroborate analogue.[38] Fluorescence spectra show a small red shift upon addition of increasing equivalents of CB[8], as well as a significant decrease of the intensity (the fluorescence quantum yield amounts to 1% free Cy3 and to 0.7% for the 1:1 complex) (Figure 4b).

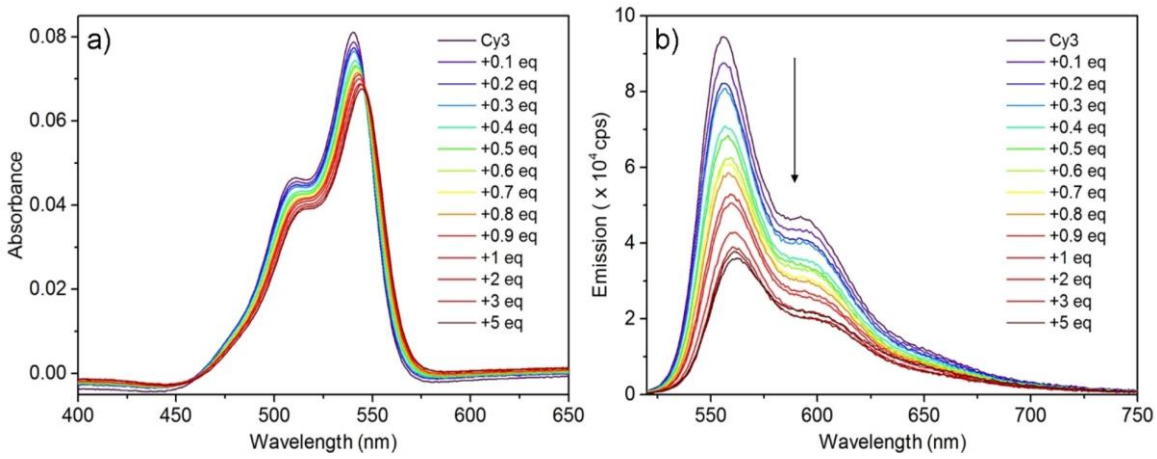

Figure 4 *a) UV Visible spectrum of Cy3 (1 μM) in aqueous solution upon addition of CB[8]. (b) Fluorescence spectrum of Cy3 in water (1 μM) upon addition of CB[8],* λ_{max} *= 510 nm.*

This last observation is in contrast with the idea of an enhanced emission upon complexation in a restricted environment and deserves more investigation. Fluorescence decays were measured, getting an average fluorescence lifetime of 3.48 ns for free Cy3 in water, and of 4.24 ns for a solution containing the supramolecular 1:1 complex (Figure 5).

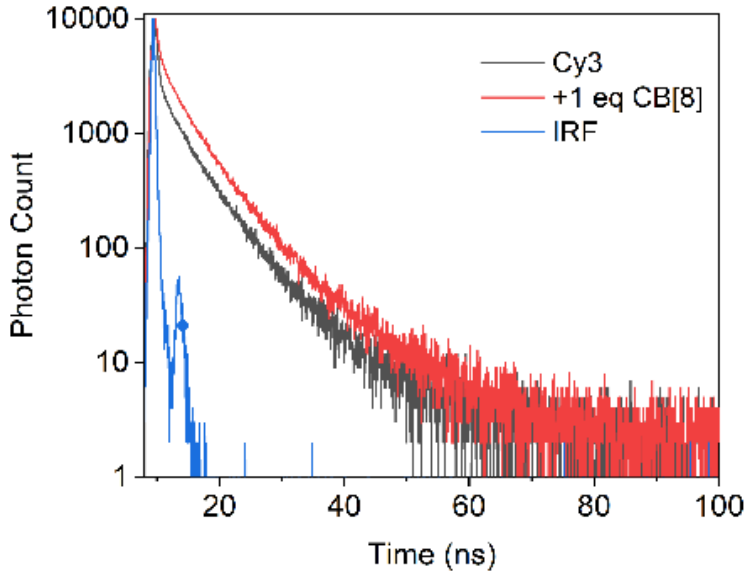

Figure 5 *Fluorescence decay traces of free Cy3 (black) and Cy3•CB[8] complex (red) in water.*

Fluorescence intensity and lifetime data unexpectedly led to a smaller radiative decay rate for Cy3 in the complex (1.62×10^{-3} ns^{-1}) than in water solution (2.99×10^{-3} ns^{-1}), consistently with the observed decrease in absorption coefficient upon complexation, while the non-radiative decay rate stayed practically constant (0.287 vs. 0.234 ns^{-1}). Since we know that only one Cy3 molecule was present in the complex, the increase of the

radiative decay constant (related to transition dipole moment) for free Cy3 in water suggested the presence of aggregates when CB[8] was not present in water (Table 1).

Table 2 *Tri-exponential fit of the fluorescence decay of free Cy3 and of the 1:1 Cy3•CB[8] complex.*

	τ1 (ns) [f1 (%)]	*τ2 (ns) [f1 (%)]*	*τ3 (ns) [f1 (%)]*	*Average lifetime (ns)*
Free Cy3	*0.239 [33.473]*	*2.806 [29.892]*	*6.911 [36.635]*	*3.48*
Cy3 +1 eq CB[8]	*0.397 [21.266]*	*3.435 [46.476]*	*8.044 [32.258]*	*4.24*

In particular, the results were consistent with slightly superradiant aggregates, which were disaggregated upon complexation with CB[8]. To prove this hypothesis, anisotropy measurements were performed for free Cy3 both in water and in a much more viscous solvent (Figure 6).

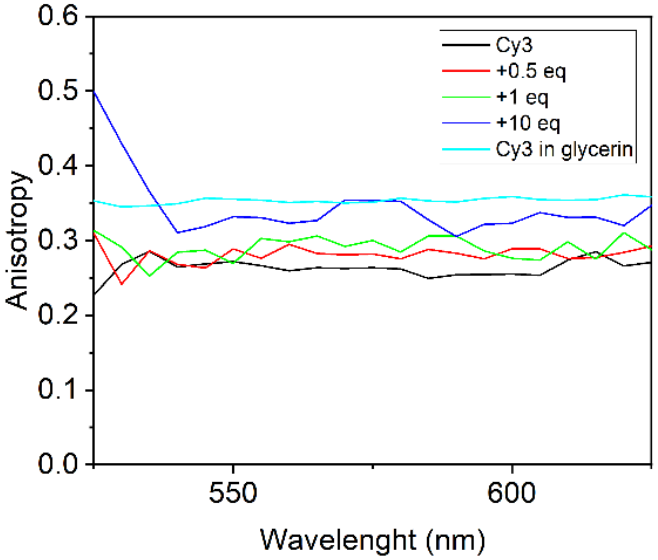

Figure 6 *Anisotropy traces for Cy3 (black), Cy3 +0.5 eq CB[8] (red), Cy3 +1 eq CB[8] (green), Cy3 +10 eq CB[8] (blue) in water and anisotropy trace for Cy3 (cyano) in glycerin.*

For free Cy3 in water a fluorescence anisotropy value r = 0.26 was found, while the measurement in glycerol gave the fundamental anisotropy value r_0 = 0.35. Exploiting the Perrin equation, a hydrodynamic volume of 4.41×10^4 Å^3 was estimated for Cy3. Scaling down this value by a factor 1.3,[39] to roughly exclude the solvation shell, we end up with a volume of 3.39×10^4 Å^3, corresponding to a sphere of radius 20 Å. This value was comparable with the molecular length, suggesting the presence of oligomeric

aggregates in water, despite the low concentration. Therefore, fluorescence anisotropy measurements confirmed the presence of small aggregates (not detected, in fact, with DLS) for free Cy3 in water. Cy3 molecules in these aggregates were probably very loosely interacting, as suggested by the small spectral variations with respect to the complex and by the ease of rupture of the aggregates when adding CB[8]. To unambiguously confirm the presence of Cy3 aggregates in water, we performed absorption and fluorescence measurements on solutions at different concentration. Since Cy3 does not have a good solubility in water already at concentrations of the order of 10^{-5} M, we prepared a mother solution and filtered it, to be sure to remove any non-solubilized compound. The filtered mother solution was then diluted by a factor 8 and by a factor 16. The corresponding spectra (Figure 7) showed a decrease of extinction coefficient and of concentration normalized emission intensity upon dilution.

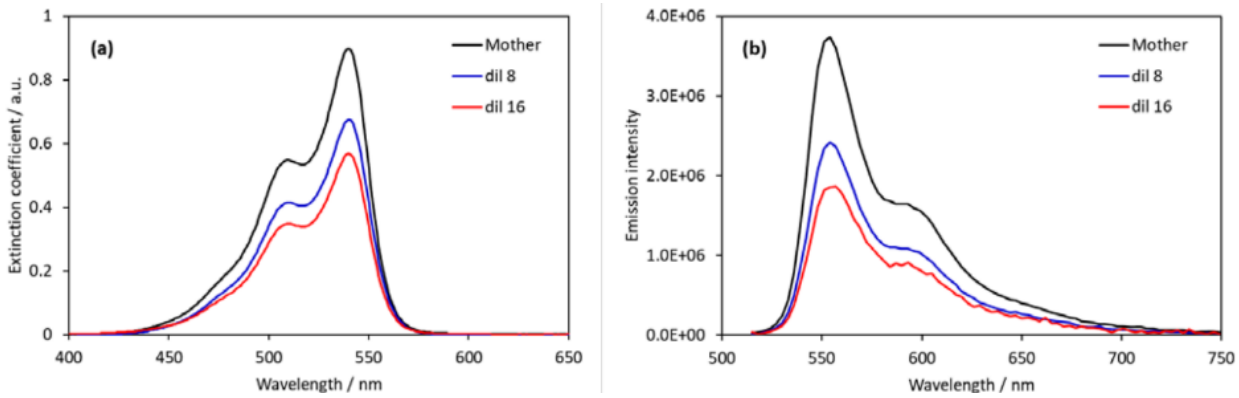

Figure 7 *(a) Absorption spectra of Cy3 water solutions having different concentration: the spectra of diluted solutions were divided by the corresponding dilution factor, to retrieve spectra proportional to the molar extinction coefficient. (b) Fluorescence spectra of Cy3 water solutions having different concentration: the spectra were corrected for inner filter effects (significant only for the mother solution); each spectrum was then divided by the absorbance of the corresponding solution at the excitation wavelength.*

This strongly supports the formation of aggregates, favored in more concentrated solutions, and the superradiant nature of the aggregates (related to increased transition dipole moment). Under the premise of dye aggregation, the K_a estimated by ITC was only an apparent binding constant. We therefore used the fluorescence titration (at much lower Cy3 concentration with respect to the ITC experiment) to obtain a more realistic (albeit still apparent) K_a. The fluorescence data could be fitted through the Benesi-Hildebrand equation and confirmed a 1:1 host: guest complex, with a K_a = 1.5×10^{6} M^{-1} (Figure 8).

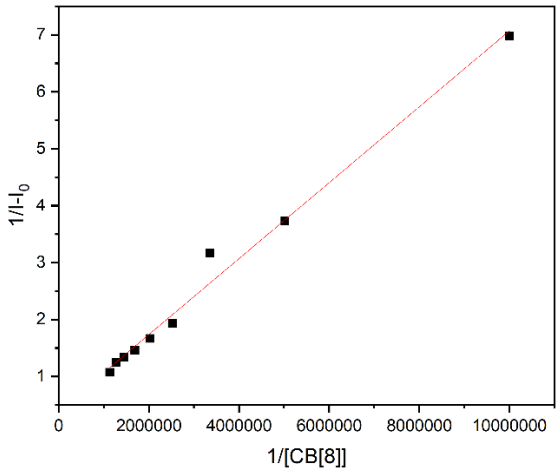

Figure 8 *Fitting of data to obtain the association constant. A linear equation well fitted the points, whose equation is y=6.667E-7x+0.4043 (R^2 = 0.9887).*

Interestingly, the major effect of complexation on fluorescence intensity seemed to be played by the rupture of aggregates upon the formation of the complex. While most complexes of CB[8] show a much higher solubility in water than the CB[8] itself, it was surprising to see that during solution studies of binding of the dye Cy3 to CB[8], upon the addition of one equivalent of CB[8] over the course of a few hours the complex started to precipitate as bright purple needle-shaped crystals. To more thoroughly investigate the arrangement of Cy3 in the cavity of CB[8], crystals suitable for X-ray diffraction (XRD) were grown in water. Diffraction data from small, twinned crystals was collected using synchrotron radiation at 100 K. The crystal belongs to the polar orthorhombic $Pna2_1$ space group. The solid state structure shows that the asymmetric unit contains one CB[8] macrocycle, one trans Cy3 cation with its chloride counterion and a total of 13 cocrystallized. water molecules (Figure 9a). Therefore, the crystal has a 1:1 host-guest ratio, as observed in solution by spectroscopic and ITC experiments. The aromatic indolinene terminals of the dye are located inside the hydrophobic cavities of CB[8] (Figure 9b). The architecture of the host-guest interactions furnishes a rationale for the upfield shifts observed for the aromatic protons in the ^{1}H NMR investigation. In fact, the crystal packing shows that both aromatic terminals of an indolenine are hosted by two adjacent CB[8] units (Figure 9b) and that each CB[8] hosts the aromatic terminals of two indolenine guests (Figure 9c). This leads to the formation of a linear supramolecular polymer, as shown in Figure 9b, generated by the periodic crystallographic translation of 12.871 Å along the *a* axes. One aromatic ring of the dye is almost exactly centered in the hydrophobic cavity, with distances of its barycenter from

the mean planes of the two CB[8] oxygen portals of 3.16 Å for the entry portal and 2.98 Å for the second portal (Figure 9c). The second aromatic ring is less deeply inserted in the hydrophobic cavity of an adjacent CB[8], with distances of 0.22 and 5.96 Å from the entry and second portals, respectively (Figure 9c). The aromatic plane of the dye is tilted by about 56° with respect to the parallel oxygen portal planes of the polymeric CB[8] chain. The two parallel phenyl rings hosted inside the same CB[8] form a weak *π-π* stacking interaction at a distance of about 3.5 Å (Figure 9c). The asymmetric interaction of the two dyes with the CB[8] produces an asymmetric deformation of the host. The CB[8] entry portal of the more deeply inserted Cy3 is more ovalized[40] with respect to the entry portal of the less inserted one. The difference between the minor and the major axes of the ellipsoidal portals are 1.41 and 1.09 Å, respectively. The aromatic terminals of the dye molecules completely fill the hydrophobic cavity of CB[8] units (Figure 4d) and the cocrystallized water molecules are all external to the cavity. The crystal packing shows that each linear polymeric chain packs against four other chains oriented in antiparallel fashion giving a checkerboard pattern when viewed along the crystallographic *a* axes (Figure 9e). Therefore, the molecules are arranged in two orthogonally oriented close packed layers parallel to the *ab* and *ac* crystallographic planes (Figure 9f). In these layers, each CB[8] of the supramolecular polymer is offset by half of the a axis length and tilted by about 30° with respect to neighboring antiparallel chains. This results in a highly distorted herringbone motive (Figure 9f). The charges of the dyes are counterbalanced by chloride anions located in alternate water channels bordered by four polymeric chains (Figure 9e). This crystal packing is similar to that observed for 1:2 host-guest complex between CB[8] and 4-(4-aminophenyl)-N-methylpyridinium[41] and for the highly disordered polymeric 1:1 host-guest complex between CB[8] and N-(4-(phenylazo)benzyl)-N′-methyl-4,4′-bipyridinium.[36] It is also interesting to note the structural similarity of the columnar arrangement of the Cy3-CB[8] complex with the reported nanotubular framework constituted by pure CB[8], obtained in the presence of a molecular chaperone,[42] which results in a slight increase (about 0.15 Å) in the distance between consecutive CB[8] molecules.

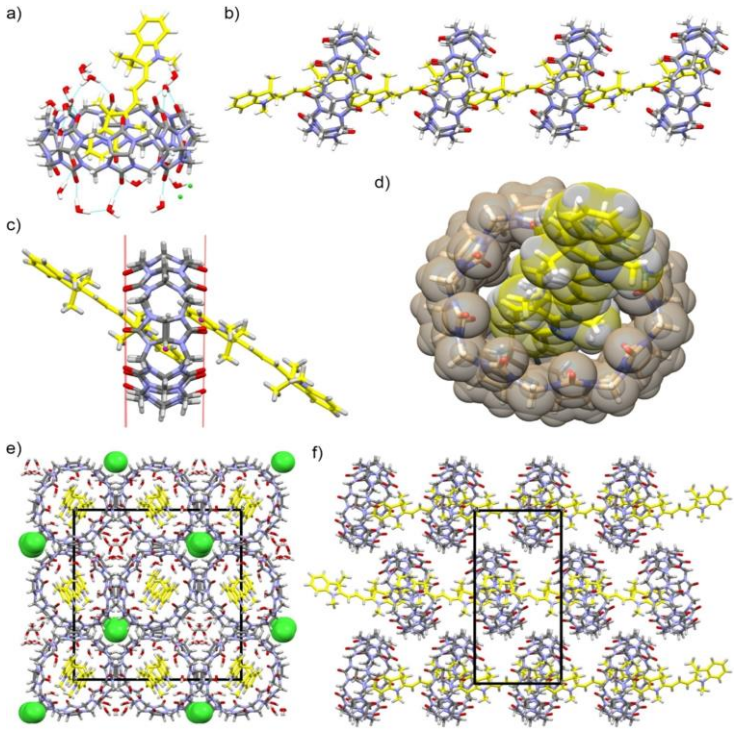

Figure 9 *(a) Stick representation in CPK colors of the asymmetric unit of Cy3·CB[8] complex. Carbon atoms of the Cy3 dye are evidenced in yellow. (b) Linear supramolecular polymeric chain assembly formed by CB[8] and Cy3 units. (c) Each CB[8] unit hosts a couple of π-π stacked Cy3 guests. The barycenters of the aromatic ring of the dyes (violet spheres) are differently inserted in the hydrophobic cavity of CB[8] delimitated by the oxygen portal planes (red lines). (d) Space fill representation of the cavity of CB[8] unit completely filled by the aromatic terminals of the Cy3 dyes. (e) Checkerboard pattern of the antiparallel polymeric chains viewed along the crystallographic a axes. The chloride counterions (green VdW spheres) are located in alternate water channels. (f) Highly distorted herringbone motive of a single layer of CB[8] units viewed along the crystallographic b axes. The CB[8] macrorings of antiparallel supramolecular polymeric chains are tilted by about 30°.*

6.3. Conclusions

We investigated the interaction of an indocyanine trimethine dye, Cy3, with CB[8] by MS, NMR, ITC, UV-Vis absorption and fluorescence spectroscopy and single crystal X-ray diffraction. The solution studies indicated the formation of a 1:1 complex of Cy3 and CB[8]. The ITC measurements revealed that the complexation was an enthalpically and entropically driven process, with an apparent association constant of 1.5×10^{6} M^{-1}, obtained via fluorescence titration. The optical spectroscopic investigation suggested the presence of Cy3 aggregates in water which were disrupted by addition of CB[8]. The ^{1}H NMR spectra confirmed the complexation process and evidenced a slow formation of a supramolecular polymer with subsequent precipitation after a few hours. The X-ray structure obtained from single crystals confirmed the formation of a polymer with 1:1 stoichiometry in the solid state. Both aromatic terminals of Cy3 were hosted by two

adjacent CB[8] units and each CB[8] hosted the aromatic terminals of two Cy3 guests, thereby forming linear supramolecular polymeric chains. The columnar arrangement of the Cy3·CB[8] complex represents an interesting nanotubular framework with incorporated dye molecules.

6.4. Experimental section

5.4.1. Guest synthesis

Synthesis of 1,2,3,3-tetramethyl-3H-indol-1-ium iodide (1)

2,3,3-Trimethyl-3H-indole (4.77 g, 30 mmol) was dissolved in a mixture of methyl iodide (24.11 mL, 300 mmol) and acetonitrile (60 mL) under Ar. The solution was refluxed for 24 h, then allowed to cool to room temperature and the resulting solid was collected by filtration. The solid was washed with acetone and recrystallized with EtOH to give compound 1 as yellow crystalline compound (4.25 g, 14.94 mmol, 45%).

^{1}H NMR (DMSO-d_6, 300 MHz): δ (ppm) = 7.93-7.90 (m, 1H), 7.85-7.82 (m, 1H), 7.64-7.61 (m, 2H), 3.98 (s, 3H), 2.78 (s, 3H), 1.53 (s, 6H).

^{13}C NMR (DMSO-d_6, 75 MHz): δ (ppm) = 196.4, 142.6, 142.1, 129.8, 129.3, 123.8, 115.6, 54.5, 35.3, 22.2, 14.7.

MS: m/z: calculated for $C_{12}H_{16}N^+$ $[M]^+$ = 174.13, experimental for $[M]^+$ = 174.25.

Synthesis of 1-methyl-2-[3-(1-methyl-3,3-dimethylindolin-2-ylidene)prop-l-enyl]-3,3-dimethyl-3H-iodolium iodide (Cy3)

Compound 1 (0.63 g, 4 mmol) was refluxed with triethylorthoformate (0.6 mL, 8 mmol) in 3 mL of pyridine at 120 °C for 1 h. The reaction mixture was then cooled to room temperature and excess diethyl ether was carefully added to the solution to precipitate the product. The crude dye was recrystallized from ethanol to give the product with a 58% yield.

^{1}H NMR (DMSO-d_6, 300 MHz): δ (ppm) = 8.34 (t, J = 13.6 Hz, 1H), 7.64 (d, J = 7.4 Hz, 2H), 7.46 (m, 4H), 7.29 (m, 2H), 6.45 (d, J = 13.6 Hz, 2H), 3.65 (s, 6H), 1.69 (s, 12H).

^{13}C NMR (DMSO-d_6, 75 MHz): δ (ppm) = 174.8, 149.9, 143.3, 141.0, 129.1, 125.8, 123.0, 112.1, 103.2, 49.3, 32.0, 27.7.

MS: m/z: calculated for $C_{25}H_{29}N_2^+$ $[M]^+$ = 357.23, experimental for $[M]^+$ = 357.95.

6.4.2. Fluorescence measurements

Hydrodynamic volume evaluation

To assess the existence of aggregates, the rotational correlation time was calculated through the Perrin equation[43]:

$$r = \frac{r_0}{1 + \left(\tau/\theta\right)}$$

where r is the anisotropy of Cy3 in water, r_0 is the fundamental anisotropy measured for a solution of Cy3 in glycerol, τ is the fluorescence lifetime and θ is the rotational correlation time. The calculated value for θ is 9.57 ns.

The rotational correlation time, θ, is proportional to the molecular volume[43]:

$$\theta = \frac{\eta V}{RT}$$

where η is the viscosity of the solvent, R is the gas constant and T is the absolute temperature.

Fluorescence quantum yield

To evaluate the fluorescence quantum yield for the guest and for the solution containing the guest and 1 equivalent of host, the following equation was used[43]:

$$Q = Q_r \frac{I}{I_r} \frac{OD_r}{OD} \frac{n^2}{n_r^2}$$

where Q is the quantum yield, I is the integrated emission intensity, OD is the optical density and n is the refractive index. The subscript "r" denotes the reference, namely Rhodamine 101 in ethanol, whose Q_r is known.

k_r and k_{nr} evaluation

To assess the radiative and the non-radiative decay rates, starting from the quantum yield and the fluorescence lifetime, the following two equations were used[43]:

$$k_r = \frac{Q}{\tau}$$

$$k_{nr} = \tau^{-1} - k_r$$

Concentration-dependent spectra

A mother solution of Cy3 in water was prepared (nominal concentration on the order of 10^{-5} M) and filtered, to be sure to remove any non-solubilized compound. The filtered mother solution was then diluted by a factor 8 and by a factor 16. A micro-cuvette of 1.5 × 1.5 mm path was used for fluorescence measurements, to reduce inner filter effects. For the mother solution, inner filter effects were non-negligible though, therefore the corresponding emission spectrum has been corrected according to the following equation[43]:

$$I_{corr}(\lambda_{em}) = I(\lambda_{em}) \times 10^{[A(\lambda_{exc})+A(\lambda_{em})]/2}$$

where $I(\lambda_{em})$ and $I_{corr}(\lambda_{em})$ are the measured and the corrected emission spectra, respectively, $A(\lambda_{exc})$ and $A(\lambda_{em})$ are the absorbance values at the excitation and emission wavelength, respectively. The absorbance values are referred to a 1.5 mm path length (as used in fluorescence).

Evaluation of the association constant by optical data

To evaluate the association constant (K_a) by fluorescence data, the Benesi-Hildebrand equation was used:

$$\frac{1}{I - I_0} = \frac{1}{K_a\,(I_{max} - I_0)[L]^n} + \frac{1}{I_{max} - I_o}$$

where $[L]$ is the host concentration, I_0 is the emission intensity in absence of host, I_{max} is the emission intensity at concentration of host beyond which the emission does not change significantly anymore (1 eq in our case) and I is the emission intensity for every added equivalent of host, n is the number of host molecules which complex the guest.

6.4.3. X-ray diffraction from single crystals

Bright purple needle needle-shaped single crystals suitable for an X-ray investigation were obtained by recrystallization in water of the Cy3·CB[8] precipitate. Data collection was carried out at the XRD1 beamline of the Elettra synchrotron (Trieste, Italy), employing the rotating-crystal method with a Dectris Pilatus 2M area detector. Single crystals were dipped in paratone cryoprotectant, mounted on a nylon loop and flash-frozen under a nitrogen stream at 100 K. Diffraction data were indexed and integrated using the XDS package,[44] while scaling was carried out with XSCALE.[45] Structures was solved using the SHELXT[46] program and structure refinement was performed with

SHELXL-18/3,[47] operating through the WinGX GUI,[48] by full-matrix least-squares (FMLS) methods on F^2. Non-hydrogen atoms were refined anisotropically, with the exception of some water molecules with occupancy factor less of equal to 0.5. Due to the low reflection/parameter ratio the ISOR and SIMU cards were used in the refinement. Hydrogen atoms were added at the calculated positions and refined using the riding model. Crystallographic data and refinement details are reported in Table 2. The asymmetric unit of the orthorhombic crystals ($Pna2_1$ space group) of Cy3·CB[8] (Figure 10) contains one crystallographically independent CB[8] molecule, one Cy3 ion, one chloride ion splits in two close positions (0.75/0.25 occupancy factors) and a total of 13 co-crystallized water molecules refined in 17 sites. The structure was refined as a 3-component non-merohedral twin. The twin laws (−1, 0, 0; 0, 0.078, 0.922; 0, 1.078, -0.078), which corresponds to two-fold axes about the [0 5 4] direct lattice direction and (−1, 0, 0; 0, 0.078, -0.922; 0, -1.078, -0.078), which corresponds to two-fold axes about the [0 5 -4] direct lattice direction (Figure S6), were detected with PLATON TwinRotMat. The fraction of overlapped reflections was calculated as about 48% for both components. The refinement as a 3-component twin with HKLF 5 card significantly reduced the R-factor. The R1 factor decreased by 0.060, with refined BASF factors of 0.17 for both components.

Table 3 *Crystal data and structure refinement for Cy3·CB[8].*

Cy3·CB[8]	
Empirical formula	$C_{48}H_{48}N_{32}O_{16}$, $C_{25}H_{29}N_2^+$, Cl^-, $13H_2O$
Formula weight	*1956.34*
Temperature (K)	*100(2)*
Wavelength (Å)	*0.7*
Crystal system	*Orthorhombic*
Space group	*P na2₁*
Unit cell dimensions (Å)	*a = 12.871(15) b = 25.367(18) c = 27.426(17)*
Volume (Å³)	*8955(13)*
Z	*4*
ρ calcd (g/cm³)	*1.451*
μ (mm⁻¹)	*0.118*
F (000)	*4112*
Reflections collected	*35107*
Indep. Reflections	*11113*
restraints/parameters	*1646/1252*
GooF	*1.174*
Final R indices [I>2σ(I)]	$R_1 = 0.1165$ $wR_2 = 0.3058$
R indices (all data)	$R_1 = 0.1581$ $wR_2 = 0.3473$
CCDC code	*2092004*

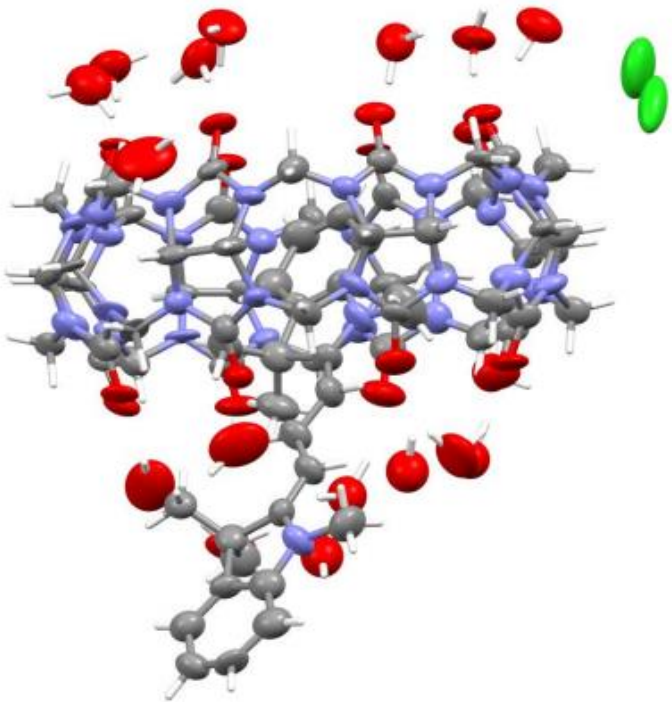

Figure 100 *Asymmetric unit of the Cy3·CB[8]. Ellipsoids in CPK colors at 50% probability. Hydrogen atoms represented in sticks.*

6.5. References

(1) Y. Li, Y. Zhou, X. Yue, Z. Dai, *Adv. Healthcare Mater.* **2020**, 9, e2001327.

(2) M. Panigrahi, S. Dash, S. Patel, B. K. Mishra, *Tetrahedron* **2012**, 68, 781–805.

(3) H. A. Shindy, *Dye Pigment.* **2017**, 145, 505–513.

(4) W. Sun, S. Guo, C. Hu, J. Fan, X. Peng, *Chem. Rev.* **2016**, 116, 7768–7817.

(5) A. P. Gorka, R. R. Nani, M. J. Schnermann, *Acc. Chem. Res.* **2018**, 51, 3226–3235.

(6) G. L. Silva, V. Ediz, D. Yaron, B. A. Armitage, *J. Am. Chem. Soc.* **2007**, 129, 5710–5718.

(7) J. Cao, T. Wu, C. Hu, T. Liu, W. Sun, J. Fan, X. Peng, *Phys. Chem. Chem. Phys.* **2012**, 14, 13702–13708.

(8) H. Xiao, P. Li, B. Tang, *Chem. Eur. J.* **2021**, 27, 6880–6898.

(9) S. Gadde, E. K. Batchelor, A. E. Kaifer, *Chem. Eur. J.* **2009**, 15, 6025–6031.

(10) J. V. Frangioni, *Curr. Opin. Chem. Biol.* **2003**, 7, 626–634.

(11) J. L. Bricks, Y. L. Slominskii, I. D. Panas, A. P. Demchenko, *Methods Appl. Fluoresc.* **2018**, 6, e012001.

(12) X. Wu, W. Zhu, *Chem. Soc. Rev.* **2015**, 44, 4179–4184.

(13) R. N. Dsouza, U. Pischel, W. M. Nau, *Chem. Rev.* **2011**, 111, 7941–7980.

(14) K. Kasatani, M. Ohashi, M. Kawasaki, H. Sato, *Chem. Lett.* **1987**, 16, 1633–1636.

(15) Y. Matsuzawa, S. I. Tamura, N. Matsuzawa, M. Ata, *J. Chem. Soc. Faraday Trans.* **1994**, 90, 3517–3520.

(16) T. V. S. Rao, J. B. Huff, C. Bieniarz, *Tetrahedron* **1998**, 54, 10627–10634.

(17) C. M. S. Yau, S. I. Pascu, S. A. Odom, J. E. Warren, E. J. F. Klotz, M. J. Frampton, C. C. Williams, V. Coropceanu, M. K. Kuimova, D. Phillips, S. Barlow, J. L. Brédas, S. R. Marder, V. Millar, H. L. Anderson, *Chem. Commun.* **2008**, 2897–2899.

(18) S. Gadde, E. K. Batchelor, J. P. Weiss, Y. Ling, A. E. Kaifer, *J. Am. Chem. Soc.* **2008**, 130, 17114–17119.

(19) N. K. Petrov, D. A. Ivanov, D. V. Golubkov, S. P. Gromov, M. V. Alfimov, *Chem. Phys. Lett.* **2009**, 480, 96–99.

(20) H. Zhang, L. Liu, C. Gao, R. Sun, Q. Wang, *Dyes Pigm.* **2012**, 94, 266–270.

(21) K. L. Kim, G. Sung, J. Sim, J. Murray, M. Li, A. Lee, A. Shrinidhi, K. M. Park, K. Kim, *Nat. Commun.* **2018**, 9, 1712.

(22) M. Li, A. Lee, S. Kim, A. Shrinidhi, K. M. Park, K. Kim, *Org. Biomol. Chem.* **2019**, 17, 6215–6220.

(23) B. Gong, B. K. Choi, J. Y. Kim, D. Shetty, Y. H. Ko, N. Selvapalam, N. K. Lee, K. Kim, *J. Am. Chem. Soc.* **2015**, 137, 8908–8911.

(24) M. Li, A. Lee, K. L. Kim, J. Murray, A. Shrinidhi, G. Sung, K. M. Park, K. Kim, *Angew. Chem. Int. Ed.* **2018**, 57, 2120–2125; *Angew. Chem.* **2018**, 130, 2142–2147.

(25) M. Li, S. Kim, A. Lee, A. Shrinidhi, Y. H. Ko, H. G. Lim, H. H. Kim, K. B. Bae, K. M. Park, K. Kim, *ACS Appl. Mater. Interfaces* **2019**, 11, 43920–43927.

(26) S. J. Barrow, S. Kasera, M. J. Rowland, J. Del Barrio, O. A. Scherman, *Chem. Rev.* **2015**, 115, 12320–12406.

(27) D. Sigwalt, M. Šekutor, L. Cao, P. Y. Zavalij, J. Hostaš, H. Ajani, P. Hobza, K. Mlinarić-Majerski, R. Glaser, L. Isaacs, *J. Am. Chem. Soc.* **2017**, 139, 3249–3258.

(28) X. Yang, R. Wang, A. Kermagoret, D. Bardelang, *Angew. Chem. Int. Ed.* **2020**, 59, 21280–21292; *Angew. Chem.* **2020**, 132, 21464–21476.

(29) A. Pedrini, A. Devi Das, R. Pinalli, N. Hickey, S. Geremia, E. Dalcanale, *Eur. J. Org. Chem.* **2021**, 2021, 1547–1552.

(30) E. Pazos, P. Novo, C. Peinador, A. E. Kaifer, M. D. García, *Angew. Chem. Int. Ed.* **2019**, 58, 403–416; *Angew. Chem.* **2019**, 131, 409–422.

(31) Y. H. Ko, E. Kim, I. Hwang, K. Kim, *Chem. Commun.* **2007**, 1305–1315.

(32) G. Wu, M. Olesińska, Y. Wu, D. Matak-Vinkovic, O. A. Scherman, *J. Am. Chem. Soc.* **2017**, 139, 3202–3208.

(33) X. Zhang, T. Sun, X. L. Ni, *Org. Chem. Front.* **2021**, 8, 32–38.

(34) Z. H. Peng, *J. Mater. Chem.* **1996**, 6, 559–565.

(35) J. Kim, I. S. Jung, S. Y. Kim, E. Lee, J. K. Kang, S. Sakamoto, K. Yamaguchi, K. Kim, *J. Am. Chem. Soc.* **2000**, 122, 540–541.

(36) J. Del Barrio, P. N. Horton, D. Lairez, G. O. Lloyd, C. Toprakcioglu, O. A. Scherman, *J. Am. Chem. Soc.* **2013**, 135, 11760–11763.

(37) F. Biedermann, V. D. Uzunova, O. A. Scherman, W. M. Nau, A. De Simone, *J. Am. Chem. Soc.* **2012**, 134, 15318–15323.

(38) G. V. Zakharova, V. G. Avakyan, V. P. Markelov, N. L. Svyatoslavskii, T. A. Svyatoslavskaya, A. K. Chibisov, *High Energy Chem.* **2015**, 49, 407–414.

(39) R. E. Di Paolo, J. O. Tocho, *J. Lumin.* **1997**, 72–74, 481–483.

(40) N. Hickey, B. Medagli, A. Pedrini, R. Pinalli, E. Dalcanale, S. Geremia, *Cryst. Growth Des.* **2021**, 21, 3650–3655.

(41) T. Y. Zhou, Q. Y. Qi, Y. Zhang, X. N. Xu, X. Zhao, *Org. Chem. Front.* **2015**, 2, 1030–1034.

(42) P. Wang, Y. Wu, Y P. Wang, Y. Wu, Y. Zhao, Y. Yu, M. Zhang, L. Cao, *Chem. Commun.* **2017**, 53, 5503–5506.

(43) J.R. Lakowicz *Principles of Fluorescence Spectroscopy*, Third Edition.

(44) Kabsch, W. XDS. *Acta Crystallogr. Sect. D Biol. Crystallogr*. **2010**, 66, 125–132.

(45) Kabsch, W. Integration, scaling, space-group assignment and post-refinement. *Acta Crystallogr. Sect. D Biol. Crystallogr.* **2010**, 66, 133–144.

(46) Sheldrick, G. M. SHELXT - Integrated space-group and crystal-structure determination. *Acta Crystallogr. Sect. A Found. Crystallogr.* **2015**, 71, 3–8.

(47) Sheldrick, G.M. Crystal structure refinement with SHELXL. *Acta Crystallogr.* **2015**, C71, 3–8.

(48) Farrugia, L. J. WinGX and ORTEP for Windows: An update. *J. Appl. Crystallogr.* **2012**, 45, 849–85